

ABSTRACT

Title of Dissertation: NEURAL FEEDBACK CONTRIBUTION TO HUMAN LOCOMOTION CONTROL

Shakiba Rafiee, Doctor of Philosophy, 2022

Dissertation directed by: Associate Professor Ross H. Miller,
Neuroscience and Cognitive Science Program

Associate Research Professor Tim Kiemel,
Neuroscience and Cognitive Science Program

The human nervous system stabilizes locomotion by continuously correcting for deviations away from the desired gait pattern through making transient changes to muscle excitations. We refer to this correction process as “muscle modulation”. It remains unknown how muscle modulations are implemented in the larger framework of human neuromuscular control to achieve stability. Such knowledge has implications across various health and engineering fields. Systematic identification of the properties of the nervous system can provide insight into the role that different muscle modulations play in human walking. Additionally, mathematical models of human walking can be used to test the validity of different neural controllers. In this thesis, we devised three studies to further our understanding of the role different muscle modulations play in human walking and hypothesize the neural mechanisms involved in producing them.

In study one, we investigated the role of the ankle dorsiflexor muscle, tibialis anterior, modulation in the control and stability of human walking. Previous research from our lab has suggested a novel role for the tibialis anterior in speed control during early stance. To investigate this role, we imposed a restriction on ankle dorsiflexion using a taping method, which limited the ability of this muscle to accelerate the body forward during early stance. We characterized the kinematic and muscular responses of this “restricted” walking to mechanical perturbations and compared the results with those from “normal” human walking. Our results support the idea that early stance modulation of tibialis anterior muscle regulates speed control.

In studies two and three, we used mathematical models of human walking to investigate the neural mechanisms involved in foot-placement. In study two, we examined whether a model of human locomotion that is purely controlled by spinal reflex mechanisms can produce muscle modulations observed in human locomotion. In study three, we developed a model of human walking and examined its response to mechanical perturbations of the leg. Together these studies provided insight into the types of neural mechanisms the human nervous system uses to stabilize walking. We observed that gated reflex mechanisms can produce some of the human responses to external perturbations, but not all.

NEURAL FEEDBACK CONTRIBUTION TO HUMAN LOCOMOTION
CONTROL

by

Shakiba Rafiee

Dissertation submitted to the Faculty of the Graduate School of the
University of Maryland, College Park, in partial fulfillment
of the requirements for the degree of
Doctor of Philosophy
2022

Advisory Committee:

Professor Ross H. Miller, Chair
Professor Tim Kiemel, Co-Chair
Professor Jae Kun Shim
Professor Rodolphe Gentili
Professor Norman M. Wereley

© Copyright by
Shakiba Rafiee
202

Acknowledgements

I would like to first thank my advisors, Tim Kiemel and Ross Miller, without whom this work would not have been possible. Thank you, for giving me the opportunity to work under your supervision and to learn from you. Thank you for your invaluable advice, support, and patience during my PhD.

I would like to thank my dissertation committee, professors Jae Kun Shim, Rodolphe Gentili, and Norman Wereley whose feedback helped shape this thesis. I am especially grateful to Jae Kun Shim for his guidance throughout my graduate studies.

I thank my lab mates in the Neuromechanics Research Core, Hossein Ehsani, Becky Krepinevich, Jessica Hunter, Sara Honarvar, Rana Karimpour, Mia Caminita, Sam Snyder, Gina Garcia, Jenna Burnett, Edward Chu, and Liz Bell for all the discussions, supports and friendships.

I want to give special thanks to my husband, Yahya, who was by my side every step of the way, my parents, Farideh and Reza, and my sister, Banafshe for their support and love. Words do not express how blessed I am to have you in my life. Thank you

Table of Contents

Acknowledgements.....	ii
Table of Contents	iii
List of Figures	v
List of Abbreviations	vi
Chapter 1 : Introduction	1
1.1 Problem Statement:.....	1
1.2 Approach:.....	4
1.3 Specific Aims:.....	5
1.4 Thesis Outline:.....	7
Chapter 2 : Background and Significance	8
2.1 Local Stability of Human Walking	8
2.2 Spinal & Supraspinal Mechanisms in the Active Control of Walking	10
2.3 Stabilizing strategies	12
2.3.1 Counteractive Strategies	13
2.3.2 Non-Counteractive Strategies	14
2.4 Control of Foot-placement in Walking	15
2.5 Methods.....	17
2.6 Significance of our method	18
Chapter 3 : Role of Tibialis Anterior in Human Gait	20
3.1 Introduction:.....	20
3.2 Methods:	24
3.2.1 Experimental Design:.....	25
3.2.2 Statistical Analysis:.....	28
3.3 Results.....	29
3.3.1 Average Waveforms:	29
3.3.2 Kinematic Responses:.....	31
3.3.3 Muscular Responses:	34
3.4 Discussion	36
3.4.1 Walking with Limited Dorsiflexion	37
3.4.2 Response to Perturbations with Limited Dorsiflexion	38
Chapter 4 : Counteractive Strategies in a Non-counteractive Model	40
4.1 Introduction.....	40
4.2 Methods.....	43
4.2.1 Overview:.....	43
4.2.2 Computer Model	43
4.2.3 Simulations	44
4.2.4 Data Analysis & Response Comparison,	45
4.3 Results.....	46
4.3.1 Kinematic Responses:.....	47
4.3.2 Spatiotemporal Responses	50
4.3.3 Muscular Responses.....	52
4.3.3.1 Swing counteractive strategy:.....	52

4.3.3.2	Ipsilateral leg early-stance compensatory strategy:	54
4.3.3.3	Contralateral leg late-stance compensatory strategy:	57
4.4	Discussion	58
4.4.1	Counteractive Mechanisms	59
4.4.2	Non-Counteractive Mechanisms.....	59
4.4.3	Two-step Recovery:	61
4.4.4	Phase-specific Characteristics & Non-Counteractive Mechanisms.....	61
Chapter 5	: Hybrid Neuromechanical Model of Human Walking	65
5.1	Introduction.....	65
5.2	Methods:	68
5.2.1	Overview:.....	68
5.2.2	Model Description:	68
5.2.3	Perturbation simulation:.....	75
5.2.4	Data Analysis & Response Comparison:	75
5.3	Results.....	76
5.3.1	Unperturbed Behavior:.....	76
5.3.2	Kinematic Responses:.....	78
5.3.3	Muscular Responses:	82
5.4	Discussion:.....	86
5.4.1	Neuromechanical Models vs Human	86
5.4.2	Reflex Model vs Reflex+CPG Model	87
Chapter 6	: Conclusions	90
Appendices	93
Appendix I	: Smoothing the Song & Geyer (2015) Model.....	93
Bibliography	101

List of Figures

Figure 2-1) Schematic diagram of the components of neural control of human walking.....	9
Figure 3-1) Application of dorsiflexion restriction.....	25
Figure 3-2) Average kinematics waveforms in the normal and restricted conditions.	30
Figure 3-3) Average Muscle excitations waveforms in the normal and restricted conditions	31
Figure 3-4) The ϕ IRF heat map describing the response of the ipsilateral ankle AP position to the mechanical perturbations	32
Figure 3-5) The ϕ IRF heat map describing the response of the ipsilateral ankle angle to the mechanical perturbations	33
Figure 3-6) TA Early stance Strategy	35
Figure 3-7) VAS Early stance Strategy	36
Figure 4-1) Musculoskeletal model used to study human locomotion	44
Figure 4-2) Comparison between model and human mean waveforms	47
Figure 4-3) Comparing the Ankle AP position response to the mechanical perturbations in the model and human	49
Figure 4-4) Comparing step length and duration responses to the mechanical perturbations in the model and human	51
Figure 4-5) Comparing ipsilateral hamstring and knee angle responses to the mechanical perturbations applied during swing, in the model and human	53
Figure 4-6) Comparing ipsilateral TA response to the mechanical perturbations applied during swing, in the model and human	55
Figure 4-7) Comparing ipsilateral HFL/RF response to the mechanical perturbations applied during swing, in the model and human	56
Figure 4-8) Comparing contralateral muscle responses to the mechanical perturbations applied during swing, in the model and human	57
Figure 5-1) Musculoskeletal model used to study human locomotion	69
Figure 5-2) Comparison between the kinematics and muscle excitations between the two models and human during unperturbed cycles.....	77
Figure 5-3) Comparing the Ankle AP position response to the mechanical perturbations in the models and human	79
Figure 5-4) Comparing the Pelvis AP position response to the mechanical perturbations in the models and human	81
Figure 5-5) Comparing ipsilateral TA response to the mechanical perturbations in the models and human	83
Figure 5-6) Comparing ipsilateral VAS response to the mechanical perturbations in the models and human	84
Figure 5-7) Comparing Contralateral GAS response to the mechanical perturbations in the models and human	85
Figure 5-8) Comparing AP Pelvis response to the mechanical vs visual perturbations applied at mid swing in human	87

List of Abbreviations

DOF degrees of freedom

ID system identification

CPG central pattern generators

COM center of mass

ϕ IRFs phase-dependent impulse response functions

AFO ankle foot orthosis

CP cerebral palsy

EMG Electromyographic

TA tibialis anterior

GAS gastrocnemius

LG gastrocnemius lateralis

MG gastrocnemius medialis

SOL soleus

VAS vastii

Vmed vastus medialis

Vlat vastus lateralis

RF rectus femoris

BFLH biceps femoris long head

BFSH biceps femoris Short Head

SemiT semitendinosus

GLU gluteus

Gmax gluteus maximus

Gmed gluteus medius

LES lumbar erector spinae

HTF harmonic transfer function

LTP linear time periodic

AP anterior posterior

RMS root mean square

RG rhythm generator

PF pattern formation

GRF ground reaction force

Chapter 1 : Introduction

1.1 Problem Statement:

Bipedal walking is arguably the signature movement of humans as a species and the most important activity of daily living for general mobility. Many pathological conditions that affect the neuromuscular system, such as Parkinson's disease (Wood et al., 2002; Allen et al., 2011) or gait disorders associated with old age (Masud and Morris, 2001) make it difficult to walk. A mechanistic understanding of neuromuscular control of walking, such that accurate predictive computer models can be created, would help in understanding the structure and function of the nervous system both in health and pathology, which is one of the central problems in motor control.

Human walking is locally stable (Dingwell and Kang, 2007), which means that humans can return to their original gait pattern after being exposed to small external or internal perturbations (Faisal et al., 2008). Maintaining locomotion stability might seem easy given that walking typically requires little conscious effort in a healthy state. However, bipedal walking is inherently unstable in the absence of sensory information. Imagine walking without visual information or any tactile feedback. Neural feedback plays a crucial role in human walking stability. When perturbations cause a kinematic deviation from a desired gait pattern, the human nervous system uses sensory information to make transient changes in the periodic patterns of muscle excitations to help the system converge back to its original behavior (i.e., stable limit cycle). The collection of the nervous system's responses to the perturbation is called "stabilizing

strategies.” Insight into how these strategies are implemented at the neural level (i.e., “neural control mechanisms”) has important implications in various research fields: e.g., designing bipedal robots (Collins et al., 2005), prostheses (Tahir et al., 2018) or assistive devices for populations with locomotor disabilities (Martelli et al., 2017). However, neural control of human locomotion is not yet fully identified.

Developing predictive models of neuromuscular control is complicated by the variety of mechanisms that contribute to neural control of human walking. Two main categories of potential neural control mechanisms have been proposed in the gait literature: counteractive mechanisms, and non-counteractive mechanisms.

Counteractive mechanisms oppose the kinematic effect of the perturbations shortly after they occur. They rely on fixed-latency gated reflex pathways to change the neural command. Due to the straightforward nature of the involved neural reflexes, which often involve a single joint, it has been relatively easy to identify the role of counteractive mechanisms in gait control (e.g., Dietz et al., 1986a; Eng et al., 1994a). However, counteractive strategies alone cannot explain gait neural control.

To optimally control human gait, the nervous system also adopts non-counteractive strategies to proactively prevent the potential effect of the perturbations (e.g., Patla, 2003a) or retroactively compensate for them (Rafiee and Kiemel, 2020). Rather than opposing the perturbation at a single joint, non-counteractive mechanisms work on a whole-body level. In addition, non-counteractive responses may be delayed until an appropriate phase, when the response can be more successful than an immediate

response. It has been suggested that to implement non-counteractive responses, the nervous system uses sensory information to estimate the future state of the system and update the neural command based on that information (Logan et al., 2017; Rafiee and Kiemel, 2020). Due to the complicated nature of the non-counteractive strategies, which involve controlling multiple degrees of freedom (DOF), identifying the non-counteractive mechanisms of walking neural control remains a challenge.

Using external mechanical perturbations in combination with system identification (ID) methods allows making inferences about the role of each muscle in human walking (Logan et al., 2017; Rafiee and Kiemel, 2020). However, full identification of the neural controller requires applying a large number of independent mechanical perturbations (equal to at least half of the system's DOF). In addition, taking the black box system ID approach which only provides information about the relationship between the inputs and outputs, it would be impossible to use experiments to infer the neural mechanisms responsible for producing those responses. Studying the response of human walking to all perturbations goes beyond the scope of this thesis. A more attainable aim is designing a set of studies to identify the response of human walking to a specific group of perturbations and to use computer simulations to test hypothesized neural controllers that can produce the observed responses.

One of the important subtasks of human locomotion is ensuring correct foot-placement. When perturbed, people initially step in the direction of the mechanical perturbation (Wang and Srinivasan, 2014) and compensate for the foot-placement errors in the following steps (Joshi and Srinivasan, 2019). If the leg is placed too far in front of the

body, is too late to bring the leg back. Instead the nervous system can use non-counteractive mechanisms to move the pelvis forward relative to the foot (Rafiee and Kiemel, 2020). Modulation of anterior muscles, including that of the tibialis anterior (TA), during early stance is hypothesized to be one of these non-counteractive strategies that helps propel the body forward and regulates the speed of the center of mass (Rafiee and Kiemel, 2020). This hypothesis is compelling because it proposes an additional role for the TA in gait, where this muscle is typically thought to be important for other tasks such as ground clearance (Boakes and Rab, 2006). However, this hypothesis needs further confirmation. The goal of this thesis is therefore 1) to verify whether the early stance modulation of TA plays a role in gait speed control, 2) to examine whether this response can be categorized as non-counteractive and 3) to examine potential neural mechanisms that contribute to this modulation.

1.2 Approach:

Various methods have been used to identify the role of muscle excitations in gait control. However, using external perturbation in combination with system ID methods can provide causal inferences about the properties of the nervous system. Our lab has developed a technique that characterizes the human walking response to small external perturbations and allows investigation of the stabilizing role of different muscle modulation in gait control (Kiemel et al., 2016). In this thesis, we use this technique to verify the previously hypothesized role of TA modulation in gait control and expand on our understanding of the neural mechanisms that contribute to it. This purpose is pursued in three specific aims.

1.3 Specific Aims:

Aim 1: To verify the role of early stance TA modulation in speed control

Early stance modulation of the TA muscle is one of the non-counteractive strategies suggested to regulate foot-placement (Rafiee and Kiemel, 2020). In study 1, to investigate the role of early stance modulation of TA in controlling gait speed, we limited the contribution of this dorsiflexor muscle to gait. We impose a restriction on ankle dorsiflexion using a taping method, which should limit the ability of this muscle to accelerate the body forward during stance. We then study how human walking is stabilized in response. We compare the mean patterns of muscle excitations in the “restricted” and “normal” conditions. More importantly, we identify differences between the stabilizing response in these conditions by characterizing their kinematic and muscular responses to lower-body mechanical perturbations. We hypothesize that if early stance TA modulation plays an important role in speed control, then restricting dorsiflexion should lead to either decreased ability to compensate for errors in foot placement or adaptation of alternative strategies by the nervous system to control speed and help the subjects maintain balance on the treadmill.

Aim 2: To examine previous categorization of foot-placement strategies as counteractive /non-counteractive using a neuromechanical model of walking

To better understand the neural mechanisms involved in the human stabilizing responses, the first step was to test if counteractive and non-counteractive responses have been previously categorized correctly (Rafiee and Kiemel, 2020). We use computer simulation of human walking to test the previous counteractive / non-

counteractive classification of the muscular responses. To this end, we examine the response of a well-known counteractive model of human walking (Geyer and Herr, 2010) to external mechanical perturbations. We compare its results to those from previous experiment (Rafiee and Kiemel, 2020). We hypothesize that if our previous classification was correct, the Geyer and Herr (2010) model would be able to reproduce responses that we have categorized as counteractive, but not the non-counteractive ones.

Aim 3: To develop a hybrid neuromechanical model of human walking with both counteractive and non-counteractive components

As a follow up to study 2, in study 3 we compare different types of neural mechanisms that can stabilize human walking. It has been suggested that the implementation of the non-counteractive strategies requires mechanisms such as a clock or a state estimator. Therefore, we develop our own neuromechanical model of human walking with both counteractive and non-counteractive components. Our new model is based on Song and Geyer (2015) counteractive model with added non-counteractive mechanisms in the form of a clock with phase-resetting (Aoi et al., 2010). We study whether adding this non-counteractive component helps the model behave more like a human in response to external mechanical perturbations. We hypothesize that adding a simple clock with phase-resetting to the model would affect the average muscle excitation waveforms and by extension the muscular responses induced by reflex mechanisms that rely on them. It is hypothesized that this clock mechanism is necessary but not sufficient for producing all non-counteractive responses. Therefore here, we expect our hybrid model

to mimic human response to external perturbations better than the counteractive model in study 2 for at least a subset of the muscular responses.

1.4 Thesis Outline:

To summarize, the overall goal of this thesis is to further our understanding of the role of different muscle modulations in foot-placement strategies and hypothesize the neural mechanisms involved in producing them. To this end, we first review the literature on human foot-placement strategies and what is known about their neural mechanisms (**Chapter 2**). Next, we use experiments to verify the role of early stance modulation of TA in gait speed control (**Chapter 3**). We then use modeling to examine previous categorization of foot-placement strategies as counteractive and non-counteractive (**Chapter 4**). Finally, we develop a new neuromechanical model of human walking to examine potential neural mechanisms that contribute to foot-placement (**Chapter 5**).

Chapter 2 : Background and Significance

In this chapter, we review how humans use foot-placement strategies to stabilize walking. Our goal is to clarify to what extent can human responses to external perturbations be explained by our current knowledge of control strategies. To this end, we review the role of the musculoskeletal system and nervous system in stabilizing walking and the mechanisms at their disposal. We then review existing knowledge on the role of counteractive and non-counteractive mechanisms of the neuromuscular controller in producing the foot-placement strategies. Lastly, we review what methods can be used to identify these foot-placement strategies and infer the mechanisms which produce them.

2.1 Local Stability of Human Walking

Human walking is locally stable, which means that in response to small perturbations it can return to its initial gait pattern. Local stability of human walking is the product of the interaction between the musculoskeletal system, which is responsible for producing movement, and the nervous system, which dictates the neural commands. From a control theory perspective, this structure consists of two entities: 1) the plant, the entity that is being controlled; and 2) the neural feedback, the entity that controls (Figure 2-1) Schematic diagram of the components of neural control of human walking (inspired by Zehr, 2005; Pearson et al., 2006). The musculoskeletal system produces movement. The neural controller, then receives information about the movement through different sensory modalities (including vision, somatosensation and vestibular

sensation) and updates the command signal at different neural levels.). Both the controller and the plant contribute to gait stability (Holmes et al., 2006). This ensemble takes advantage of passive mechanisms of the plant and active mechanisms of the neural feedback to achieve stability in the face of continual perturbations that arise from internal sources (e.g., neuromuscular and sensory noise (Faisal et al., 2008)) and external sources (e.g., variation in walking surfaces or changes in optic flow due to environmental motion).

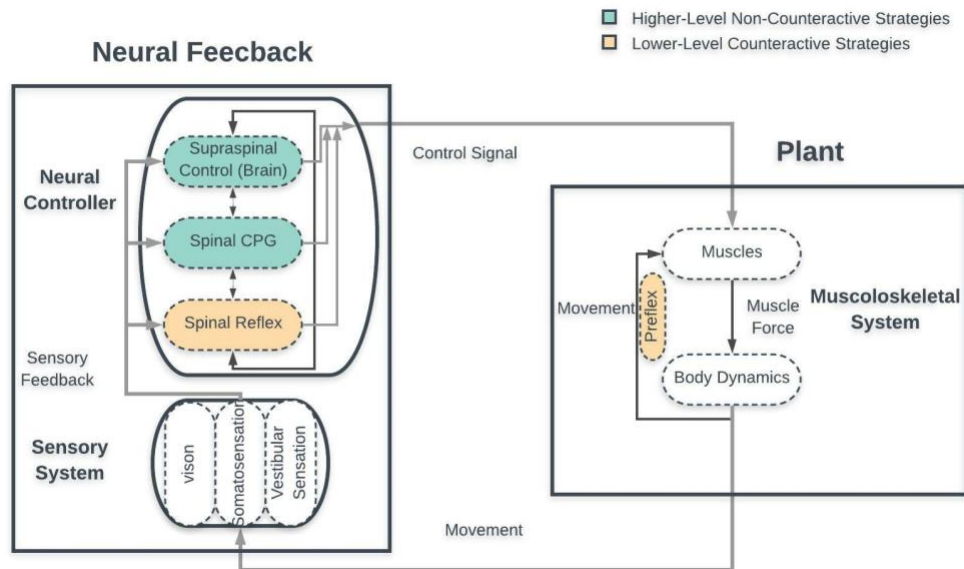


Figure 2-1) Schematic diagram of the components of neural control of human walking (inspired by Zehr, 2005; Pearson et al., 2006). The musculoskeletal system produces movement. The neural controller, then receives information about the movement through different sensory modalities (including vision, somatosensation and vestibular sensation) and updates the command signal at different neural levels.

Passive Components: The musculoskeletal system contributes to the control of locomotion through passive mechanisms. Due to intrinsic viscoelastic properties of the musculoskeletal system, in human walking, the plant can partially correct for small perturbations and help resume walking behavior. These mechanisms that are due to the

viscoelastic properties of the musculoskeletal system contributes to gait stability and robustness by producing zero-delay intrinsic responses to the perturbations. Muscle force-length and force-velocity relationships are examples of these viscoelastic properties. It has been established that in addition to the neural component, force production depends on the muscle dynamics (Hill, 1938). Therefore, any perturbation that affects these dynamics (for instance by increasing the muscle length) would also change the muscle forces and joint kinetics. That is why these passive stabilizing mechanisms, that change the muscle dynamics after zero neural delay, are thought of as instantaneous feedback loops and are called reflexes (Brown and Loeb, 2000). The contribution of reflexes to gait stability, even though hard to measure experimentally, has been extensively studied and established in the computer modeling literature (Gerritsen et al., 1998; Loeb et al., 1999; Proctor and Holmes, 2010). These passive stabilizing mechanisms are involved in both single joint as well as multi joints strategies.

Active Components: The other category of strategies, i.e. active control strategies, are implemented by the nervous system, predominantly through changing muscle excitations from their average waveforms. Sensory information is essential for active locomotor control and coordinating the muscle modulations required for stabilizing walking. We use sensory information to set the timing of muscle excitations, regulate their magnitude and alter their pattern (Pearson et al., 2006). To better understand the role of sensory information in active control of human walking, in the next section we

review the literature on known and hypothesized neural mechanisms involved in gait control at both spinal and supraspinal levels.

2.2 Spinal & Supraspinal Mechanisms in the Active Control of Walking

Animal studies have shown that the spinal cord contains neural circuits, called central pattern generators (CPG), that can generate rhythmic patterns of muscular excitations and produce locomotor movements, even in the absence of sensory information (Grillner and Wallen, 1985). According to cat studies, a CPG consists of reciprocally interacting flexor and extensor half centers that receive parallel excitatory and inhibitory commands from rhythm generators and are responsible for the rhythmic movement production. Recent literature suggests a hierarchical nature for the CPGs that control the upper leg and lower leg muscles (Duysens and Forner-Cordero, 2018). In addition, modular rhythm generators have been suggested for the swing and stance (Duysens and Forner-Cordero, 2018). CPGs are responsible for coordinating movement for several joints through an intricate web of connections between neighboring neurons. Even though CPGs do not need sensory information, they integrate sensory information (Duysens and Forner-Cordero, 2018). Indirect evidence suggests that the CPGs may also play a role in generating basic patterns of human locomotion (Hultborn and Nielsen, 2007). These neural circuits that produce the basic patterns of human locomotion can also be regulated by the supraspinal neural circuits (Taga, 1995; Aoi et al., 2010)

The other group of spinal mechanisms involved in regulating human walking are the population of interneurons that mediate somatosensory reflex pathways. Three main reflex categories are known to contribute to human locomotion. 1) Muscle stretch reflex is a length feedback mechanism. Afferent fibers from the primary (Ia) and secondary (II muscle spindles provide information about the muscle length and its rate of change respectively and directly synapse unto the motoneurons in the spinal cord and modulate their excitation (Purves et al., 2014). 2) Similarly, the Golgi tendon reflex is a force feedback mechanism. Afferent neurons (Ib) from the Golgi tendon organs carry information about the tendon tension which reflects the muscle force (Purves et al., 2014). 3) Lastly, cutaneous reflexes regulate other spinal pathways. Afferent neurons carry information about touch to modify the limb movement trajectories (Purves et al., 2014). The stumbling correction reaction is one of the most well-known examples of the cutaneous reflexes. These spinal reflexes are known to be highly task and phase-dependent (Zehr et al., 1997). In addition, they are suggested to potentially bypass the CPG (Hultborn and Nielsen, 2007).

The human walking is also regulated at the supraspinal level. At this level, the nervous system can directly regulate walking by controlling subtasks of locomotion such as postural stability (Takakusaki, 2013). Some researchers have suggested involvement of internal models in the direct control of locomotion (Wolpert et al., 1995; Takakusaki, 2013). In addition, the supraspinal network can indirectly regulate walking, through sending simple commands to the spinal level. The supraspinal networks can both modulate CPGs and regulate transcortical reflexes (Matthews, 1991). **Figure 2-1)**

Schematic diagram of the components of neural control of human walking (inspired by Zehr, 2005; Pearson et al., 2006). The musculoskeletal system produces movement. The neural controller, then receives information about the movement through different sensory modalities (including vision, somatosensation and vestibular sensation) and updates the command signal at different neural levels. Illustrates a schematic diagram of the components of neural control of human walking as described above.

2.3 Stabilizing strategies

Humans use the amalgam of the abovementioned mechanisms to stabilize locomotion in response to internal and external perturbations. In this section, we revisit the original question: to what extent can human responses to external perturbations be explained by our current knowledge of control strategies. To address this question, it is helpful to distinguish between gait stabilization strategies. Human walking is proposed to use two main classes of strategies for stabilization: counteractive and non-counteractive strategies. In this section, we review both categories of strategies in foot placement.

2.3.1 Counteractive Strategies

As mentioned in the introduction chapter, the term counteractive refers to a group of strategies in response to unexpected internal or external perturbation. Counteractive strategies rely on sensory information to directly counteract the effect of the perturbations (Patla, 2003). For instance, in response to mechanical perturbations that displace the leg, counteractive foot-placement strategies are implemented through modulation of muscles that move the leg in the opposite direction of the applied

perturbations (Eng et al., 1994; Rafiee and Kiemel, 2020). In general, the majority of these counteractive strategies take advantage of proprioceptive spinal reflexes with length-feedback (e.g., Eng et al., 1994) and force-feedback characteristics (Yang et al., 1991; Sinkjær et al., 1996; Van de Crommert et al., 1996; Grey et al., 2004). Some of the counteractive strategies described in the literature involve only a single joint, but others involve several joints, such as the stumbling correction reaction. Due to the properties of the mono- and polysynaptic reflex pathways, these counteractive responses, in general, happen a fixed latency after the onset of the perturbation. By virtue of having easy to detect characteristics in combination with the extended literature that exist on the structure of the involved spinal reflex mechanisms, it has been relatively easy to understand the goal of most counteractive strategies.

2.3.2 Non-Counteractive Strategies

Optimal control of human walking also includes proactive (Patla et al., 1991) and compensatory strategies (Rafiee and Kiemel, 2020) that are categorized as non-counteractive. Proactive strategies are not directly related to local stability of human walking, but they provide insight into the structure of non-counteractive mechanisms. Proactive strategies rely on vision to predict future sensory and motor events. Obstacle avoidance is one of the best known proactive strategies where using visual information, the gait pattern is altered to avoid collisions (Patla et al., 1991). The other group of non-counteractive strategies arise in response to mechanical perturbations, but rather than opposing them, these strategies compensate for the effect of the perturbations (Rafiee and Kiemel, 2020). For instance, in responses to mechanical perturbations that result

in forward displacement of the swing leg just prior to heel strike, it has been observed that the muscles are modulated at specific phases of the gait cycle to compensate for the leg being pushed forward, by propelling the pelvis forward and controlling the speed of the contralateral leg in the next cycle.

As discussed in the introduction chapter, these non-counteractive strategies are delayed until an appropriate phase, rather than producing an immediate response. It has been suggested that when implementing non-counteractive strategies, the nervous system considers the biomechanics of the body and its interaction with the environment. Since the body biomechanics is phase-dependent, the non-counteractive strategies should use knowledge about the state (e.g., phase) of the system to implement the correct response. Therefore, the non-counteractive responses cannot be easily described by reflex mechanisms. Rather they presumably rely on mechanisms that provide information about the state of the system. To this day, identifying role of the muscle modulation in non-counteractive strategies has remained difficult due to two reasons. 1) The non-counteractive strategies often involve several joints, and 2) a full neural pathway from the sensory input to motor output that explains the proactive responses is not known.

This section reviewed the general characteristics of counteractive and non-counteractive strategies. We conclude here that compared to counteractive strategies, the neural mechanisms underlying non-counteractive strategies remain to be further investigated. In the next section, we review the literature on the contribution of these categories of responses to human foot placement.

2.4 Control of Foot-placement in Walking

Maintaining stability is one of the main subtasks of human walking. Foot-placement is one of the most important control strategies that the nervous system adopts to stabilize gait in both the mediolateral (Rankin et al., 2014) and anterior-posterior (Hof, 2008) directions. Experimental studies have found that the timing and placement of the foot at heel strike contributes to walking stability (Nashner, 1980). Similarly, in simulation studies, controlling the angle of the leg at heel strike ensures stability in simple models of human locomotion (Srinivasan and Ruina, 2006). Both counteractive and non-counteractive strategies have been reported to play a crucial role in foot placement. In the broad sense, foot-placement strategies contribute to walking stability by 1) positioning the foot (Dietz et al., 2004; Eng et al., 1994) and 2) correcting for the errors in foot-placement in the following steps (Hof, 2008; Wang and Srinivasan, 2014; Vlutters et al., 2018) through controlling the center of mass (COM) movement, as well as the walking speed and cadence.

Different muscle modulations regulate foot placement. For instance, gait research has suggested that modulation of the hamstring muscle group during swing contributes to foot positioning (Dietz et al., 1986; Eng et al., 1994) and modulation of leg plantarflexors during late stance contributes to leg progression (Neptune et al., 2001), which can be used to compensate for the errors in foot placement in the previous step. Recent studies in our lab (Logan et al., 2017; Rafiee and Kiemel, 2020) have suggested an addition to this list: modulation of anterior leg-muscle activities during early stance

as a mechanism to regulate the speed of the pelvis relative to the foot and thus compensate for errors in foot placement. However, as discussed earlier, our interpretation of the responses involving more than a single joint remain as hypotheses. Lack of sufficient understanding of muscle-level control prevents us from developing a model that can simulate human-like response in a predictive fashion. To paraphrase Feynman:

“What we cannot create, we do not understand.”

The overarching goal of the proposed studies is therefore to examine the role of previously hypothesized muscle modulations in foot-placement, hypothesize potential components of the neuromuscular controller for producing these responses and develop a predictive model of human locomotion control that can produce these responses.

2.5 Methods

Various methods have been used to identify the role of muscle excitations in gait control. As mentioned in the introduction chapter, having knowledge about the underlying mechanism of the musculoskeletal and nervous system can provide intuition on the role of the muscle modulations in control of walking. Similarly, having knowledge of the biomechanics of the human gait can help identify some of the muscle excitation roles. For example, using a biomechanical model of gait, Neptune et al. (2001) showed that the late stance excitation of gastrocnemius muscles, and not the soleus, contribute to swing initiation.

Aside from modeling approaches, experimental studies have helped shape our current understanding of different strategies of walking control. Part of our knowledge comes from looking at gait variability by studying the correlation between muscle excitations and the outcome strategies (Bauby and Kuo, 2000; Dingwell and Marin, 2006). For instance, the role of late-stance rectus femoris (RF) modulation in cadence control has been studied in this paradigm (Den Otter et al., 2004). Studying variability is essentially studying the system behavior in response to the intrinsic perturbations (that exist due to sensory and motor noise). However, the downside of using variability is that it cannot be used to identify the role of sensory information in the adopted control strategies. This is because the intrinsic perturbations in the system cannot be measured; therefore, it is difficult to identify which component of the closed-loop system has caused the observed deviations in the kinematics and muscular excitations. The alternative is studying the response of the system under external perturbations. For instance, using external perturbations, researchers have identified the role of modulation of the hamstring muscle group during swing in foot placement strategies (Eng et al., 1994) and the role of modulation of leg plantarflexors during mid-stance in balance control (Nashner, 1980; Sinkjær et al., 1996).

2.6 Significance of our method

One of the significant aspects of the proposed study is that our lab has developed a technique that characterizes the human walking response to small external perturbations (Kiemel et al., 2016). This approach feature is important because small

perturbations reflect the natural fluctuations which always occur during locomotion. In addition, compared to the large perturbations commonly used in the literature, small perturbations might evoke different responses in human movement, for example, the sway vs stepping responses to posture perturbations (Maki and McIlroy, 1997). Our method calculates the phase-dependent impulse response functions (ϕ IRFs) that describe system responses to small, brief perturbations applied at any phase of the gait cycle. This feature is invaluable to us as calculating these ϕ IRFs for large perturbations can be very difficult. Large perturbations are often discrete, and the system requires relatively long time for recovery. Therefore, to fully characterize the human walking response to large discrete perturbations, researchers should perturb the system at range of phase of the gait cycle, using several different amplitudes. Our method does not suffer from these problems.

In the following chapters, we will discuss how we will use this method to understand the role of the several muscle modulations in gait control and their potential neural mechanisms and specifically the role of early stance modulation of the ankle dorsiflexor TA muscle in speed control

Chapter 3 : Role of Tibialis Anterior in Human Gait

In this Chapter, we investigated the role of early-stance tibialis anterior (TA) muscle modulation in the control and stability of human walking. We proposed an experiment that limits the TA contribution to gait by restricting the ankle dorsiflexion through taping. The results support the idea that early stance modulation of tibialis anterior muscle regulates speed control. They also indicate adaptation of the neural feedback to the restriction.

3.1 Introduction:

Our previous study suggested a role of TA in maintaining treadmill walking speed during the stance phase (Rafiee and Kiemel, 2020). This finding is novel since gait literature typically focuses on the role of TA during swing phase, where its modulation prevents toe-dragging (Boakes and Rab, 2006). TA excitation during early stance has been suggested to prevent foot-slapping (Boakes and Rab, 2006), and induced-acceleration analysis suggest TA acts to decrease forward COM velocity during early stance (Liu et al., 2006). However, recent studies from our lab combining small continuous visual and mechanical perturbations with system ID (Logan et al., 2017; Rafiee and Kiemel, 2020) have suggested that TA modulation soon after heel strike acts to control COM velocity. We found that in response to mechanical perturbations (forward push of the ankle) and visual perturbations (forward displacement of the visual scene), the TA excitation in early stance increased, presumably to increase

walking speed and compensate for errors in foot placement by helping propel the COM forward relative to the foot (Rafiee and Kiemel, 2020). This early-stance modulation was found to be a general control strategy, observed in response to both visual and mechanical perturbations. However, few studies have recognized such a role for TA. These exceptions could be found in older literature; for instance, Perry and Davids (1992) proposed that excitation of the dorsiflexor muscles during early stance controls the rate of plantarflexion and through that contributes to limb progression and consequently forward body propulsion. However, the role of early stance TA modulating in speed control needs more evidence.

To further examine the potential role of TA in controlling forward body propulsion, we restricted the TA contribution to gait using an ankle taping method. The idea is that if the primary dorsiflexor (TA) is indeed playing an important role in propulsion, then by increasing resistance to dorsiflexion, two scenarios are possible. Either the system will have a decreed ability to compensate for errors in foot placement or the nervous system would have to adopt alternative strategies to control propulsion and help the subjects maintain their balance on the treadmill.

Studies on pathological gaits have revealed that the greatest negative effect of limited dorsiflexion/ excessive plantarflexion during stance has been on body progression (Perry and Davids, 1992). People suffering from these types of pathological gaits, such as children with cerebral palsy (Norlin and Odenrick, 1986) or stroke survivors (Olney and Richards, 1996), generally walk at slower speeds. Limited ankle dorsiflexion forces compensatory gait modifications. If pronation is available to them, it can substitute for

dorsiflexion to an extent (Karas and Hoy, 2002). However, in absence of pronation, more metabolically costly compensation strategies have to be implemented, such as walking with shorter step lengths or early heel rise during stance (Karas and Hoy, 2002). In addition, rehabilitation studies conclusively have shown that in the clinical populations, wearing ankle foot orthosis (AFOs) increases walking speed as they help restore partial dorsiflexion (Lehmann et al., 1987).

Similarly, experiments on limiting dorsiflexion have shown that the greatest negative effect is on speed (Delafontaine et al., 2017; Ota et al., 2014; Vistamehr et al., 2014). In most of these experiments AFOs were used. There are few studies that have tried to specifically restrict ankle dorsiflexion using mechanical devices (Ota et al., 2014). In healthy populations, wearing AFOs have decreased the ability to change forward propulsive momentum quickly and consequently have affected the ability to change walking speed (Vistamehr et al., 2014). However, caution must be exercised in interpreting these results AFOs can also restrict the plantarflexors' contribution to gait whose modulation at late-stance has a significant role in propulsion. More specifically, it has been reported that using mechanical dorsiflexion restrictors forces the individuals to take shorter steps and reduce their single support duration (Ota et al., 2014). In summary, dorsiflexion limitations affect the average walking speed as well as the ability to quickly make changes in it, which point to a role for the primary dorsiflexor muscles in speed control.

In the closed-loop structure of movement production, changes in the movement cause changes in the muscle excitations and vice versa. For instance, Romkes and Brunner

(2007) demonstrated that healthy subjects with taped joints that mimicked the cerebral palsy (CP) population toe-walk with similar abnormal muscle excitation patterns, such as a decreased TA excitation during early stance. In another study, Romkes and Brunner (2006) found that in children with CP, wearing AFOs decreases the TA excitation by one third at heel strike. Similarly, in healthy individuals wearing AFOs decreases TA excitation during early stance (Geboers et al., 2002) and during gait initiation (Delafontaine et al., 2017). Dorsiflexion restriction can affect walking either by changing the plant or neural feedback or some combination of both. However, to our knowledge the properties of the neural feedback (i.e., the mapping from the kinematics to the muscle excitations) or the properties of the plant (i.e., the mapping from the muscle excitations to the produced kinematics) have never been investigated. Here, we have the tools to study these mappings.

In this study, we seek to extend our previous work where we used a combination of perturbation and system ID methods to identify the role of muscle modulations in gait. Here, we will identify the role of early stance TA modulation in speed control by adding a restriction that limits the contribution of the primary dorsiflexor muscle to gait and study the “restricted” gait response to external lower-body mechanical perturbations.

The restriction will directly affect the plant through changing the body mechanics (for instance by increasing the joint stiffness). Similarly, based on previous studies, both the average waveform of kinematics and muscle excitations are expected to change. Particularly, we expect to see a decrease in the dorsiflexion angle, and a decrease in average TA excitation at heel strike. Importantly, here, we hypothesize that the

restriction will affect the neural feedback. We expect to see changes in the mapping from movement to the neural command due to the neural feedback adapting to this new plant. Previously, we saw adaptation of the neural feedback to the mechanical perturbation apparatus, where phase-specific muscular excitation changed to guarantee conventional kinematic patterns (Rafiee and Kiemel, 2020). Here, we expect the nervous system to adopt alternative strategies to control speed on the treadmill. Some potential strategies could be an increase in modulation of the quadriceps muscle group during early stance in response to the external perturbations. Absence of alternative responses would suggest TA modulation is not important for controlling speed.

3.2 Methods:

We have collected data from 10 healthy young adults (4 men and 6 women aged 18 to 35 years) in accordance with the University of Maryland IRB. Prior to the test, a single standing trial was collected as a reference for a neutral position. The participants walked on a treadmill (Cybex Trotter 900T, Cybex International, Inc., USA) in two conditions: 1) normal and 2) restricted, where their ankle dorsiflexion was restricted using a standard Achilles tendon taping method ((Perrin and McLeod, 2018), **Error! Reference source not found.**).

For the taping procedure, the subjects were asked to put their ankles in maximum dorsiflexion position. Anchor strips (2.5 cm 3M Micropore tape) were applied proximally and distally. Elastic athletic tapes (7.6 cm, Elastikon, Johnson & Johnson) were stretched fully, then relaxed slightly



Figure 3-1) Application of dorsiflexion restriction

and placed across the posterior ankle to limit dorsiflexion (Figure 3-1) Application of dorsiflexion restriction).

3.2.1 Experimental Design:

Twelve trials of walking, each 250 s long, were collected per subject. In the first 3 trials and last 3 trials, participants walked normally; in the middle 6 trials, participants walked with restricted ankle dorsiflexion. This design allows us to better understand the source of differences in the average muscle excitation between these two walking conditions. Fatigue could affect the muscle excitation and result in a decrease in the overall excitation over time, therefore we designed the experiment so that both conditions occurred the same number of times at the beginning and end of each session. In addition, individuals could implement different walking strategies, and therefore, we decided against randomizing the order of conditions between subjects. Throughout the middle 220 s portion of all trials, the subjects' walking were perturbed by small

continuously-changing forces applied to their legs through a spring-motor (LX80L; ParkerHannifin Corporation) mechanism (Rafiee and Kiemel, 2020).

The mechanical perturbation signal (position of the motor) was specified with a white noise signal with power spectral density of $3.1 \text{ cm}^2/\text{Hz}$ filtered by an 8th-order Butterworth low-pass filter with a cutoff frequency of 2.6 Hz. Since we are interested in the local stability of human walking using small perturbations, there is the threat that the system's responses to perturbations might be buried under the intrinsic variability of human gait. Applying several long random signals allow separating the effect of perturbation and the intrinsic variability of human gait (Rafiee and Kiemel, 2020).

Data Collection: Lower-body and trunk kinematic data was collected using a 2D marker set in a ten-camera VICON-MX motion analysis system (VICON, Inc, Oxford, UK). Reflective markers (diameter, 1.4 cm) were placed on the right and left sides of the body at external landmarks: base of the 5th metatarsal, posterior calcaneus (heel), lateral malleolus (ankle), lateral femoral condyle (knee), greater trochanter (hip), posterior superior iliac spine (PSIS), iliac crest, and superior acromion process (shoulder). Additionally, markers were placed at the midline of the spine at the level of C7, T10 and L1 vertebrae. All markers were attached at the skin of these bony prominences except those that were placed on the shoe (at the 5th metatarsal and heel).

Electromyographic (EMG) data was recorded from the legs and the trunk using the wireless TRIGNO system (DELSYS, USA), which has a built-in bandwidth of 20–450 Hz. The EMG were collected from: right and left tibialis anterior (TA), right

gastrocnemius lateralis (LG), right and left gastrocnemius medialis (MG), right soleus (SOL), right vastus medialis (Vmed), right vastus lateralis (Vlat), right and left rectus femoris (RF), right biceps femoris long head (BFLH), right semitendinosus (SemiT), right gluteus maximus (Gmax), right gluteus medius (Gmed), and right lumbar erector spinae (LES, recorded at L1-L2).

Data Analysis: The kinematic and EMG data were analyzed in MATLAB (MathWorks, USA). The kinematic data were analyzed in the sagittal plane to calculate the joint and segment angles as well as segment displacement in the anterior-posterior (AP) direction. The segment angles were computed relative to vertical, with positive indicating that the upper end of the segment moved forward relative to the lower end. The joint angles were calculated by subtracting the upper segment angle from the lower segment, so that ankle plantarflexion, knee flexion and hip extension are all in the positive direction. The hip joint angle was approximated using markers on lateral femoral condyle, greater trochanter and iliac crest. Since the process of taping the ankle and then removing it affected the position of the ankle marker, we approximated the ankle joint angle using markers on the base of the 5th metatarsal, posterior calcaneus and lateral femoral condyle. For all joint angles, the reference configuration obtained from the average of the joint angle during the standing trial were subtracted from the data. We also used the sagittal plane kinematic data to calculate the step length and durations (see Rafiee and Kiemel, 2020). The heel-strike times were approximated as the times of local minima of the heel marker in the vertical axis, and toe-off times

were approximated as the times of the local maxima of sagittal-plane hip marker relative to the toe marker angle.

Using MATLAB, the EMG data were synchronized with kinematics by correcting for 48 ms delay in the TRIGNO system (DELSYS, USA). The EMG signals were then high-pass filtered with a zero-lag forward-backward cascade of a 4th-order Butterworth filter with a cutoff frequency 20 Hz and full-wave and rectified. Lastly, for each subject and each muscle the EMG signals were normalized to the root mean square (RMS) of the normal walking data for that muscle.

We used harmonic transfer functions (HTF) to characterize the response of human walking to the applied perturbations. An HTF describes the input-output mapping for a linear time periodic (LTP) system (Wereley, 1990), which human walking can be approximated as. The kinematic and muscular (muscle excitation as measured by EMG) responses to the perturbations were analyzed in the frequency domain, using HTFs (Kiemel et al., 2016) and then converted to the time (phase) domain to compute phase-dependent impulse response functions (ϕ IRFs) that describe the response of the system to small brief perturbations (impulses) applied at any phase of the gait cycle. See Kiemel et al. (2016) and Rafiee and Kiemel (2020) for details.

Finally, the kinematic and EMG mean waveforms were compared between the normal and restricted walking conditions as well as across the trials to explore adaptation.

3.2.2 Statistical Analysis:

For each kinematic or EMG variable, paired t-tests were performed to determine if the difference between the mean waveforms of normal and restricted conditions was significantly different than zero. For each response variable, statistical tests were performed on the ϕ IRF for all perturbation phases and for response times up to 3 cycles following the perturbation. t-tests were also used to determine whether ϕ IRF values were significantly different than zero.

3.3 Results

We compared the average waveforms of kinematic and muscle excitations between the two different gait conditions. In addition, we compared how humans responded to the mechanical perturbations by characterizing the kinematic and muscular responses and study the differences in ϕ IRFs of the normal and restricted gaits.

3.3.1 Average Waveforms:

Kinematics: The taping method indeed resulted in the desired effect. We saw significant decreases in the ankle dorsiflexion angle in the restricted condition, particularly during late stance and swing (indicated by the asterisks in **Error! Reference source not found..A**). In addition, during early stance, the taping method significantly decreased the plantarflexion angle (**Error! Reference source not found..A**). We also saw that the dorsiflexion restriction caused changes in the other joint kinematics. Similar to other studies (e.g., Ota et al., 2014), we observed that the restriction resulted in a significant increase in the knee extension during single-support

and swing (**Error! Reference source not found..B**). On the other hand, no significant difference was found for the hip flexion angle (**Error! Reference source not found..C**) or the trunk angle (**Error! Reference source not found..D**).

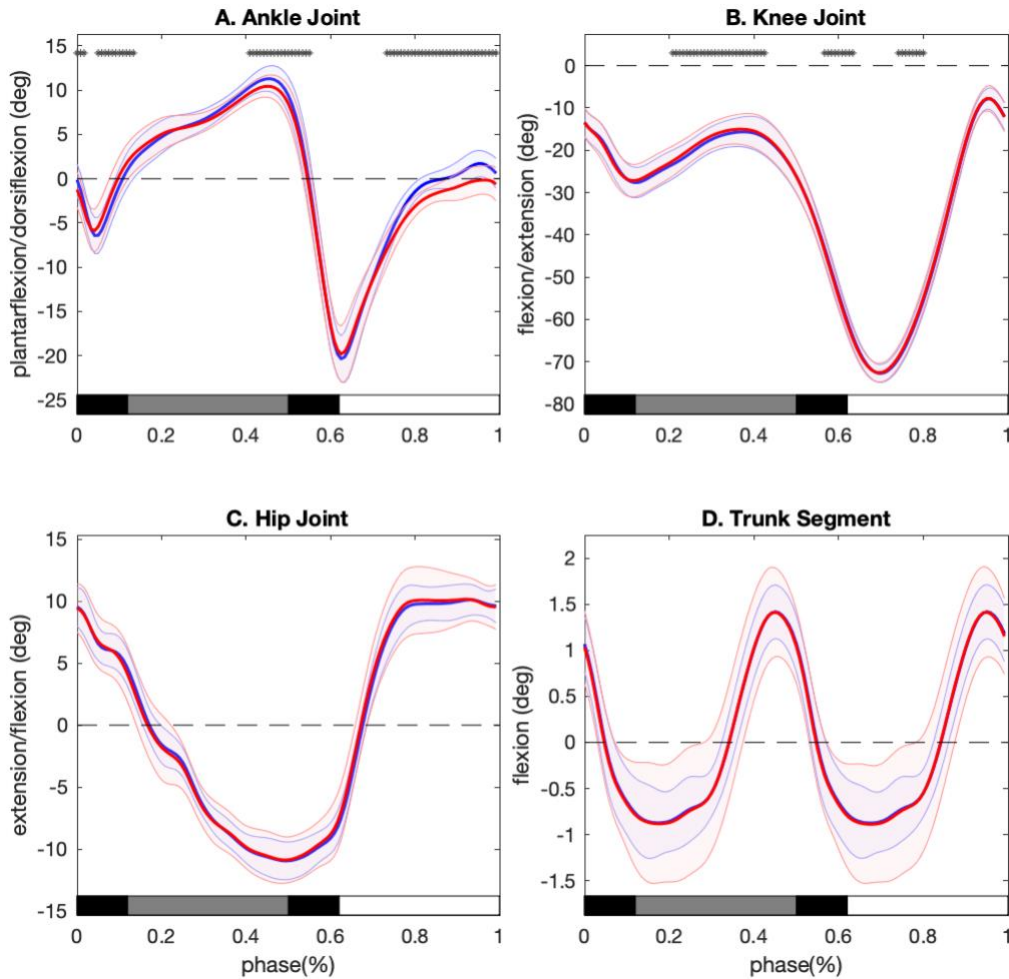


Figure 3-2) Average waveforms of kinematics: the ankle joint (A), knee joint (B), Hip joint (C) and trunk segment (D) angles in the normal (blue) and restricted (red) conditions. The shaded areas indicate 95% confidence intervals. Asterisks indicate significant differences ($p < 0.05$). The bars on the horizontal axes indicate gait phase: (white = swing, gray = single support, and black = double support). The ankle plantarflexion, knee flexion and hip extension are in the positive direction.

Spaciotemporal parameters: the average step and stride durations were found to be significantly shorter in the restricted gait ($\bar{T}_{\text{step}} = 0.5243$ s, $\bar{T} = 1.0486$ s) compared

to the normal gait ($\bar{T}_{\text{step}} = 0.5289$ s, $\bar{T} = 1.0578$). However, our preliminary results did not show a significant difference in the single support, double support or their respected ratios to the step duration between conditions. We also saw that the average step length was significantly shorter in the restricted condition (71.4 cm), compared to the normal gait (72.6 cm).

Muscle Excitations: We observed significant differences between conditions at the peak muscle excitation for 3 muscles. TA muscle and VAS muscles demonstrated a significant decrease in their peak excitation at early stance in the restricted walking condition (**Error! Reference source not found..A - C**).

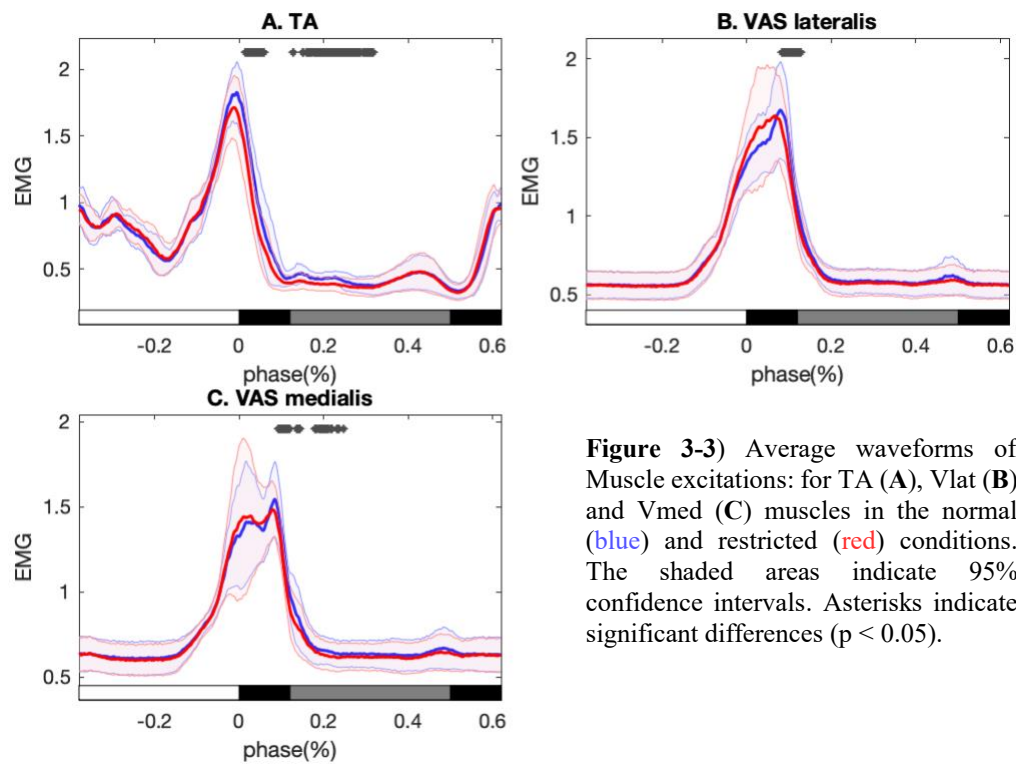


Figure 3-3) Average waveforms of Muscle excitations: for TA (A), Vlat (B) and Vmed (C) muscles in the normal (blue) and restricted (red) conditions. The shaded areas indicate 95% confidence intervals. Asterisks indicate significant differences ($p < 0.05$).

3.3.2 Kinematic Responses:

In response to the forward mechanical perturbation, we observed that the legs were displaced forward in both conditions (**Figure 3-4**) The ϕ IRF heat map describing the response of the ipsilateral ankle AP position to the mechanical perturbation in the (A) normal condition, (B) restricted condition and (C) the difference between the two conditions. The ϕ IRF heat maps have two independent variables: perturbation phase on the horizontal axis and normalized response time on the vertical axis. Normalized response time indicates the phase of the gait cycle at which a given response occurs. The single dependent variable of the ϕ IRF is the response to the perturbation, and it is indicated using a color map. Yellows and reds indicate a response in the same direction as the perturbation; blues indicate a response in the opposite direction, and white indicates no response. The diagonal line in the heat map corresponds to a response measured at the same time the perturbation is applied. The black arrows in the heat maps indicate the response time in the experiment when the peak significant t -value occurs.). Generally, we did not find many significant conditional differences in the early kinematic responses. This was somewhat expected as the transient kinematic responses to the mechanical perturbation are passive responses. The one kinematic response that was significantly different between the two walking conditions was the ankle angle response. In response to the forward push of the ankles, we observed an increase in the ankle dorsiflexion angle at heel strike in both gaits (**Figure 3-5**) The ϕ IRF heat map describing the response of the ipsilateral ankle angle to the mechanical perturbation in the (A) normal condition, (B) restricted condition and (C) the difference

between the two conditions. **D**) takes a slice of the first two heat maps and shows the IRF for perturbations applied at phase -0.3 in normal (blue) and restricted (red) conditions. The arrows in the heat maps and asterisks in the slice IRF indicate the time where significant differences between conditions took place ($p < 0.05$). The yellow arrows indicate the perturbation phase (-0.3). The black arrows in the heat maps indicate the response time in the experiment when the peak significant t -value occurs.). However, in the restricted condition, the perturbation resulted in a smaller dorsiflexion response compared to the normal condition (indicated by the asterisks in **Figure 3-5**)

The ϕ IRF heat map describing the response of the ipsilateral ankle angle to the mechanical perturbation in the (A) normal condition, (B) restricted condition and (C) the difference between the two conditions. **D**) takes a slice of the first two heat maps and shows the IRF for perturbations applied at phase -0.3 in normal (blue) and restricted (red) conditions. The arrows in the heat maps and asterisks in the slice IRF indicate the time where significant differences between conditions took place ($p < 0.05$). The yellow arrows indicate the perturbation phase (-0.3). The black arrows in the heat maps indicate the response time in the experiment when the peak significant t -value occurs.**D**). This result could indicate that in the restricted condition the person was not able to use the ankle dorsiflexion mechanism during early stance phase to compensate for the errors in foot placement, by propelling the body forward.

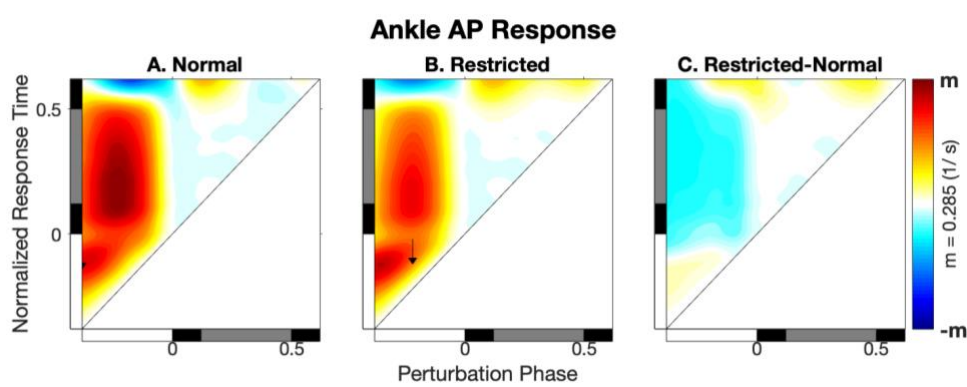


Figure 3-4) The ϕ IRF heat map describing the response of the ipsilateral ankle AP position to the mechanical perturbation in the (A) normal condition, (B) restricted condition and (C) the difference between the two conditions. The ϕ IRF heat maps have two independent variables: perturbation phase on the horizontal axis and normalized response time on the vertical axis. Normalized response time indicates the phase of the gait cycle at which a given response occurs. The single dependent variable of the ϕ IRF is the response to the perturbation, and it is indicated using a color map. Yellows and reds indicate a response in the same direction as the perturbation; blues indicate a response in the opposite direction, and white indicates no response. The diagonal line in the heat map corresponds to a response measured at the same time the perturbation is applied. The black arrows in the heat maps indicate the response time in the experiment when the peak significant t -value occurs.

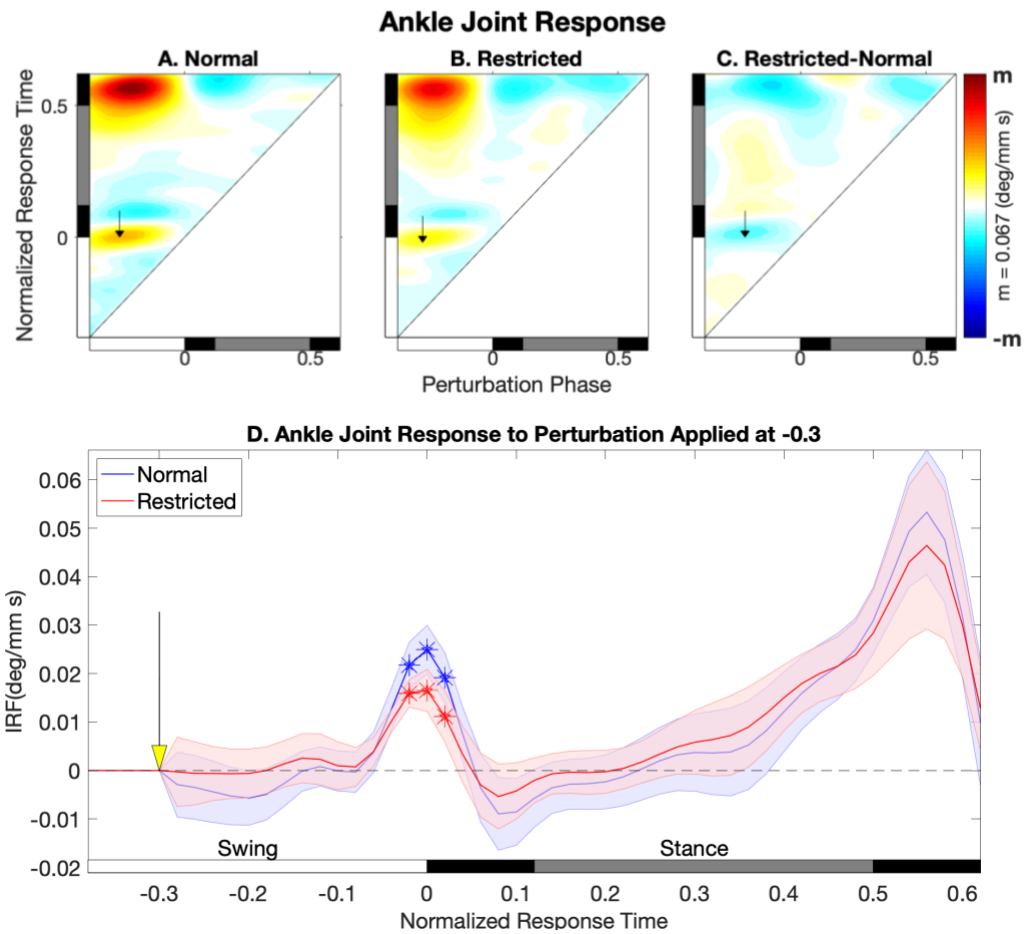


Figure 3-5) The ϕ IRF heat map describing the response of the ipsilateral ankle angle to the mechanical perturbation in the (A) normal condition, (B) restricted condition and (C) the difference between the two conditions. (D) takes a slice of the first two heat maps and shows the IRF for perturbations applied at phase -0.3 in normal (blue) and restricted (red) conditions. The arrows in the heat maps and asterisks in the slice IRF indicate the time where significant differences between conditions took place ($p < 0.05$). The yellow arrows indicate the perturbation phase (-0.3). The black arrows in the heat maps indicate the response time in the experiment when the peak significant t -value occurs.

3.3.3 Muscular Responses:

In this study we were mostly interested in the neural control of the restricted gait compared to normal gait and the changes in the muscle excitations in response to the perturbations. We found an indication of one muscular strategy that differed between the two conditions; that is the early-stance responses of the anterior muscles. Like the normal walking condition, in the restricted walking we observed increases in the excitation of the anterior muscles TA and Vlat at early stance. Even though the strategies differed from person to person, our results show that, on average, the TA muscle showed a significantly smaller increase in its early stance excitation in the restricted condition (indicated by the asterisks in **Figure 3-6**)

TA Early stance Strategy: The ϕ IRF heat map describing the response of the TA muscle to the mechanical perturbation in the (A) normal condition, (B) restricted condition and (C) the difference between the two conditions. (D) takes a slice of the first two heat maps and shows the IRF for perturbations applied at phase -0.2 in normal (blue) and restricted (red) conditions. The arrows in the heat maps and asterisks in the slice IRF indicate the time where significant differences between conditions took place ($p < 0.05$). The yellow arrows indicate the perturbation phase (-0.2). The black arrows in the heat maps indicate the response time in the experiment when the peak significant t -value occurs. (D). On the other hand, Vlat showed a significantly greater increase in its early stance excitation in the restricted condition comparing to the normal gait (indicated by the asterisks in **Figure 3-7**)

VAS Early stance Strategy: The ϕ IRF heat map describing the response of the VAS muscle to the mechanical perturbation in the (A) normal

condition, **(B)** restricted condition and **(C)** the difference between the two conditions. **(D)** takes a slice of the first two heat maps and shows the IRF for perturbations applied at phase -0.3 in normal (**blue**) and restricted (**red**) conditions. The arrows in the heat maps and asterisks in the slice IRF indicate the time where significant differences between conditions took place ($p < 0.05$). The yellow arrows indicate the perturbation phase (-0.3). The black arrows in the heat maps indicate the response time in the experiment when the peak significant t -value occurs.**(D)**. It is hypothesized that the modulation of anterior muscles including VAS and TA during early stance is a mechanism used to accelerate the pelvis relative to the foot to compensate for errors in foot placement. Since the TA contribution to this early stance strategy is compromised, modulation of the Vlat compensates for the foot placement errors.

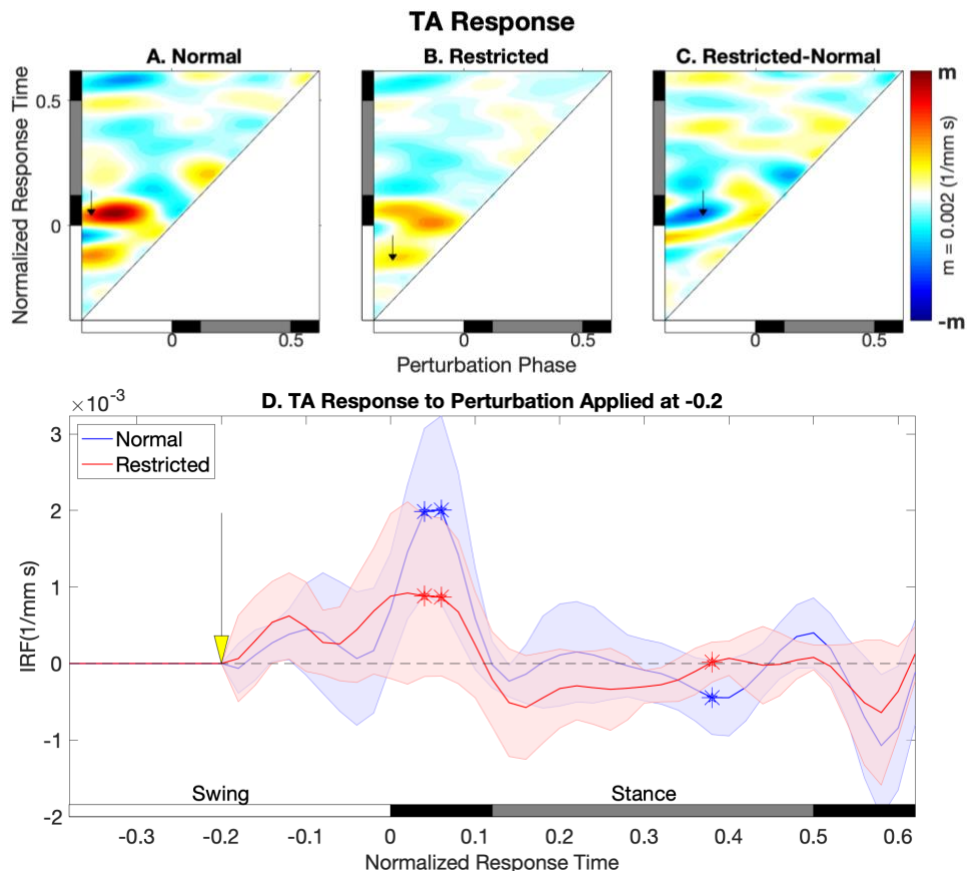


Figure 3-6) TA Early stance Strategy: The ϕ IRF heat map describing the response of the TA muscle to the mechanical perturbation in the (A) normal condition, (B) restricted condition and (C) the difference between the two conditions. (D) takes a slice of the first two heat maps and shows the IRF for perturbations applied at phase -0.2 in normal (blue) and restricted (red) conditions. The arrows in the heat maps and asterisks in the slice IRF indicate the time where significant differences between conditions took place ($p < 0.05$). The yellow arrows indicate the perturbation phase (-0.2). The black arrows in the heat maps indicate the response time in the experiment when the peak significant t -value occurs.

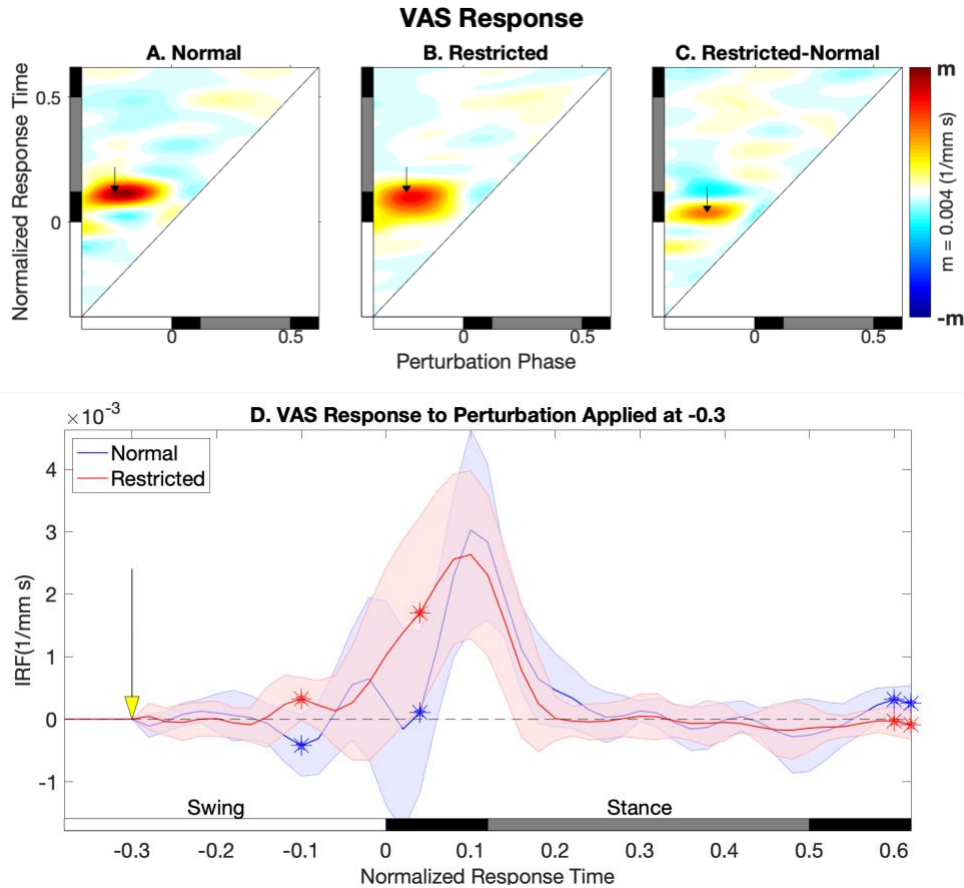


Figure 3-7) VAS Early stance Strategy: The ϕ IRF heat map describing the response of the VAS muscle to the mechanical perturbation in the (A) normal condition, (B) restricted condition and (C) the difference between the two conditions. (D) takes a slice of the first two heat maps and shows the IRF for perturbations applied at phase -0.3 in normal (blue) and restricted (red) conditions. The arrows in the heat maps and asterisks in the slice IRF indicate the time where significant differences between conditions took place ($p < 0.05$). The yellow arrows indicate the perturbation phase (-0.3). The black arrows in the heat maps indicate the response time in the experiment when the peak significant t -value occurs.

3.4 Discussion

In this study we wanted to investigate the role of early stance TA modulation in correcting for errors in foot placement by regulating forward body propulsion. To this end, we used an Achilles tendon taping method to restrict ankle dorsiflexion and therefore limit the contribution of the primary dorsiflexor muscle (TA) to gait. As

planned, we found that when the ankle was taped, the increased resistance to dorsiflexion reduced the ankle range of motion (Error! Reference source not found..A). Our hypothesis was that when TA's ability to contribute to forward body propulsion is diminished, due to limited dorsiflexion, the nervous system would compensate by using other speed control strategies. The observed increase in the VAS muscle excitation at early stance supports this hypothesis.

3.4.1 Walking with Limited Dorsiflexion

Generally, our kinematic results resembled those from the literature. Similar to previous findings (e.g. Ota et al., 2014), we observed that the dorsiflexion restriction resulted in greater knee extension angles during single support phases (**Figure 3-2**). Average waveforms of kinematics: the ankle joint (**A**), knee joint (**B**), Hip joint (**C**) and trunk segment (**D**) angles in the normal (**blue**) and restricted (**red**) conditions. The shaded areas indicate 95% confidence intervals. Asterisks indicate significant differences ($p < 0.05$). The bars on the horizontal axes indicate gait phase: (white = swing, gray = single support, and back = double support). The ankle plantarflexion, knee flexion and hip extension are in the positive direction.**B**). The combination of these changes in ankle and knee angles produced a significantly shorter step lengths in the restricted condition, which is also consistent with the dorsiflexion restriction literature when walking on a treadmill (Cho et al., 2015). It has been established that reduced dorsiflexion takes the greatest toll on leg progression (Perry and Davids, 1992). Taking shorter steps and spending more time in double support is a characteristic of slow human walks in general (Karas and Hoy, 2002; Wu et al., 2019). In this study,

where the subjects walked on a treadmill with a roughly constant speed, we expected the step frequency to be greater in the restricted condition, given that the step length was shorter. Our expectations were met for both the step and stride frequencies. However, this was not the case for the ratios of the SS to DS durations. Even though the single support duration tended to be shorter in the restricted condition, this value was not found to be significantly different between the two walking conditions.

Taping the ankle affected the plant through changing the body mechanics (**Figure 3-2**) Average waveforms of kinematics: the ankle joint (**A**), knee joint (**B**), Hip joint (**C**) and trunk segment (**D**) angles in the normal (**blue**) and restricted (**red**) conditions. The shaded areas indicate 95% confidence intervals. Asterisks indicate significant differences ($p < 0.05$). The bars on the horizontal axes indicate gait phase: (white = swing, gray = single support, and black = double support). The ankle plantarflexion, knee flexion and hip extension are in the positive direction.). More importantly, we saw that the restriction indirectly affected the neural feedback, as supported by the observed changes in average muscle excitation waveforms that ensure adaptability of gait to the new walking condition (**Figure 3-3**) Average waveforms of Muscle excitations: for TA (**A**), Vlat (**B**) and Vmed (**C**) muscles in the normal (**blue**) and restricted (**red**) conditions. The shaded areas indicate 95% confidence intervals. Asterisks indicate significant differences ($p < 0.05$).). The TA excitation during early stance was significantly reduced in the taped gait condition, which is consistent with the literature on restricting dorsiflexion with AFOs (Geboers et al., 2002). By increasing the resistance to dorsiflexion, the subjects adopted a gait strategy that required less TA

excitation during early stance. This strategy resulted in a gait with shorter steps, which as discussed earlier is a characteristic of gaits with limited dorsiflexion (Perry and Davids, 1992). At the same time, we also observed a significant decrease in the early stance VAS excitation (**Figure 3-3**) Average waveforms of Muscle excitations: for TA (**A**), Vlat (**B**) and Vmed (**C**) muscles in the normal (**blue**) and restricted (**red**) conditions. The shaded areas indicate 95% confidence intervals. Asterisks indicate significant differences ($p < 0.05$). **B&C**). We argue that the VAS muscle group works with the other leg anterior muscles at early stance to propel the body forward. The reduction in the early stance excitation of the anterior muscles is consistent with the decrease in the step length.

3.4.2 Response to Perturbations with Limited Dorsiflexion

The other goal of this study was to further understand neural control strategies implemented by the nervous system to stabilize walking with limited dorsiflexion. We observed distinct differences in two muscular responses that were significantly different across normal and restricted gaits. Both muscular responses belonged to the non-counteractive early stance strategy that was hypothesized to compensate for errors in foot placement.

The mechanical perturbation, applied during swing, displaces the swing leg forward (**Figure 3-4**) The ϕ IRF heat map describing the response of the ipsilateral ankle AP position to the mechanical perturbation in the (**A**) normal condition, (**B**) restricted condition and (**C**) the difference between the two conditions. The ϕ IRF heat maps have

two independent variables: perturbation phase on the horizontal axis and normalized response time on the vertical axis. Normalized response time indicates the phase of the gait cycle at which a given response occurs. The single dependent variable of the ϕ IRF is the response to the perturbation, and it is indicated using a color map. Yellows and reds indicate a response in the same direction as the perturbation; blues indicate a response in the opposite direction, and white indicates no response. The diagonal line in the heat map corresponds to a response measured at the same time the perturbation is applied. The black arrows in the heat maps indicate the response time in the experiment when the peak significant t -value occurs.). The nervous system tries to compensate for this effect. We have argued previously that in normal gait, early stance modulation of anterior muscles, including TA and VAS, compensate for the leg being too far in front of the body by propelling the hip forward (Rafiee and Kiemel, 2020). The dorsiflexion restriction compromises the TA's ability to perform work. In the restricted gait, we observed a smaller increase in the TA modulation at early stance compared to the normal gait (**Figure 3-6**) TA Early stance Strategy: The ϕ IRF heat map describing the response of the TA muscle to the mechanical perturbation in the (A) normal condition, (B) restricted condition and (C) the difference between the two conditions. D) takes a slice of the first two heat maps and shows the IRF for perturbations applied at phase -0.2 in normal (blue) and restricted (red) conditions. The arrows in the heat maps and asterisks in the slice IRF indicate the time where significant differences between conditions took place ($p < 0.05$). The yellow arrows indicate the perturbation phase (-0.2). The black arrows in the heat maps indicate the response time

in the experiment when the peak significant t -value occurs.). This change in the dorsiflexor muscle excitation could also explain the smaller dorsiflexion response at early stance (**Figure 3-5**) The ϕ IRF heat map describing the response of the ipsilateral ankle angle to the mechanical perturbation in the (A) normal condition, (B) restricted condition and (C) the difference between the two conditions. D) takes a slice of the first two heat maps and shows the IRF for perturbations applied at phase -0.3 in normal (blue) and restricted (red) conditions. The arrows in the heat maps and asterisks in the slice IRF indicate the time where significant differences between conditions took place ($p < 0.05$). The yellow arrows indicate the perturbation phase (-0.3). The black arrows in the heat maps indicate the response time in the experiment when the peak significant t -value occurs.). With the diminished contribution of TA to speed control, the nervous system increases the excitation of another anterior muscle group, namely VAS modulation at early stance (**Figure 3-7**) VAS Early stance Strategy: The ϕ IRF heat map describing the response of the VAS muscle to the mechanical perturbation in the (A) normal condition, (B) restricted condition and (C) the difference between the two conditions. D) takes a slice of the first two heat maps and shows the IRF for perturbations applied at phase -0.3 in normal (blue) and restricted (red) conditions. The arrows in the heat maps and asterisks in the slice IRF indicate the time where significant differences between conditions took place ($p < 0.05$). The yellow arrows indicate the perturbation phase (-0.3). The black arrows in the heat maps indicate the response time in the experiment when the peak significant t -value occurs.). This strategy would accelerate the COM forward and compensates for the errors in foot placement.

In conclusion, our results support our hypothesis that the TA modulation at early stance plays an important role in forward body propulsion and speed control. Since we found that when TA's ability to perform work was diminished, to compensate for the errors in foot placement, the nervous system had to use other speed control strategies, namely early stance modulation of VAS.

Chapter 4 : Counteractive Strategies in a Non-counteractive Model

In this chapter we used computer simulation of human walking to test the previous counteractive/non-counteractive classification of the muscular responses. We examined the response of a well-known counteractive model of human walking (Geyer and Herr, 2010) to external mechanical perturbations and compared the results to human responses (Rafiee and Kiemel, 2020). The results suggest that our previous classifications were correct in most cases.

4.1 Introduction

Neuromechanical simulation of human walking is a useful approach in investigating the role of sensory information in gait stabilizing strategies. Using experiments to infer how these stabilizing strategies are implemented at the neural level (i.e., neural control mechanisms) is difficult due to the complexity of the locomotor neural networks. In such cases, computer models of human gait and sensorimotor control can help test different neural controllers and give insight into the neural mechanisms that contribute to the control of human walking (e.g., Jo, 2007; Song and Geyer, 2017)

A source of complexity in using computer models to investigate the neural control mechanisms of human gait is that different controllers can produce similar realistic limit cycles (Kuo, 2002). Validity of a possible controller therefore cannot be gauged well by only examining the limit cycle. However, different controllers would be expected to show qualitatively different muscular responses to perturbations, with the

responses of some models being more similar to human responses than others. Therefore, examining model responses to external perturbations is necessary to assess the plausibility of neuromechanical control.

Both Counteractive and non-counteractive models have been proposed in the gait modelling literature. Some models solely rely on counteractive mechanisms (e.g., Günther and Ruder, 2003; Geyer and Herr, 2010; Song and Geyer, 2015), while others use both counteractive and non-counteractive mechanisms (Aoi et al., 2010; Dzeladini et al., 2014; Jo and Massaquoi, 2007; Ogihara and Yamazaki, 2001; Taga, 1995).

A small number of studies in the literature have evaluated neuromechanical models by comparing their responses to external perturbations with those of humans. These models were successful in producing *some* of the counteractive (Jo, 2007; Murai and Yamane, 2011; Song and Geyer, 2017) and non-counteractive (Jo, 2007; Taga, 1998) human responses to large perturbations. However, to our knowledge, the responses of models to small perturbation have not been investigated, even though experimental studies has shown that small and large perturbations might evoke different responses (e.g., Maki and McIlroy, 1997). In particular, the neural mechanisms responsible for producing non-counteractive responses to small perturbations largely remain debated.

In a previous study (Rafiee and Kiemel 2020), we classified responses of human walking to small mechanical perturbations that result in forward displacement of the swing leg as counteractive and non-counteractive based on the latency of the responses and whether we could hypothesize a reflex mechanism to produce them or not. In

addition to the known foot-placement strategies that counteract kinematic displacement, we found phase-specific muscle modulations that compensated for the leg being pushed forward by helping 1) propel the pelvis forward and 2) control speed of the contralateral leg in the next cycle. Perturbations applied at different phases of gait cycle did not produce fixed response latencies for these compensatory behavior (as a simple reflex mechanism would predict), and the timing of the responses suggested involvement of phase-specific mechanisms (Rafiee and Kiemel, 2020). In addition, a subset of these compensatory responses was found to be a general control mechanism shared between the response to mechanical and visual perturbations. Therefore, we proposed that the observed compensatory responses should be categorized as non-counteractive (Rafiee and Kiemel, 2020).

The goal of our study is to validate the previous counteractive / non-counteractive classification of the muscular responses. If our classification was correct, we expect that a model with only counteractive mechanisms to reproduce human responses that we have classified as counteractive but not those we have classified as non-counteractive. Here, to test this prediction, we perturbed an existing model of human locomotion that is dominantly controlled through counteractive mechanisms. We chose to study the Geyer and Herr (2010) model since it is a well established model of locomotion inspired by several physiological studies on the counteractive control strategies. However, this model does not rely on any non-counteractive mechanism proposed to be important for producing compensatory responses (Rafiee and Kiemel, 2020).

4.2 Methods

4.2.1 Overview:

In a previous study with experiments on human subjects, we used springs to apply small mechanical perturbations to the ankle in the form of force impulses during walking, and inferred the neural control using impulse response functions (Rafiee and Kiemel, 2020). Here we repeated this experiment virtually by applying the same perturbations to a computer model that includes only counteractive mechanisms (Geyer and Herr, 2010) to determine whether our previous classifications of the responses to counteractive and non-counteractive were accurate.

4.2.2 Computer Model

In the current simulation study, we directly applied impulses of force to perturb the Geyer and Herr (2010) model. The Geyer and Herr (2010) model is popular a 2D sagittal-plane computer model of human walking with nine mechanical degrees of freedom, developed in MATLAB SimMechanics (**Figure 4-1**) Musculoskeletal model used to study human locomotion (Geyer & Herr, 2010). This model has 9 degrees of freedom: 3-DoF planar joint between the pelvis and the ground, and each leg has hip, knee and ankle flexion/extension. The model is actuated by 7 muscles per leg: gluteus maximus (GLU), hamstrings (HAMS), hip flexor (HFL), Vasti (VAS), gastrocnemius medialis (GAS), soleus (SOL), and tibialis anterior (TA).). The model consists of a HAT segment (a lumped head, arms, and torso) and two legs. Each leg consists of three pin joints (hip, knee, ankle) actuated by seven Hill-type muscles. The muscles receive excitation control signals and response by developing forces per their activation and contractile dynamics, producing moments at the joints that actuate the

model. The muscle excitations are controlled through gated fixed-latency reflex mechanisms, where the involved reflex mechanisms change based on whether the foot of a given leg is in contact with the ground (i.e., stance vs swing). The model has 4 groups of reflexes using feedback information about muscle force, muscle length, joint angle, and ground contact forces. In the current study, we adapted the (Geyer and Herr, 2010) model in the MATLAB SimMechanics environment by applying simultaneous equal impulses of force to the ankles in the anterior direction to mimic the experimental setup.

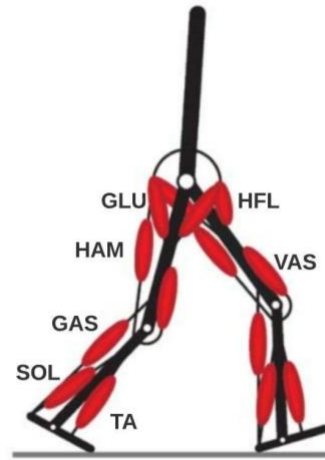


Figure 4-1) Musculoskeletal model used to study human locomotion (Geyer & Herr, 2010). This model has 9 degrees of freedom: 3-DoF planar joint between the pelvis and the ground, and each leg has hip, knee and ankle flexion/extension. The model is actuated by 7 muscles per leg: gluteus maximus (GLU), hamstrings (HAMS), hip flexor (HFL), Vasti (VAS), gastrocnemius medialis (GAS), soleus (SOL), and tibialis anterior (TA).

4.2.3 Simulations

We simulated a total of 101 runs (1 unperturbed walking and 100 perturbed walking) using a Simulink ode15s solver, with maximum timestep size of 10^{-1} s and relative and absolute error tolerance of 10^{-9} and 10^{-10} , respectively. Small error tolerances were necessary to ensure that the perturbation responses were not critically confounded numerical errors. All the simulations began from the same initial states, when the AP speed was 1.3 m/s, the hip, knee and ankle angles were 140° , 175° , 90° for the right leg and 175° , 175° , 85° for the left leg. In the perturbed walking simulations, before

applying the mechanical perturbations, we let the model run for at least 15 s to get close to its limit cycle. In each perturbed walking simulations, an identical mechanical perturbation was applied at one of 100 different phases uniformly distributed throughout the gait cycle. The mechanical perturbation was an impulse of force approximated by a scaled Gaussian function of time: $F(t) = \frac{A}{\sigma\sqrt{2\pi}} e^{-\frac{(t-t_0)^2}{2\sigma^2}}$, where $\sigma = 0.005$ s is the standard deviation, t_0 is the perturbation time, and $A = 0.1$ Ns is the integral of $F(t)$. With these parameters, the maximum of $F(t)$ was $\frac{A}{\sigma\sqrt{2\pi}} = 7.98$ N. Each leg was exposed to half of this impulse force to mimic the experimental string-pulley perturbation system. The simulation continued at least 5 cycles after the perturbation was applied

4.2.4 Data Analysis & Response Comparison,

We analyzed muscle excitations, spatiotemporal variables including step length and step duration and kinematic variables including hip, knee, and ankle flexion angles and the position of the foot relative to the pelvis in the AP direction. To compare the human and model muscular behavior, we used electromyography (EMG) signals from the experimental study as a proxy for muscle excitations. For both human data and the model, we normalized the muscle excitation value by dividing by the root mean square (RMS) of the mean waveform of unperturbed cycles for each muscle.

To compare the average kinematic and muscle excitation waveforms between model and human, we first expressed all the variables as a function of normalized time, which is time divided by the unperturbed period T . A new time step was then defined as $T/100$.

We used linear interpolation to fit the kinematic variables and muscle excitations in all simulations (perturbed and unperturbed) to this 100-point phase cycle. The human data were also fitted to a 100-point phase cycle. To compare the average behavior of models with human, for each variable we calculated the root mean square of the variable's Z-

score:
$$RMS_Z = \sqrt{\frac{1}{n} \sum_{\vartheta=0}^{n-1} \left(\frac{x_{\text{exp}}(\vartheta) - x_{\text{sim}}(\vartheta)}{std_{\text{exp}}(\vartheta)} \right)^2}$$
, where $x_{\text{sim}}(\vartheta)$ is the simulated value at

phase (ϑ); $x_{\text{exp}}(\vartheta)$ is the mean experimental value; $std_{\text{exp}}(\vartheta)$ is the experimental between-subject standard deviation, and $n=100$ is the number of points in the phase cycle.

Finally, to obtain the ϕ IRFs for all variables, for each perturbation phase, the unperturbed signals were subtracted from the perturbed ones, and the difference signals were then divided by the integral of the impulse force (A). In the experimental ϕ IRFs, the mechanical perturbation was the displacement of the motor rather than the applied forces. To approximate the responses to a force perturbation, we divided the experimental ϕ IRFs by the stiffness of the spring in the experiment (Rafiee and Kiemel, 2020). In the result section we compare the “direct ϕ IRFs” from this simulation study to the “inferred ϕ IRFs” from experiment (Rafiee and Kiemel, 2020) in terms of the amplitude, direction and timing of the responses between model and human data.

4.3 Results

In the unperturbed condition, the model walked with the average speed of 1.37 m/s over ground, which was close to the experimental average speed of 1.39 m/s on

treadmill. The average muscular and kinematic waveforms were also relatively similar to those of human walking (**Figure 4-2**) Comparison between model (in black) and human mean waveforms (in blue) of **A.** the kinematics variables and **B.** muscle excitations during unperturbed cycles. The experimental data includes 95% confidence intervals. **For** each joint angle the average value is subtracted from the signal. The Gray and white bars on the horizontal axes correspond to single support phase (white for swing and gray for stance) for the reference leg. The black bars indicate double support.), with average kinematic and muscular $RMS_z = 3.15$. However, some differences to the human walking patterns were found in the model's trunk angle (trunk $RMS_z = 6.95$), hamstring muscle excitation (HAM $RMS_z = 6.04$ SD), and hip flexor muscle excitation (HFL $RMS_z = 4.80$ SD). In addition, the double support duration relative to the stride duration was smaller in the model (0.09) compared to humans (0.13).

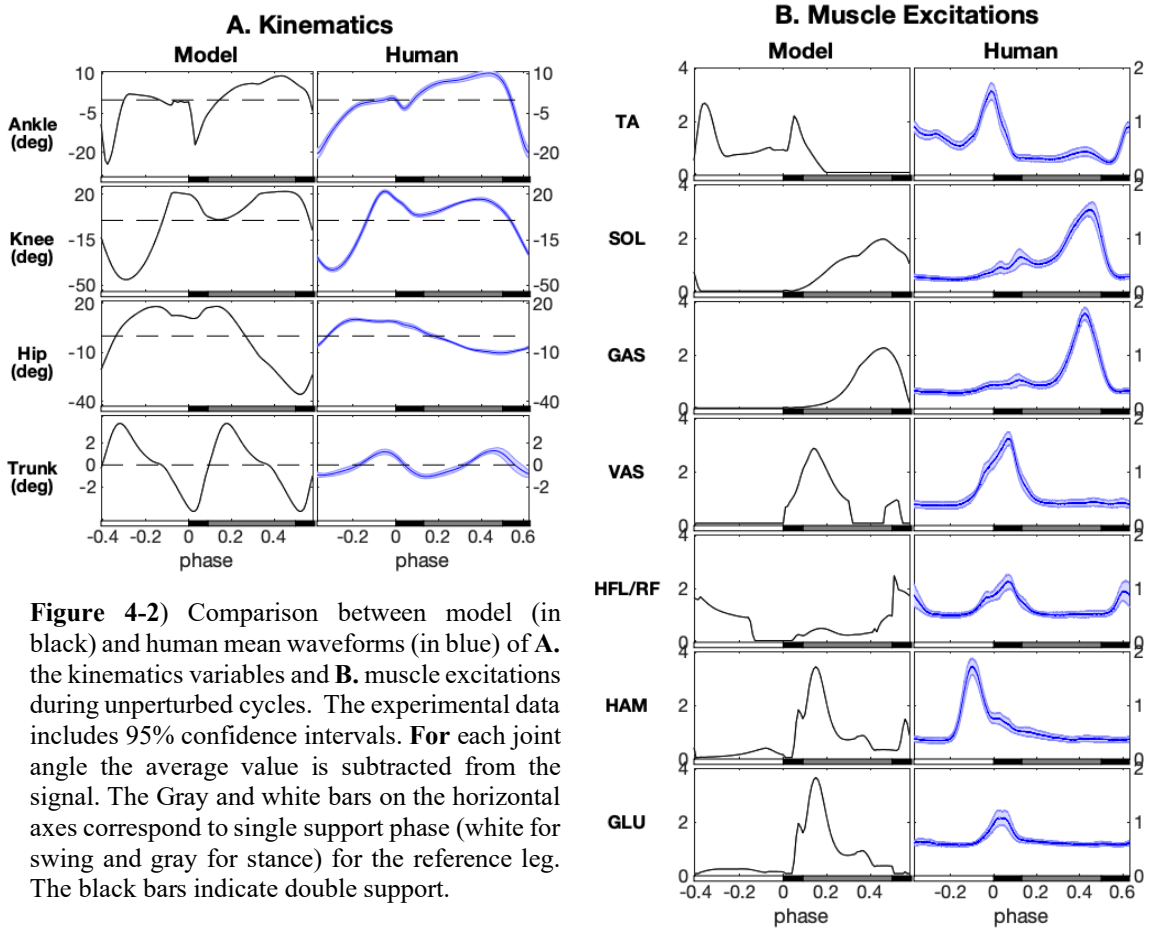


Figure 4-2) Comparison between model (in black) and human mean waveforms (in blue) of **A.** the kinematics variables and **B.** muscle excitations during unperturbed cycles. The experimental data includes 95% confidence intervals. **For** each joint angle the average value is subtracted from the signal. The Gray and white bars on the horizontal axes correspond to single support phase (white for swing and gray for stance) for the reference leg. The black bars indicate double support.

4.3.1 Kinematic Responses:

The initial kinematic responses across the model and human were relatively similar. As an example, **Figure 4-3)** Comparing the Ankle AP position response to the mechanical perturbations in the model and human. A. demonstrates the ϕ IRF responses in heat maps that have two independent variables: perturbation phase on the horizontal axis and normalized response time on the vertical axis. The color coding of the heat maps from cold to hot indicates the value of the ϕ IRFs (white for 0, yellow and red for positive, and blue for negative). The value m , specified above each heatmap, is the

maximum absolute response value which we used to define the color map (see color bar). The diagonal line in the heat map corresponds to a response measured at the same time the perturbation is applied. By definition, the ϕ IRF is 0 (white) below this line. The black arrow indicates the response time in the experiment when the peak significant t -values occurs. **B.** takes a vertical slice of the ankle AP response heat maps and depicts the ϕ IRF for the perturbations applied at 3 specific phases during swing. Blue shaded areas depict experimental ϕ IRFs with 95% confidence interval, and solid black lines shows model's the direct ϕ IRFs. Yellow arrows indicate the time of perturbation. **A** illustrates the direct ϕ IRFs from the model and the inferred ϕ IRFs from human data in heatmaps for the ankle position relative to the pelvis in the anterior posterior (AP) direction. These heatmaps describe how a perturbation at any phase of the gait cycle, indicated on the horizontal axis, produces responses at times indicated on the vertical axis. In both cases, we observed initial positive responses to the forward force perturbations applied during swing (**Figure 4-3**) Comparing the Ankle AP position response to the mechanical perturbations in the model and human. **A.** demonstrates the ϕ IRF responses in heat maps that have two independent variables: perturbation phase on the horizontal axis and normalized response time on the vertical axis. The color coding of the heat maps from cold to hot indicates the value of the ϕ IRFs (white for 0, yellow and red for positive, and blue for negative). The value m , specified above each heatmap, is the maximum absolute response value which we used to define the color map (see color bar). The diagonal line in the heat map corresponds to a response measured at the same time the perturbation is applied. By definition, the

ϕ IRF is 0 (white) below this line. The black arrow indicates the response time in the experiment when the peak significant t -values occurs. B. takes a vertical slice of the ankle AP response heat maps and depicts the ϕ IRF for the perturbations applied at 3 specific phases during swing. Blue shaded areas depict experimental ϕ IRFs with 95% confidence interval, and solid black lines shows model's the direct ϕ IRFs. Yellow arrows indicate the time of perturbation. A). Notice that in both cases the positive results start immediately with zero latency and are approximately parallel to the black diagonal line of stimulus onset. In other words, in both cases, the positive force perturbations (forward push) applied during swing, resulted in instantaneous forward displacement of the ankle relative to the pelvis in the AP direction. These results show that the model was able to reproduce the expected initial passive kinematic responses.

To better illustrate the zero-latency nature of these responses, **Figure 4-3**) Comparing the Ankle AP position response to the mechanical perturbations in the model and human. A. demonstrates the ϕ IRF responses in heat maps that have two independent variables: perturbation phase on the horizontal axis and normalized response time on the vertical axis. The color coding of the heat maps from cold to hot indicates the value of the ϕ IRFs (white for 0, yellow and red for positive, and blue for negative). The value m , specified above each heatmap, is the maximum absolute response value which we used to define the color map (see color bar). The diagonal line in the heat map corresponds to a response measured at the same time the perturbation is applied. By definition, the ϕ IRF is 0 (white) below this line. The black arrow indicates the response time in the experiment when the peak significant t -values occurs. B. takes a vertical

slice of the ankle AP response heat maps and depicts the ϕ IRF for the perturbations applied at 3 specific phases during swing. Blue shaded areas depict experimental ϕ IRFs with 95% confidence interval, and solid black lines shows model's the direct ϕ IRFs. Yellow arrows indicate the time of perturbation. **B** takes vertical slices of the heat maps and depicts single impulse responses for perturbations applied at early-swing (phase = -0.3), mid-swing (phase = -0.2) and late-swing (phase = -0.1). It is evident from **Figure 4-3**) Comparing the Ankle AP position response to the mechanical perturbations in the model and human. A. demonstrates the ϕ IRF responses in heat maps that have two independent variables: perturbation phase on the horizontal axis and normalized response time on the vertical axis. The color coding of the heat maps from cold to hot indicates the value of the ϕ IRFs (white for 0, yellow and red for positive, and blue for negative). The value m , specified above each heatmap, is the maximum absolute response value which we used to define the color map (see color bar). The diagonal line in the heat map corresponds to a response measured at the same time the perturbation is applied. By definition, the ϕ IRF is 0 (white) below this line. The black arrow indicates the response time in the experiment when the peak significant t -values occurs. B. takes a vertical slice of the ankle AP response heat maps and depicts the ϕ IRF for the perturbations applied at 3 specific phases during swing. Blue shaded areas depict experimental ϕ IRFs with 95% confidence interval, and solid black lines shows model's the direct ϕ IRFs. Yellow arrows indicate the time of perturbation. **B** that the initial behavior, in terms of the timing, direction and the slope of the responses were similar between model and human at times before heel strike. In both cases, these initial

positive responses were then followed by successive negative and positive values, which are partially due to the effect of the perturbations shifting the time of heel strike (see the Spatiotemporal section below).

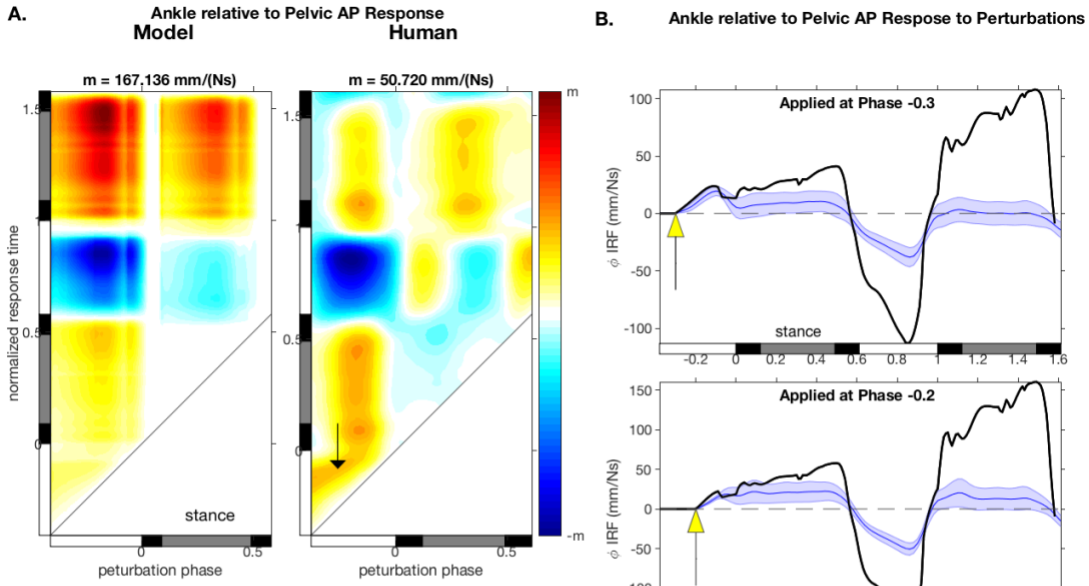


Figure 4-3) Comparing the Ankle AP position response to the mechanical perturbations in the model and human. A. demonstrates the ϕ IRF responses in heat maps that have two independent variables: perturbation phase on the horizontal axis and normalized response time on the vertical axis. The color coding of the heat maps from cold to hot indicates the value of the ϕ IRFs (white for 0, yellow and red for positive, and blue for negative). The value m , specified above each heatmap, is the maximum absolute response value which we used to define the color map (see color bar). The diagonal line in the heat map corresponds to a response measured at the same time the perturbation is applied. By definition, the ϕ IRF is 0 (white) below this line. The black arrow indicates the response time in the experiment when the peak significant t -values occurs. B. takes a vertical slice of the ankle AP response heat maps and depicts the ϕ IRF for the perturbations applied at 3 specific phases during swing. Blue shaded areas depict experimental ϕ IRFs with 95% confidence interval, and solid black lines shows model's the direct ϕ IRFs. Yellow arrows indicate the time of perturbation.

4.3.2 Spatiotemporal Responses

Figure 4-4) Comparing step length and duration responses to the mechanical perturbations in the model and human. As you go from right to left, the time delay between perturbation and response is increasing. The gray bars on the horizontal axis indicate values corresponding to single stance for the reference leg; the white bars indicate values corresponding to swing, and the black bars correspond to double support. illustrates the value of the spatiotemporal variables ϕ IRFs from the model and human data at mid-step for perturbations applied at different phases during previous steps. The response of the model and human were relatively similar during the cycle where the perturbations were applied. In both model and human, the forward push of the ankles increased the step length (**Figure 4-4)** Comparing step length and duration responses to the mechanical perturbations in the model and human. As you go from right to left, the time delay between perturbation and response is increasing. The gray bars on the horizontal axis indicate values corresponding to single stance for the reference leg; the white bars indicate values corresponding to swing, and the black bars correspond to double support.**A)** and duration (**Figure 4-4)** Comparing step length and duration responses to the mechanical perturbations in the model and human. As you go from right to left, the time delay between perturbation and response is increasing. The gray bars on the horizontal axis indicate values corresponding to single stance for the reference leg; the white bars indicate values corresponding to swing, and the black bars correspond to double support.**B)**. It is worth mentioning that for all variables the

magnitudes of the same step responses were greater in the model compared to human participants.

However, the response of the model and human diverged in the following steps. In the experimental data, we observed that in response to the forward push of the ankles, the length of the first step after perturbation decreased (**Figure 4-4**) Comparing step length and duration responses to the mechanical perturbations in the model and human. As you go from right to left, the time delay between perturbation and response is increasing. The gray bars on the horizontal axis indicate values corresponding to single stance for the reference leg; the white bars indicate values corresponding to swing, and the black bars correspond to double support.**A**) whereas the duration of the first step after perturbation was not significantly affected (**Figure 4-4**) Comparing step length and duration responses to the mechanical perturbations in the model and human. As you go from right to left, the time delay between perturbation and response is increasing. The gray bars on the horizontal axis indicate values corresponding to single stance for the reference leg; the white bars indicate values corresponding to swing, and the black bars correspond to double support.**B**). These results could be interpreted as a mechanism implemented by the human participants to compensate for the previous increase in the step length. Such strategy was not implemented by the model. In the model, in response to the forward push of the ankle, the length of the next step after the perturbation increased (**Figure 4-4**) Comparing step length and duration responses to the mechanical perturbations in the model and human. As you go from right to left, the time delay between perturbation and response is increasing. The gray bars on the

horizontal axis indicate values corresponding to single stance for the reference leg; the white bars indicate values corresponding to swing, and the black bars correspond to double support. A) and so did the step duration (Figure 4-4) Comparing step length and duration responses to the mechanical perturbations in the model and human. As you go from right to left, the time delay between perturbation and response is increasing. The gray bars on the horizontal axis indicate values corresponding to single stance for the reference leg; the white bars indicate values corresponding to swing, and the black bars correspond to double support. B).

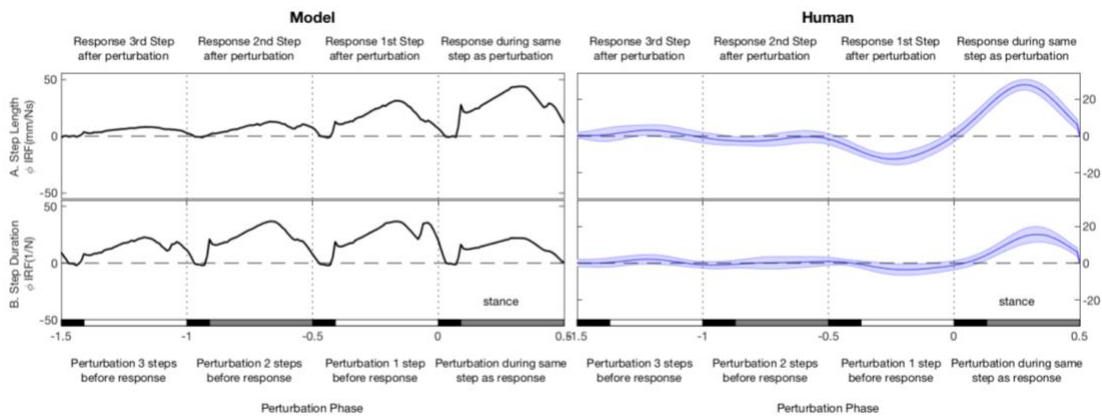


Figure 4-4) Comparing step length and duration responses to the mechanical perturbations in the model and human. As you go from right to left, the time delay between perturbation and response is increasing. The gray bars on the horizontal axis indicate values corresponding to single stance for the reference leg; the white bars indicate values corresponding to swing, and the black bars correspond to double support.

Figure 4-4) Comparing step length and duration responses to the mechanical perturbations in the model and human. As you go from right to left, the time delay between perturbation and response is increasing. The gray bars on the horizontal axis indicate values corresponding to single stance for the reference leg; the white bars indicate values corresponding to swing, and the black bars correspond to double

support. **B** also illustrates that in both model and human, the perturbations resulted in an increase in the same step duration that was not negated in the following cycles. The accumulated effect of these changes in the step duration was a phase delay imposed on both model and human participants. This phase delay was manifested as successive negative and positive values in the ϕ IRF graphs: as in the kinematic example above (**Figure 4-3**) Comparing the Ankle AP position response to the mechanical perturbations in the model and human. A. demonstrates the ϕ IRF responses in heat maps that have two independent variables: perturbation phase on the horizontal axis and normalized response time on the vertical axis. The color coding of the heat maps from cold to hot indicates the value of the ϕ IRFs (white for 0, yellow and red for positive, and blue for negative). The value m , specified above each heatmap, is the maximum absolute response value which we used to define the color map (see color bar). The diagonal line in the heat map corresponds to a response measured at the same time the perturbation is applied. By definition, the ϕ IRF is 0 (white) below this line. The black arrow indicates the response time in the experiment when the peak significant t -values occurs. B. takes a vertical slice of the ankle AP response heat maps and depicts the ϕ IRF for the perturbations applied at 3 specific phases during swing. Blue shaded areas depict experimental ϕ IRFs with 95% confidence interval, and solid black lines shows model's the direct ϕ IRFs. Yellow arrows indicate the time of perturbation.), and other kinematic and muscular responses.

The greatest difference between the response of the model and human, however, was how long the effect of the perturbation was sustained. Humans largely returned to their

baseline step length and duration within 2 steps (**Figure 4-4**) Comparing step length and duration responses to the mechanical perturbations in the model and human. As you go from right to left, the time delay between perturbation and response is increasing. The gray bars on the horizontal axis indicate values corresponding to single stance for the reference leg; the white bars indicate values corresponding to swing, and the black bars correspond to double support.). On the other hand, the model was not able to return to its baseline step duration in the first 3 step (**Figure 4-4**) Comparing step length and duration responses to the mechanical perturbations in the model and human. As you go from right to left, the time delay between perturbation and response is increasing. The gray bars on the horizontal axis indicate values corresponding to single stance for the reference leg; the white bars indicate values corresponding to swing, and the black bars correspond to double support.); the step duration errors lasted roughly for 10 steps (not shown here). In the rest of this paper, we seek to understand why the model was not as successful as human participants in rapidly converging back to the baseline waveforms.

4.3.3 Muscular Responses

To understand the underlying neural control mechanisms of human walking and why the model was not able to correct for the perturbations rapidly, we compared muscular responses between model and human. Previously, we have hypothesized that the humans use three different strategies to rapidly correct for the errors in foot-placement (Rafiee and Kiemel, 2020). Here, we compare if these strategies could be implemented in this model.

4.3.3.1 Swing counteractive strategy:

The first step to rapidly correct for the effect of perturbation, which is forward displacement of the foot (**Figure 4-3**) Comparing the Ankle AP position response to the mechanical perturbations in the model and human. A. demonstrates the ϕ IRF responses in heat maps that have two independent variables: perturbation phase on the horizontal axis and normalized response time on the vertical axis. The color coding of the heat maps from cold to hot indicates the value of the ϕ IRFs (white for 0, yellow and red for positive, and blue for negative). The value m , specified above each heatmap, is the maximum absolute response value which we used to define the color map (see color bar). The diagonal line in the heat map corresponds to a response measured at the same time the perturbation is applied. By definition, the ϕ IRF is 0 (white) below this line. The black arrow indicates the response time in the experiment when the peak significant t -values occurs. B. takes a vertical slice of the ankle AP response heat maps and depicts the ϕ IRF for the perturbations applied at 3 specific phases during swing. Blue shaded areas depict experimental ϕ IRFs with 95% confidence interval, and solid black lines shows model's the direct ϕ IRFs. Yellow arrows indicate the time of perturbation.), is to slow down the progression of the swing leg. Previously we have hypothesized that humans use a counteractive strategy that takes advantage of swing-phase hamstring modulations to flex the knee and slow down the swing leg (Rafiee and Kiemel, 2020). We expected that the model would be able to reproduce this short-latency “counteractive” response.

In both the model and human, the hamstring (Ham) muscle group showed initial positive responses to perturbations applied during swing after short delays from the onset of the perturbations (**Figure 4-5**) Comparing ipsilateral **A.** hamstring and **B.** knee angle responses to the mechanical perturbations applied during swing, in the model and human. The black arrows in the human response column indicate the response time in the experiment when the peak significant *t*-value occurs.**A**). The magnitude of these initial responses was greater in the human semitendinosus muscle (SemiT) compared to model's Ham. The maximum initial impulse response magnitude for times before heel strike was found to be 0.03 1/Ns in the model and 0.21 1/Ns in humans. However, the direction and, importantly, the timing of these initial response peaks were found to be very similar (**Figure 4-5**) Comparing ipsilateral **A.** hamstring and **B.** knee angle responses to the mechanical perturbations applied during swing, in the model and human. The black arrows in the human response column indicate the response time in the experiment when the peak significant *t*-value occurs.**A**).

In both model and human, these initial positive responses could be explained by the contribution of the hamstring tendon reflex mechanism (Van de Crommert et al., 1996), which is implemented in the model through a force-feedback component. Comparing **Figure 4-5**) Comparing ipsilateral **A.** hamstring and **B.** knee angle responses to the mechanical perturbations applied during swing, in the model and human. The black arrows in the human response column indicate the response time in the experiment when the peak significant t -value occurs.**A** with **Figure 4-5**) Comparing ipsilateral **A.** hamstring and **B.** knee angle responses to the mechanical perturbations applied during swing, in the model and human. The black arrows in the human response column indicate the response time in the experiment when the peak significant t -value occurs.**B**, gives insight into this mechanism and the correlation between the hamstring muscle modulation and the knee joint angle. **Figure 4-5**) Comparing ipsilateral **A.** hamstring and **B.** knee angle responses to the mechanical perturbations applied during swing, in the model and human. The black arrows in the human response column indicate the response time in the experiment when the peak significant t -value occurs.**B**, illustrates that in both model and human, in response to the forward push of the

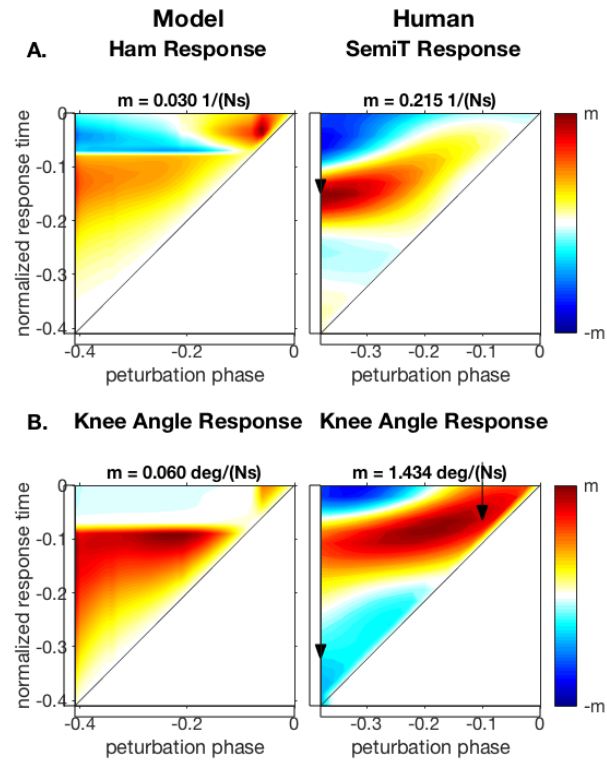


Figure 4-5) Comparing ipsilateral **A.** hamstring and **B.** knee angle responses to the mechanical perturbations applied during swing, in the model and human. The black arrows in the human response column indicate the response time in the experiment when the peak significant t -value occurs.

legs, the knee angle increases for response times after mid-swing. Knee extension response after mid-swing, lengthens the hamstring muscle. Based on the muscle force-length relationship, as the hamstring muscle length gets longer and closer to its optimal value, it becomes capable of producing more force. Since in the model the hamstring muscle group excitation is controlled through a fixed-latency force reflex mechanism, we observe that in response to the perturbations applied during swing that increase the hamstring muscle force, the hamstring muscle excitation also increases after short delays. This counteractive force-feedback mechanism eventually helps the model retreat the leg in response to the forward push applied during swing. This observation supports our hypothesis that humans could also be using this mechanism to slow down the swing leg progression.

4.3.3.2 Ipsilateral leg early-stance compensatory strategy:

Another strategy to rapidly correct for the effect of the perturbation is using compensatory strategies to prevent further error accumulation. As shown in **Figure 4-3**) Comparing the Ankle AP position response to the mechanical perturbations in the model and human. A. demonstrates the ϕ_{IRF} responses in heat maps that have two independent variables: perturbation phase on the horizontal axis and normalized response time on the vertical axis. The color coding of the heat maps from cold to hot indicates the value of the ϕ_{IRF} s (white for 0, yellow and red for positive, and blue for negative). The value m , specified above each heatmap, is the maximum absolute

response value which we used to define the color map (see color bar). The diagonal line in the heat map corresponds to a response measured at the same time the perturbation is applied. By definition, the ϕ IRF is 0 (white) below this line. The black arrow indicates the response time in the experiment when the peak significant t -values occurs. B. takes a vertical slice of the ankle AP response heat maps and depicts the ϕ IRF for the perturbations applied at 3 specific phases during swing. Blue shaded areas depict experimental ϕ IRFs with 95% confidence interval, and solid black lines shows model's the direct ϕ IRFs. Yellow arrows indicate the time of perturbation. . the mechanical perturbation pushes the leg forward relative to the pelvis, thus increasing the leg angle. Previously, we have hypothesized that the early-stance modulation of anterior muscles, including tibialis anterior (TA) and rectus femoris serves to compensate for the error in the leg angle relative to pelvis by producing a torque that propels the COM forward (Rafiee and Kiemel, 2020). However, due to the configuration of the joint angles, the modulation of these muscles before heel strike does not have the same effect. We expected that since the model does not possess any mechanism to produce such phase-specific non-counteractive strategy, the TA and HFL muscular responses would be different in the model comparing to humans.

Figure 4-6) Comparing ipsilateral TA response to the mechanical perturbations applied during swing, in the model and human. Since in the model, the magnitude of the initial response is much smaller, compared to the phase shift effect, in the heatmaps, the muscle responses were depicted only at time prior to ipsilateral leg heel strike. The black arrows in the human response column indicate the response time in the experiment when the peak significant t -value occurs. illustrates the TA response to the

mechanical perturbations in model and humans. In human participants, the TA excitation increased in early stance in response to forward push of the ankles during swing. The maximum value of these initial positive responses was 0.39 1/Ns. On the other hand, the model's initial response occurred during swing, after short delays from the onset of perturbation. The increase in TA excitation in the model was the result of a short-latency stretch reflex (i.e. length feedback) mechanism that served to counteract the ankle plantarflexion introduced by the perturbation. This initial positive response in the model had a maximum value of 0.04 1/Ns and was much smaller compared to the effect caused by the time shift (**Figure 4-6**) Comparing ipsilateral TA response to the mechanical perturbations applied during swing, in

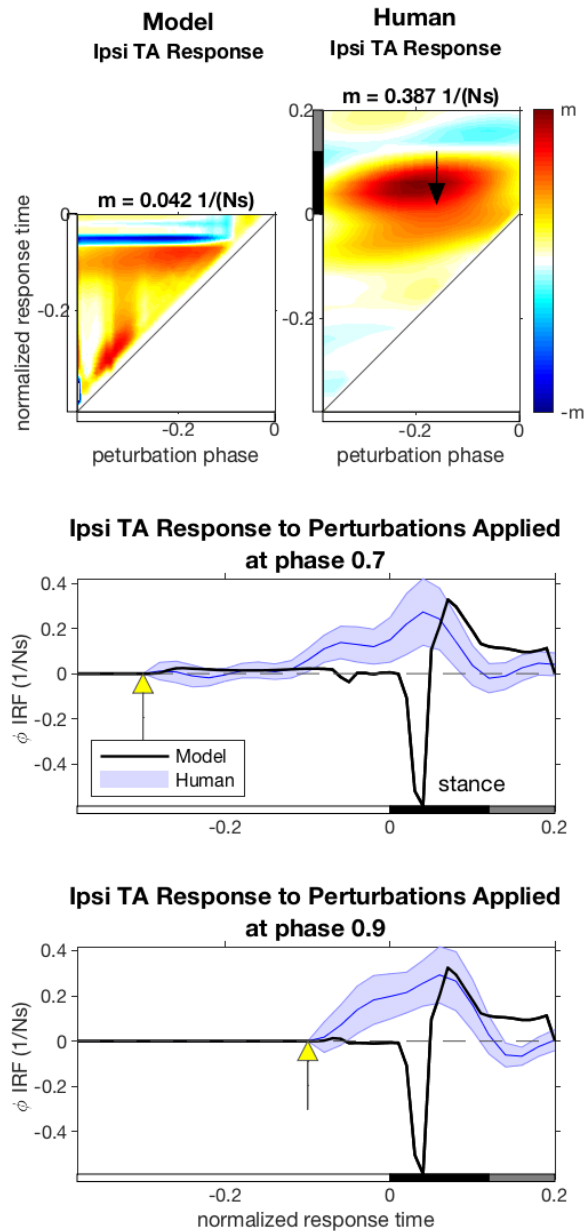


Figure 4-6) Comparing ipsilateral TA response to the mechanical perturbations applied during swing, in the model and human. Since in the model, the magnitude of the initial response in much smaller, compared to the phase shift effect, in the heatmaps, the muscle responses were depicted only at time prior to ipsilateral leg heel strike. The black arrows in the human response column indicate the response time in the experiment when the peak significant *t*-value occurs.

the model and human. Since in the model, the magnitude of the initial response is much smaller, compared to the phase shift effect, in the heatmaps, the muscle responses were depicted only at time prior to ipsilateral leg heel strike. The black arrows in the human response column indicate the response time in the experiment when the peak significant t -value occurs.). In other words, the model rather than compensating for the increase in leg angle relative to the pelvis, effectively responded to the perturbations by delaying the excitation of TA.

Figure 4-7) Comparing ipsilateral HFL/RF response to the mechanical perturbations applied during swing, in the model and human. The black arrows in the human response column indicate the response time in the experiment when the peak significant t -value occurs compares the rectus femoris (RF) muscle response in humans with the HFL response in the model. In this case, the muscular response was different in terms of both the direction of the response and its timing. The experimental data showed initial positive responses for RF at early stance (**Figure 4-7)** Comparing ipsilateral HFL/RF response to the mechanical perturbations applied during swing, in the model and human. The black arrows in the human response column indicate the response time in the experiment when the peak significant t -value occurs). On the other hand, the model demonstrated negative responses at mid swing (**Figure 4-7)** Comparing ipsilateral HFL/RF response to the mechanical perturbations applied during swing, in the model and human. The black arrows in the human response column indicate the response time in the

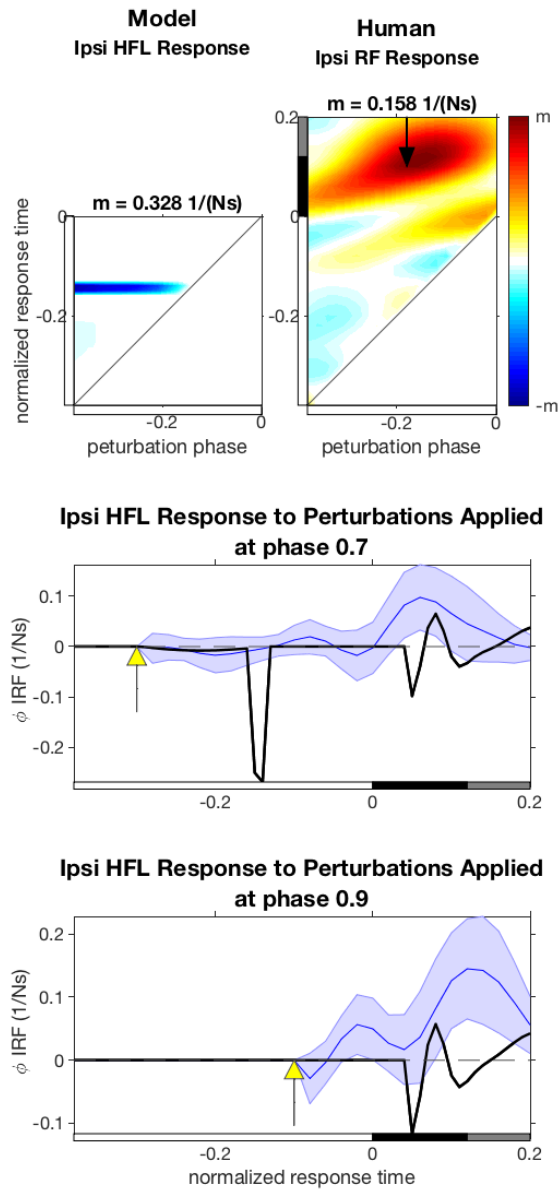


Figure 4-7) Comparing ipsilateral HFL/RF response to the mechanical perturbations applied during swing, in the model and human. The black arrows in the human response column indicate the response time in the experiment when the peak significant t -value occurs

experiment when the peak significant t -value occurs): at the phase -0.15, which corresponds to the toe-off time of the contralateral leg. This difference in response can be explained by the dependency of the HFL muscle in the model on the trunk lean at toe-off. Regardless of the source of this difference, the decrease in the HFL excitation in the model, further decreases the forward torque on COM and can be partially responsible for the slower recovery of the model.

4.3.3.3 Contralateral leg late-stance compensatory strategy:

Lastly, one additional strategy to rapidly converge back to the original gait patterns is to compensate for the initial effects of the perturbations in the following steps. Previously we have hypothesized that in response to the mechanical perturbations that increases the length of the step, humans use a compensatory strategy to reduce the length of the next step after perturbation by reducing the excitation of the contralateral leg GAS muscle (Rafiee and Kiemel, 2020). Since the studied model does not use any non-counteractive mechanism to control the GAS modulation, we did not expect its response to be similar to human response. In addition, we knew from the spatiotemporal data that the length of the next step after perturbation increases in the model (Figure 4-4) Comparing step length and duration responses to the mechanical perturbations in the

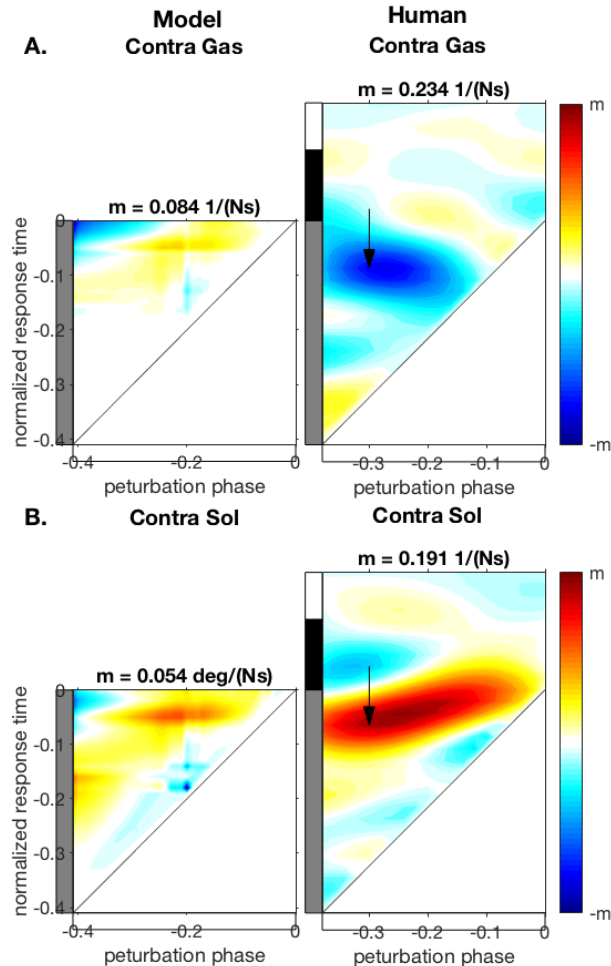


Figure 4-8) Comparing contralateral muscle responses to the mechanical perturbations applied during swing, in the model and human: A. Gas, B. Sol. The black arrows in the heat maps indicate the response time in the experiment when the peak significant *t*-values occur.

model and human. As you go from right to left, the time delay between perturbation and response is increasing. The gray bars on the horizontal axis indicate values corresponding to single stance for the reference leg; the white bars indicate values corresponding to swing, and the black bars correspond to double support.**A**). Therefore, we predicted that the model's contralateral GAS would respond to the perturbation by increasing its excitation.

Figure 4-8) Comparing contralateral muscle responses to the mechanical perturbations applied during swing, in the model and human: A. Gas, B. Sol. The black arrows in the heat maps indicate the response time in the experiment when the peak significant t -values occur. illustrates the contralateral plantarflexor muscles response to the mechanical perturbations in model and humans. In response to the forward push of the ankles during swing, the contralateral GAS (**Figure 4-8**) Comparing contralateral muscle responses to the mechanical perturbations applied during swing, in the model and human: A. Gas, B. Sol. The black arrows in the heat maps indicate the response time in the experiment when the peak significant t -values occur.**A**) and SOL muscles (**Figure 4-8**) Comparing contralateral muscle responses to the mechanical perturbations applied during swing, in the model and human: A. Gas, B. Sol. The black arrows in the heat maps indicate the response time in the experiment when the peak significant t -values occur.**B**) in the model demonstrated short-latency positive responses at mid-stance. These positive responses were product of a counteractive strategy. The mechanical perturbations caused dorsiflexion of the contralateral leg ankle and lengthened the plantarflexors. Due to the muscle force-length relationship,

the changes in the GAS and SOL lengths increased their forces, thus increasing the force-feedback induced excitations. The kinematic consequence of this mechanism was an increase in the length of the next step after perturbations (**Figure 4-4**) Comparing step length and duration responses to the mechanical perturbations in the model and human. As you go from right to left, the time delay between perturbation and response is increasing. The gray bars on the horizontal axis indicate values corresponding to single stance for the reference leg; the white bars indicate values corresponding to swing, and the black bars correspond to double support.**A**), which could have contributed to delaying of the recovery in the model.

On the other hand, comparing the contralateral SOL muscle response in model and human, it appears that the increased activity of the contralateral SOL muscle in humans can be explained by similar counteractive strategy implemented in the model (**Figure 4-8**) Comparing contralateral muscle responses to the mechanical perturbations applied during swing, in the model and human: A. Gas, B. Sol. The black arrows in the heat maps indicate the response time in the experiment when the peak significant *t*-values occur.**B**).

4.4 Discussion

The goal of this study was to test and further our understanding of what types of neural mechanisms the nervous system uses to stabilize walking. In order to better understand the neural mechanisms involved in the human stabilizing behavior, the first step is to make sure that the counteractive and non-counteractive responses have been previously

categorized correctly (Rafiee and Kiemel, 2020). We hypothesized that Geyer and Herr (2010) model, which is a counteractive model of locomotion that only uses gated reflex mechanisms, will be able to reproduce responses that we have categorized as counteractive, but not the non-counteractive ones. We tested Geyer and Herr (2010) model and found out that our previous classification was correct in most cases.

4.4.1 Counteractive Mechanisms

We observed that the model did a decent job in reproducing experimental data that we have categorized as fixed-latency counteractive responses. The ipsilateral Ham muscle group (**Figure 4-5**) Comparing ipsilateral **A.** hamstring and **B.** knee angle responses to the mechanical perturbations applied during swing, in the model and human. The black arrows in the human response column indicate the response time in the experiment when the peak significant t -value occurs.**A**) and the contralateral SOL muscle response (**Figure 4-8**) Comparing contralateral muscle responses to the mechanical perturbations applied during swing, in the model and human: **A.** Gas, **B.** Sol. The black arrows in the heat maps indicate the response time in the experiment when the peak significant t -values occur.**B**) to the perturbations were similar across the model and the experimental data in terms of the direction and the timing of the responses. The magnitudes of the responses were smaller in the model. However, this issue can be addressed by adding additional phase-specific reflex pathways to the model (Song and Geyer, 2017). In addition, the model's underlying mechanisms were designed to represent the existing physiological studies and thus were similar between model and human. In the model, both muscles used a force-feedback mechanism. The experimental literature also suggests force-feedback

mechanism from Golgi tendon organs contributes to regulating Ham muscle group during late swing (Van de Crommert et al., 1996) and SOL muscle at late stance (Grey et al., 2007).

4.4.2 Non-Counteractive Mechanisms

On the other hand, generally, the model could not reproduce the strategies that we have classified as non-counteractive. For all such strategies observed in human participants, the corresponding muscular response were different between model and human. First and foremost, the response time of these muscular responses were different, which resulted in different subsequent kinematic effect. For instance, in response to the forward push of the ankle, TA showed initial positive responses at swing in the model and at early stance in humans (**Figure 4-6** Comparing ipsilateral TA response to the mechanical perturbations applied during swing, in the model and human. Since in the model, the magnitude of the initial response is much smaller, compared to the phase shift effect, in the heatmaps, the muscle responses were depicted only at time prior to ipsilateral leg heel strike. The black arrows in the human response column indicate the response time in the experiment when the peak significant t -value occurs.). In humans, the early stance increase in TA excitation is thought to contribute to displacing the pelvis forward relative to the stance foot, which compensates for errors in foot placement (Logan et al., 2017; Rafiee and Kiemel, 2020). On the other hand, in the model, the increased TA excitation during swing does not substantially affect the position of the pelvis relative to the stance foot.

In addition to the difference in timing, in some cases the direction of the initial muscular responses was found to be different between model and human, which resulted in

opposite subsequent kinematic responses. For instance, the GAS modulation during mid stance is thought to contribute to leg progression (Neptune et al., 2001) and control the next step length. The experimental data showed that humans modulate the contralateral GAS muscle at mid-stance (**Figure 4-8**) Comparing contralateral muscle responses to the mechanical perturbations applied during swing, in the model and human: A. Gas, B. Sol. The black arrows in the heat maps indicate the response time in the experiment when the peak significant t -values occur. **A**) to presumably decrease the length of the next step after the perturbation and compensate for the increase in the previous step length (**Figure 4-4**) Comparing step length and duration responses to the mechanical perturbations in the model and human. As you go from right to left, the time delay between perturbation and response is increasing. The gray bars on the horizontal axis indicate values corresponding to single stance for the reference leg; the white bars indicate values corresponding to swing, and the black bars correspond to double support. **A**). On the other hand, in the model, the increase in the contralateral GAS muscle excitation (**Figure 4-8**) Comparing contralateral muscle responses to the mechanical perturbations applied during swing, in the model and human: A. Gas, B. Sol. The black arrows in the heat maps indicate the response time in the experiment when the peak significant t -values occur. **A**) resulted in an increase in the following step length (**Figure 4-4**) Comparing step length and duration responses to the mechanical perturbations in the model and human. As you go from right to left, the time delay between perturbation and response is increasing. The gray bars on the horizontal axis indicate values corresponding to single stance for the reference leg; the white bars indicate values corresponding to swing, and the black bars correspond to double

support.A). Part of the difference in behavior could be attributed to the fact that human participants had to walk on a treadmill with a limited space, where increases in step length or cadence can have high penalties. The model was not developed to obey these constraints.

4.4.3 Two-step Recovery:

The aforementioned observations confirm that humans use different mechanisms from those implemented in the model to control walking. The models' inability to use whole-body mechanical degrees of freedom to compensate for the effect of the perturbation may explain why it is slower than human participants in converging back to its baseline gait (**Figure 4-4**) Comparing step length and duration responses to the mechanical perturbations in the model and human. As you go from right to left, the time delay between perturbation and response is increasing. The gray bars on the horizontal axis indicate values corresponding to single stance for the reference leg; the white bars indicate values corresponding to swing, and the black bars correspond to double support.B). Other experimental studies have also shown that in general, people plan two steps ahead (Matthis and Fajen, 2014) and can correct for perturbations within two steps (Hof et al., 2010). Similarly, it has been recently established that with appropriate control, simple models of gait can correct for small perturbations in a single step (Zaytsev et al., 2015). Even though it is not obvious what this appropriate control would look like in the human neural system, neuromechanical models of gait that could achieve a single-step recovery (e.g., Zaytsev et al., 2015) were not limited to using counteractive responses. Here, we argue that inclusion of non-counteractive control

could also considerably help humans to rapidly correct for perturbations. In the rest of this section, we compare characteristics of counteractive and non-counteractive strategies, in hope of developing a future neuromechanical model of human locomotion that can produce these compensatory strategies.

4.4.4 Phase-specific Characteristics & Non-Counteractive Mechanisms

One of the main discrepancies between model and human behavior lay in the timing of the responses. In the model, since the system is controlled by counteractive mechanisms, most of the responses had short latencies. They occurred with a fixed delay after the onset of perturbation. One exception to this behavior, was mechanisms that have both fixed latency and gating such that the gating delays the response, for example the HFL reflex dependency on the trunk lean angle at the heel take-off. On the other hand, experimental responses were much more phase-specific. In both model and humans, the responses occurred during phases at which the muscles were normally active. The model implemented this response mainly by turning the muscles off during undesired phases. However, in the humans even when the muscles were “on” earlier, the responses occurred at specific phases later on, usually around the peak of the muscle’s excitation. Ipsilateral TA response to the mechanical perturbation of a leg in humans is a good example of such behavior. Even though, this muscle is active during swing (**Figure 4-2**) Comparison between model (in black) and human mean waveforms (in blue) of **A.** the kinematics variables and **B.** muscle excitations during unperturbed cycles. The experimental data includes 95% confidence intervals. **For** each joint angle the average value is subtracted from the signal. The Gray and white bars on the

horizontal axes correspond to single support phase (white for swing and gray for stance) for the reference leg. The black bars indicate double support.), the response occurs at early stance phase (**Figure 4-6**) Comparing ipsilateral TA response to the mechanical perturbations applied during swing, in the model and human. Since in the model, the magnitude of the initial response is much smaller, compared to the phase shift effect, in the heatmaps, the muscle responses were depicted only at time prior to ipsilateral leg heel strike. The black arrows in the human response column indicate the response time in the experiment when the peak significant t -value occurs.).

Such phase-specific modulation of the muscle excitations in humans suggests the existence of a non-counteractive mechanism in the system. This non-counteractive controller could be a simple clock: similar to models that control the system at a spinal level through central pattern generators (CPGs, e.g., Aoi et al., 2010). Alternatively, this non-counteractive controller could be an internal model that uses information about the position of the system to estimate the current state/phase (Wolpert et al., 1995; Kuo, 2002). Typically, such state-estimator mechanisms have been implemented at the supraspinal level in neuromechanical models (e.g., Taga, 1995) with the task of providing the phase to the spinal rhythm generators. Either way, this non-counteractive controller takes advantage of the knowledge about the phase of the system to dictate the control strategies.

Nonetheless, one should be cautious in generalizing the phase-specific responses to non-counteractive mechanisms. We found some muscles in the model whose initial responses were short-latency, however, the peak responses occurred at specific phases. Contralateral SOL response is a good example for such a behavior (**Figure 4-8**)

Comparing contralateral muscle responses to the mechanical perturbations applied during swing, in the model and human: A. Gas, B. Sol. The black arrows in the heat maps indicate the response time in the experiment when the peak significant t -values occur. **B**). This phase-specific response is the result of a force-feedback mechanism that depends on the muscle length, and therefore, the peak response occurs where the muscle length is close to its optimal value. Similar passive control strategies that take advantage of reflexes have been suggested to contribute to the robustness of human locomotion (Gerritsen et al., 1998).

However, aside from the timing of the responses, the compensatory nature of the response can be best explained, in a parsimonious manner, with a non-counteractive model. Since these compensatory responses often control movement at a whole-body level, they have to be implemented at a higher level of control, most likely the cerebellum (Takakusaki, 2013). The requirement of knowledge about the state of the system, potentially explains why the Geyer and Herr (2010) model could not reproduce the more complex compensatory strategies observed in human walking that were phase-specific, such as the modulation of the ipsilateral anterior muscles at early stance, or the contralateral RF in double support.

Additionally, non-counteractive mechanisms are essential for compensatory strategies that do not necessarily oppose the effect of the perturbations, but rather implement an optimal alternative. Previously, studying upper-body movement, Wolpert et al. (1995) established that a model with only feedback components, similar to those used in counteractive mechanisms, is not optimal. Here, we showed that, a counteractive model

of human locomotion does not produce human-like features. The discrepancy in behavior between model and human might be due to the fact that the model does not respond optimally to the perturbations, whereas the humans might.

Chapter 5 : Hybrid Neuromechanical Model of Human Walking

In this chapter, we developed a neuromechanical model of walking with a hybrid controller including both counteractive mechanisms and a CPG. In chapter 4, we observed that a purely counteractive model of human locomotion cannot reproduce strategies that we have categorized as non-counteractive. Here, we investigated whether a hybrid model can reproduce human responses to external perturbations better than a purely counteractive model. Our results suggest that the structure of the chosen counteractive model is such that it behaves as if it already has a CPG.

5.1 Introduction

Phase-specific changes in the periodic muscle excitation waveforms play an important role in the control and stabilization of human locomotion. Due to the differences in the configurations of the joint and segment angles as well as the condition of the foot on the ground, modulation of the muscles at different phase of the gait cycle can cause different kinematic consequences. Therefore, one of the more important tasks of the neural controller is the timely regulation of the muscular responses to perturbations. To implement phase-specific responses, the neural controller should have information about the phase of the system. However, the mechanisms responsible for producing these phase-specific muscular responses is not yet understood.

In theory, both gated counteractive mechanisms, and non-counteractive ones can produce phase-specific responses to perturbations. In chapter 4, we compared the

responses of a counteractive model of human locomotion to mechanical perturbations of the leg with those from human participants. We observed that a counteractive model of human locomotion that is controlled by simple reflex mechanisms is not able to reproduce most phase-specific responses that we have categorized as non-counteractive. We hypothesized two reasons for this observation: (i) the model ignored the phase-dependency of non-counteractive responses in general, and (ii) it lacked the underlying mechanisms for specific strategies. For instance, our previous studies have suggested that the early stance TA modulation compensates for errors in foot-placement using a phase-dependent mechanism that considers the position of the foot relative to the pelvis (Rafiee and Kiemel, 2020). Such a mechanism is absent in the Geyer and Herr (2010) model.

Perhaps, more importantly, since the Geyer and Herr (2010) model only has gated reflexes, those reflex mechanisms are responsible for producing both realistic periodic muscle excitation waveforms as well as realistic responses to the perturbations. This balance is difficult to achieve in a model. In addition, the literature on central pattern generators (CPGs) suggest that gated reflexes are probably not solely responsible for producing the periodic muscle excitation waveforms in humans (Hultborn and Nielsen, 2007). Rather, animal studies suggest that CPGs, which are non-counteractive spinal mechanisms, generate rhythmic locomotor muscle excitations similar to those seen during closed-loop walking (Grillner and Wallen, 1985). It has been hypothesized that the phase-dependent reflex mechanisms that contribute to gait stability are regulated through CPGs (Duysens et al., 1992). Gait simulation literature has also shown that

using CPGs, neuromechanical models of human locomotion were able to mimic some non-counteractive human gait responses to large perturbations, such as obstacle avoidance (Taga, 1998) or recovery strategies (Jo, 2007).

Thus, we argue that having a CPG in a model is both rational and perhaps it allows one the modeling flexibility necessary to produce both realistic mean waveforms and realistic responses to perturbations. In this study, we examined whether adding a CPG to a model of human walking that is primarily controlled by counteractive mechanisms, would help the model behave more like a human.

For the counteractive model, we chose Song and Geyer (2015), which is a newer version of the model studied in chapter 4 (Geyer and Herr, 2010). We then added a CPG to a version of this model and analyzed and compared the responses of the counteractive model and the hybrid model to external perturbations.

We hypothesized that having a mechanism to account for the phase-dependency of the muscle modulations, such as a CPG, might be necessary but not sufficient for producing all non-counteractive responses. We expected that adding a CPG to the model to affect the average muscle excitation patterns and the reflex mechanisms that rely on them. Such a mechanism might help the model produce some of the phase-specific responses observed in humans. On the other hand, for the model to produce all human responses it should include additional control mechanisms. Therefore, we expect our hybrid model to reproduce only a subset of the human response to external perturbations better than the counteractive model.

5.2 Methods:

5.2.1 Overview:

The goal of the current simulation study was to compare different types of neural mechanisms that can stabilize human walking. To this end, we studied 2 neuromechanical models of human walking with the same plant but different controllers. We then characterized and compared the responses of these models to the same external perturbations. The first model was a established model of human locomotion with a counteractive controller (Song and Geyer, 2015). The second model had a hybrid controller including both counteractive and non-counteractive mechanism. We built this hybrid model by adding a CPG (inspired by Aoi et al., 2010) to our version of the Song and Geyer (2015) counteractive model. In what follows, we first describe the original counteractive model and the modifications we made to it. We then describe the elements of the non-counteractive mechanism that we added to the model. Lastly, we describe the perturbation simulation process and detail evaluation of the models' responses.

5.2.2 Model Description:

Counteractive Model:

The counteractive model of human locomotion is a 3D neuromechanical model developed in OpenSim; however, the body mechanics do not have all the mechanical degrees of freedom of a fully 3D model (**Figure 5-1**) Musculoskeletal model used to study human locomotion. This model had 14 degrees of freedom. It had a 6-DoF joint between the pelvis and

the ground. In addition, each leg had a 2-DoF hip joint, a 1-DoF knee joint, and a 1-DoF ankle joint. The model is actuated by 11 muscles per leg: hip abductor (HAB), hip adductor (HAD), gluteus maximus (GLU), hamstrings (HAMS), hip flexor (HFL), rectus femoris (RF), vasti (VAS), biceps femoris short head (BFSH), gastrocnemius medialis (GAS), soleus (SOL), and tibialis anterior (TA).

). This model is adapted from a version of the Song and Geyer (2015) model, which is publicly shared on a repository on GitHub. The musculoskeletal system of this model is comprised of 7 rigid segments (two 3-segmented legs and a torso) connected by rotational joints, and it has 14 mechanical degrees of freedom. The model is actuated by 11 Hill-type muscles on each leg that receive excitations from the neural controller.

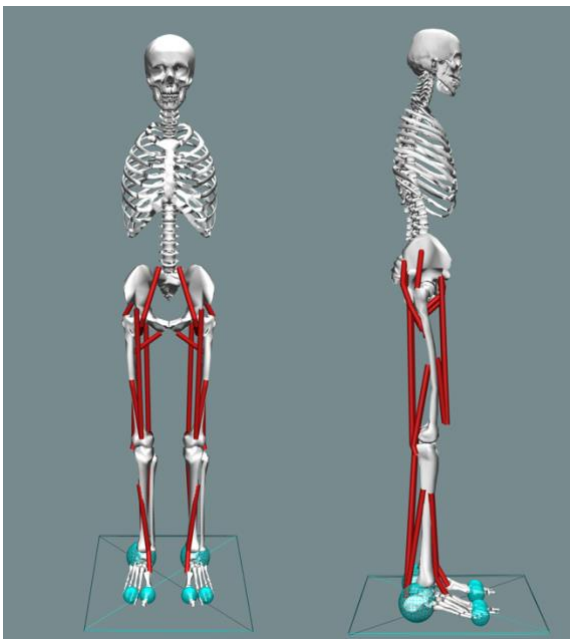


Figure 5-1) Musculoskeletal model used to study human locomotion. This model had 14 degrees of freedom. It had a 6-DoF joint between the pelvis and the ground. In addition, each leg had a 2-DoF hip joint, a 1-DoF knee joint, and a 1-DoF ankle joint. The model is actuated by 11 muscles per leg: hip abductor (HAB), hip adductor (HAD), gluteus maximus (GLU), hamstrings (HAMS), hip flexor (HFL), rectus femoris (RF), vasti (VAS), biceps femoris short head (BFSH), gastrocnemius medialis (GAS), soleus (SOL), and tibialis anterior (TA).

The model controls the muscle excitations by gated fixed-latency reflex mechanisms involving four groups of feedback information (muscle forces, muscle lengths, joint angles, and ground contact forces). The controller is organized into nine modules, sets of reflexes, which are activated based on the conditional role they play during stance

and swing. These conditional roles are: 1) control the stance leg, 2) control the stance leg when the contralateral leg is in swing 3) keep leg is stance, 4) initiate swing, 5) control the swing leg, 6) flex the knee when the leg is in swing, 7) hold the knee when the leg is in swing, 8) stop the leg when it is in swing, and 9) hold the leg when it is in swing. Even though some of these modules are independent of each other, there are constraints in the model which dictate the sequence in which most of the modules become active.

Each module can contribute to several muscles, and each muscle excitation is the sum of a baseline excitation and the relevant control module reflexes.

Inspired by physiological studies on the role of sensory information from Golgi tendon organs, muscle spindles, and cutaneous receptors, the modules operate at the spinal level. In addition to the modules, this model has a simple supraspinal counteractive controller that alters the reflex gains. This supraspinal component uses information about the AP position and velocity of the COM relative to the ankle of the stance foot to adjust the foot placement of the swing leg.

Since in this study, we wanted to investigate the responses of the models to small external perturbations, we had to make sure that the perturbation responses were greater than the numerical error in the model. Therefore, we modified the conditional modules in the Song and Geyer (2015) model and used smooth approximations for them (see Appendix I)

Counteractive Model + CPG without Phase-Resetting

We adapted our smooth version of the Song and Geyer (2015) model in OpenSim by adding non-counteractive components to it. In this study, we used a CPG as the core non-counteractive component of our model. Like the original counteractive Song and Geyer (2015) model, in our adaptation, each muscle excitation is a function of a baseline excitation and the relevant counteractive reflexes. However, here, we reduced the contribution of the reflexes by half and had the CPG regulate the muscles' baseline excitations. Therefore, for each muscle, the excitation was defined as a weighted sum of the counteractive reflex excitation and the non-counteractive CPG excitation.

Inspired by Aoi et al. (2010), in our model, we implemented the CPG as a “synergy” network that turns a subset of muscles “on” during a portion of the gait cycle. The CPG in Aoi et al. (2010) model consists of a rhythm generator (RG) and a pattern formation (PF).

In this model, RG operates as a clock. It consists of two simple phase oscillators: one for each leg. These oscillators encourage the legs to move anti-phase and have the same frequency, ω (Aoi et al., 2010):

$$\dot{\varphi}_{\text{ipsi}} = \omega - K \sin(\varphi_{\text{ipsi}} - \varphi_{\text{contra}} - \pi)$$

where, $K=1.7$ is a constant, φ_{ipsi} is the phase of the ipsilateral leg, $\dot{\varphi}_{\text{ipsi}}$ is its derivative and φ_{contra} is the phase of the contralateral leg. When the system is on its limit cycle, phase resetting has no effect on the system, and ω is equal to $2\pi/T$. Therefore, on its

limit cycle ω specifies the walking period, T . Since our counteractive model walked with the period of $T = 1.032$, here we set ω to be 6.08 rad/s .

PF uses information about the phase of the gait cycle, provided by RG, to produce five basic rectangular patterns (Aoi et al., 2010):

$$CPG_i(\varphi) = \begin{cases} 1 & \varphi_i^{on} \leq \varphi \leq \varphi_i^{off} \\ 0 & \text{otherwise} \end{cases} \quad i = 1, \dots, 5$$

in a fixed sequence, where, $0 \leq \varphi_1^{on} < \varphi_1^{off} < \varphi_2^{on} < \varphi_2^{off} < \varphi_3^{on} < \varphi_3^{off} < \varphi_4^{on} < \varphi_4^{off} < \varphi_5^{on} < \varphi_5^{off} \leq 2\pi$

Therefore, for each muscle the CPG excitation, S_{CPG_M} , was the weighted sum of these five rectangular pulses (CPG_i):

$$S_{CPG_M}(\varphi) = \sum_{i=1}^5 W_{Mi} CPG_i(\varphi)$$

W_{Mi} is the weighting coefficient of muscle M and CPG_i , and its matrix has the following form:

$$W = \begin{bmatrix} 0 & 0 & 0 & 0 & W_{VAS1} & 0 & 0 & 0 & W_{TA1} \\ 0 & 0 & 0 & 0 & 0 & 0 & W_{GAS2} & W_{SOL2} & 0 \\ W_{HFL3} & 0 & 0 & W_{RF3} & 0 & W_{BFSH3} & 0 & 0 & 0 \\ 0 & 0 & 0 & 0 & W_{VAS4} & 0 & 0 & 0 & W_{TA4} \\ 0 & W_{GLU5} & W_{HAM5} & 0 & 0 & W_{BFSH5} & 0 & 0 & 0 \end{bmatrix}^T$$

Optimization:

To determine the parameters of these 5 synergies (10 parameters: $\varphi_i^{on}, \varphi_i^{off}$), and the weighting coefficient W_{Mi} (12 parameters: 9 muscles, 3 of them use 2 synergies), we used optimization to maximize a reward function J :

$$J = 10 T_{\text{Alive}} - 0.1 C_{\text{Effort}} - C_{\text{Velocity}} - 5 C_{\text{Trunk}}$$

$$C_{\text{Effort}} = \frac{1}{T_{\text{sim}}} \sum_{i=1}^{T_{\text{sim}}/\Delta t} \sum_{M=1}^{11} act_{M_i}^2 \Delta t$$

$$C_{\text{Velocity}} = \frac{1}{T_{\text{sim}}} \sum_{i=1}^{T_{\text{sim}}/\Delta t} \|\vec{v}_i - \vec{v}_{tg}\| \Delta t$$

$$C_{\text{Trunk}} = \frac{1}{T_{\text{sim}}} \sum_{i=1}^{T_{\text{sim}}/\Delta t} (\theta_{\text{Trunk}_i})^2 \Delta t$$

which maximizes the reward for the time model can walk without falling (T_{Alive}) and minimizes an effort cost (C_{Effort}), the cost of deviation from a target velocity (C_{Velocity}), and the cost of the trunk angle deviations from upright (C_{Trunk}). $T_{\text{sim}} = 6$ s is the optimization simulation duration; $\Delta t = 0.001$ s is the simulation time step; act_M is the muscle M activation level; \vec{v} is the pelvis velocity vector, and $\vec{v}_{tg} = [1.4, 0, 0]$ m/s is its velocity target. θ_{Trunk} is the trunk lean angle.

The optimization procedure was implemented via a steady state genetic algorithm (Gad, 2021). To initiate the optimization, an initial guess of 20 possible solutions was randomly generated, each solution was used to perform a simulation and each simulation was scored per the reward function. The 10 simulations with the best scores

were retained and used to generate new feasible solutions. We included a 10% element of randomness to allow for a broad evaluation of the solution space. This process was repeated over 40 generations and the solution with the highest reward function score was retained for further analysis as follows:

$$\begin{aligned}
W_{VAS1} &= 0.446, W_{TA1} = 0.392, W_{V=GAS2} = 0.783, W_{SOL2} = 0.134, W_{HFL3} = 0.981, W_{RF3} \\
&= 1.08, W_{BF3H3} = 0.950, W_{VAS4} = 0.329, W_{TA4} = 0.389, W_{GLU5} = 0.951, W_{HAM5} = 0.728, \\
W_{BF5H5} &= 0.831, \varphi_1^{on} = 0.000, \varphi_1^{off} = 0.160(2\pi), \varphi_2^{on} = 0.237(2\pi), \varphi_2^{off} = 0.410(2\pi), \\
\varphi_3^{on} &= 0.557(2\pi), \varphi_3^{off} = 0.735(2\pi), \varphi_4^{on} = 0.755(2\pi), \varphi_4^{off} = 0.863(2\pi), \varphi_5^{on} = \\
&0.889(2\pi), \varphi_5^{off} = (2\pi).
\end{aligned}$$

Counteractive Model + CPG

In the final version of the model, the non-counteractive component is comprised of a CPG that has phase-resetting capabilities. In this case, the RG is no longer a simple clock, but it uses information about the ipsilateral leg heel-strike time, t_{ipsi}^{con} , and toe-off time, t_{ipsi}^{off} , to reset the phase of the ipsilateral leg (Aoi et al., 2010):

$$\begin{aligned}
\dot{\varphi}_{ipsi} &= \omega - K \sin(\varphi_{ipsi} - \varphi_{contra} - \pi) - (\varphi_{ipsi} - \varphi^{off})\delta(t - t_{ipsi}^{off} - \tau) \\
&\quad - (\varphi_{ipsi} - \varphi^{con})\delta(t - t_{ipsi}^{con} - \tau)
\end{aligned}$$

where $\delta(t)$ approximates the Dirac delta function. φ^{con} and φ^{off} are constant values for the phase to be reset when the leg contacts and leaves the ground, respectively. Here, the delta function ensures that after a short delay, τ , from the onset of the heel

strike or toe-off time, the phase resets to φ^{Con} or φ^{Off} . In our adaptation, we approximated the Dirac delta function as $\delta(t) = \frac{e^{-(t/a)^2}}{a\sqrt{\pi}}$, with $a = 0.01$.

To find φ^{Con} and φ^{Off} , we ran the previously optimized model without phase resetting. We found a range of initial phases for the right and left legs with which the model was stable. Throughout this range, after a few cycles, the period always converged to $T = 1.033$ s, and the phase at heel strike and toe-off converged to $0.98(2\pi)$ and $0.52(2\pi)$ respectively. Considering the delay of $\tau = 50$ ms in the phase-resetting algorithm, we found $\varphi^{Con} = 0.02(2\pi)$ and $\varphi^{Off} = 0.57(2\pi)$.

5.2.3 Perturbation simulation:

For each model, we simulated 101 runs: 100 perturbed walking simulations and a single unperturbed one. The simulations were done in OpenSim with the default integrator (Runge-Kutta-Merson) and integrator accuracy of 5×10^{-8} . An identical mechanical perturbation was applied to all models, at a different phase of the gait cycle in each simulation. Like chapter 4, the mechanical perturbation was an impulse of force, approximated by a scaled Gaussian function of time: $F(t) = \frac{A}{\sigma\sqrt{2\pi}} e^{-\frac{(t-t_0)^2}{2\sigma^2}}$, where σ was 0.005 s, and A was 0.5 Ns. With these parameters, the maximum force applied to both legs was $\frac{A}{\sigma\sqrt{2\pi}} = 39.9$ N. In order to mimic the experimental string-pulley perturbation system (Rafiee and Kiemel, 2020), each leg was exposed to half of this impulse force. Before applying the mechanical perturbations, we let the models run for

at least 6 s to get close to their limit cycle and the simulation continued at least 4 cycles after the perturbation was applied.

5.2.4 Data Analysis & Response Comparison:

We analyzed kinematic and muscular responses to the perturbations. Like chapter 4, all the variables were expressed as a function of normalized time, which is time divided by the unperturbed period T . We used linear interpolation to fit the kinematic variables and muscle excitations to the phase cycle with the step length of $T/100$. The human data were also fitted to a 100-point phase cycle. To compare the average behavior of models with human, for each variable we calculated the root mean square of the

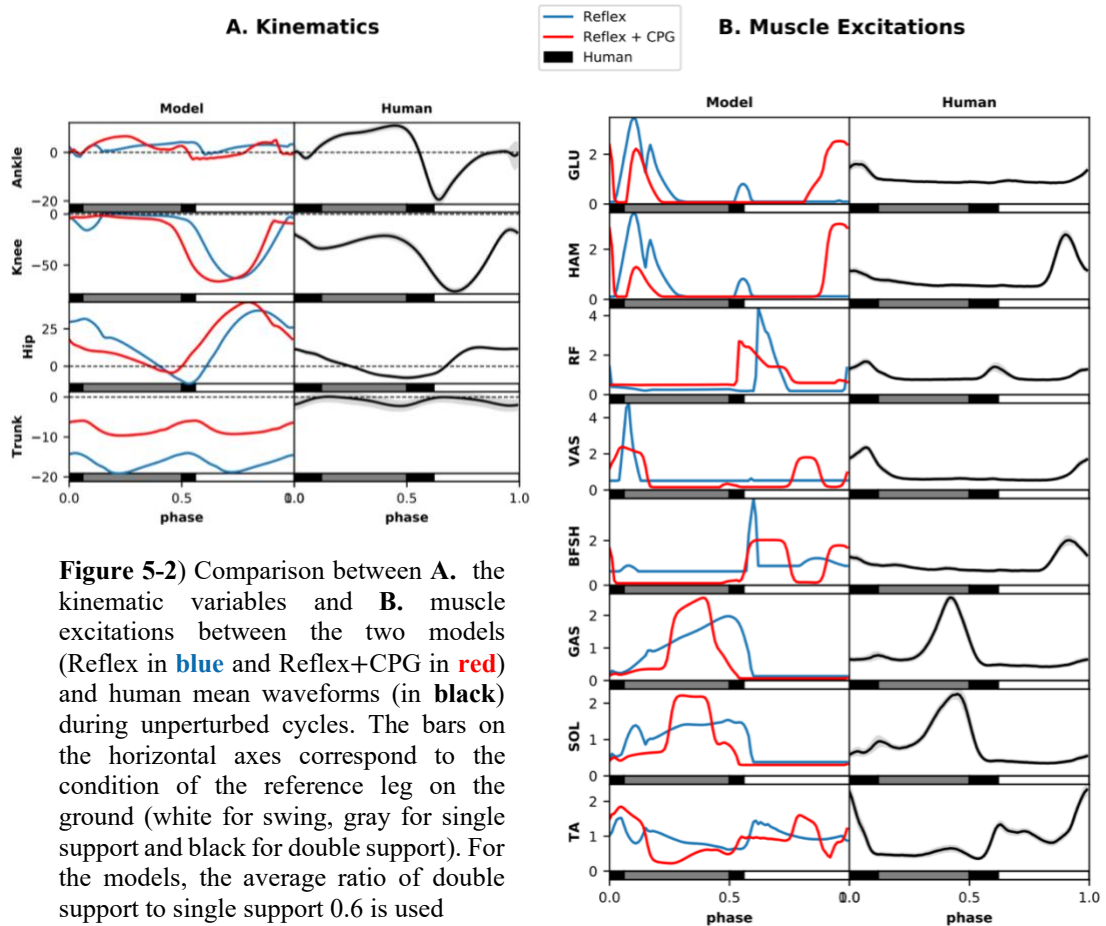
variable's Z-score: $RMS_Z = \sqrt{\frac{1}{n} \sum_{\vartheta=0}^{n-1} \left(\frac{x_{\text{exp}}(\vartheta) - x_{\text{sim}}(\vartheta)}{std_{\text{exp}}(\vartheta)} \right)^2}$, where, $x_{\text{sim}}(\vartheta)$ is the

simulated value at phase (ϑ); $x_{\text{exp}}(\vartheta)$ is the mean experimental value; $std_{\text{exp}}(\vartheta)$ is the experimental between-subject standard deviation, and $n=100$ is the number of points in the phase cycle. Finally, to analyze the response of the two models to a forward force perturbation at the ankles we calculated the direct ϕ IRFs for all variables, by subtracting the unperturbed signals from the perturbed ones, and dividing the difference signals by the integral of the impulse force, A .

5.3 Results

5.3.1 Unperturbed Behavior:

The average velocity of the human walking in the experimental study was 1.39 m/s (Rafiee and Kiemel 2020). The Reflex model walked with an average velocity of 1.44 m/s and the average velocity for the Reflex+CPG model was 1.25 m/s. **Figure 5-2)** Comparison between **A.** the kinematic variables and **B.** muscle excitations between the two models (Reflex in **blue** and Reflex+CPG in **red**) and human mean waveforms (in **black**) during unperturbed cycles. The bars on the horizontal axes correspond to the condition of the reference leg on the ground (white for swing, gray for single support and black for double support). For the models, the average ratio of double support to single support 0.6 is used compares the mean kinematics waveforms and muscles excitations between the two models and human data measured in the experimental study. In general, both models were relatively successful in replicating the mean human kinematics. The Reflex model had an average RMS_z of 3.52 for the lower-body joint angles, and the Reflex+CPG model had an average RMS_z of 3.17. In addition, the Reflex+CPG model deviated less from the mean periodic waveform of human trunk angle (trunk $RMS_z = 2.88$) than the Reflex model (trunk $RMS_z = 6.30$). On the other hand, the double support duration relative to the stride duration was closer to human data (0.13) in the Reflex model (0.08) comparing to the Reflex+CPG model (0.04).



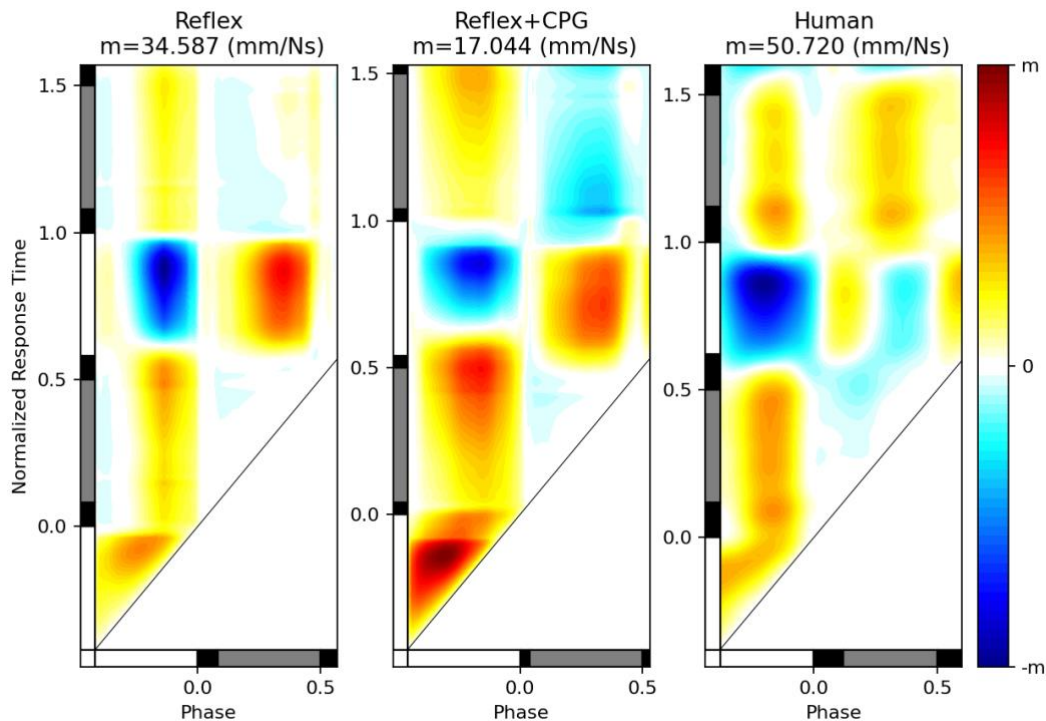
Both models were also successful in replicating the mean patterns of human muscular waveforms. The Reflex model deviated less from average human muscle excitation (with an average RMS_Z of 3.94) than the Reflex+CPG model (with an average RMS_Z of 4.11). Part of these deviations can be attributed to the differences in the double support durations between models and human. On the other hand, the on/off timing of the muscle excitation patterns agreed more with the human data in the Reflex+CPG model comparing to the Reflex model. This finding was not surprising since the primary function of the CPG was producing the basic patterns of muscle excitations.

5.3.2 Kinematic Responses:

In general, we found that the initial kinematic responses to the perturbations applied during swing were similar across the models and human data. In response to the forward force perturbation, the position of the swing leg ankle relative to the pelvis increased right after the onset of the perturbation in all cases (**Figure 5-3**) Comparing the Ankle AP position response to the mechanical perturbations in the models and human. **A.** demonstrates the ϕ IRF responses in heat maps that have two independent variables: perturbation phase on the horizontal axis and normalized response time on the vertical axis. The color coding of the heat maps from cold to hot indicates the value of the ϕ IRFs (white for 0, yellow and red for positive, and blue for negative). The value m , specified above each heatmap, is the maximum absolute response value which we used to define the color map (see color bar). The diagonal line in the heat map corresponds to a response measured at the same time the perturbation is applied. The ϕ IRF is 0 (white) below this line. **B.** takes a vertical slice of the ankle AP response heat maps and depicts the ϕ IRF for the perturbations applied at mid swing (phase = -0.3). Black shaded areas depict experimental ϕ IRFs with 95% confidence interval, and solid blue and red lines show the Reflex model and the Reflex+CPG direct ϕ IRFs.). In other words, the leg was displaced forward without any delay after the perturbation was applied. The initial response was of the same order of magnitude across the models and human data, with the maximum value of 16.58 mm/Ns, 17.04 mm/Ns and 22.99 mm/Ns respectively for the Reflex model, the Reflex+CPG model and the human responses.

However, the initial response of both models to the perturbations applied during the stance phase, when the contralateral leg was in swing, was in the opposite direction of human responses. The negative response observed in human data indicates the effect of the perturbation shifting and delaying the timings of the gait cycle. On the other hand, in both models, the swing phase perturbation of the contralateral leg, resulted in an initial time advance in the stance leg, which produced the opposite kinematic effects. The models had slower transients than human participants (not shown here). However, once the models converged back to the limit cycle, allowing the phase shift to be computed, those phase shifts were negative, thus mimicking human behavior

A. AP Ankle relative to Pelvis Response



B. AP Ankle Relative to Pelvis IRF for Perturbations Applied at Phase -0.3

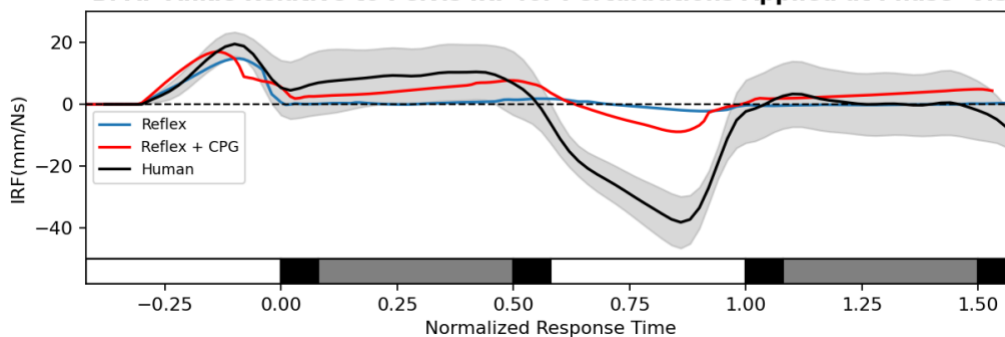
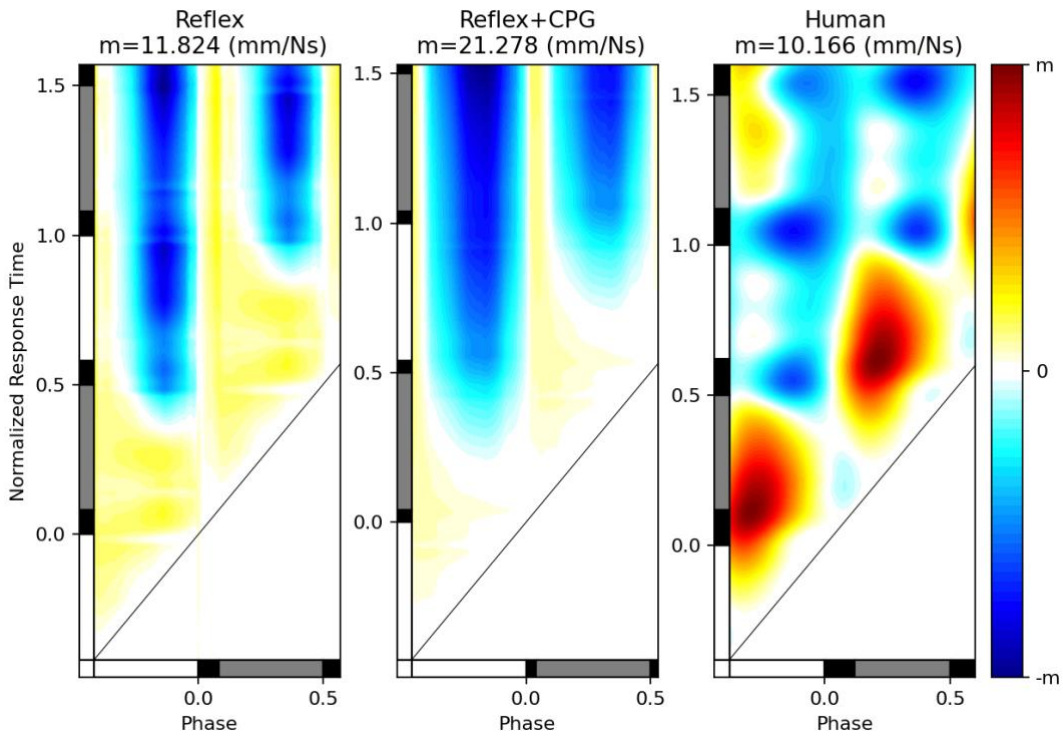


Figure 5-3) Comparing the Ankle AP position response to the mechanical perturbations in the models and human. **A.** demonstrates the ϕ IRF responses in heat maps that have two independent variables: perturbation phase on the horizontal axis and normalized response time on the vertical axis. The color coding of the heat maps from cold to hot indicates the value of the ϕ IRFs (white for 0, yellow and red for positive, and blue for negative). The value m , specified above each heatmap, is the maximum absolute response value which we used to define the color map (see color bar). The diagonal line in the heat map corresponds to a response measured at the same time the perturbation is applied. The ϕ IRF is 0 (white) below this line. **B.** takes a vertical slice of the ankle AP response heat maps and depicts the ϕ IRF for the perturbations applied at mid swing (phase = -0.3). Black shaded areas depict experimental ϕ IRFs with 95% confidence interval, and solid blue and red lines show the Reflex model and the Reflex+CPG direct ϕ IRFs.

The initial AP pelvis response to the mechanical perturbations were also similar across the models and human; however, the magnitude of the response was much smaller in the models (**Figure 5-4**). In response to the mechanical perturbations applied during swing, the pelvis showed initial positive responses parallel to the diagonal line of the perturbations onset, which indicates that these responses were due to the inertial properties of the system. The behavior of the models and humans diverged in the following steps. **Figure 5-4B** compares the IRFs up to 4 cycles after the cycle in which the perturbation was applied. In humans, after the initial positive response, the AP pelvis IRF converged back to zero. In other words, in response to the perturbations during swing the pelvis was initially displaced forward but returned to its original position in the next cycle. However, in the models, the initial positive response was followed by a negative response that persisted even when walking returned to the limit cycle.

A. Pelvis AP Response



B. AP Pelvis IRF for Perturbations Applied at Phase -0.2

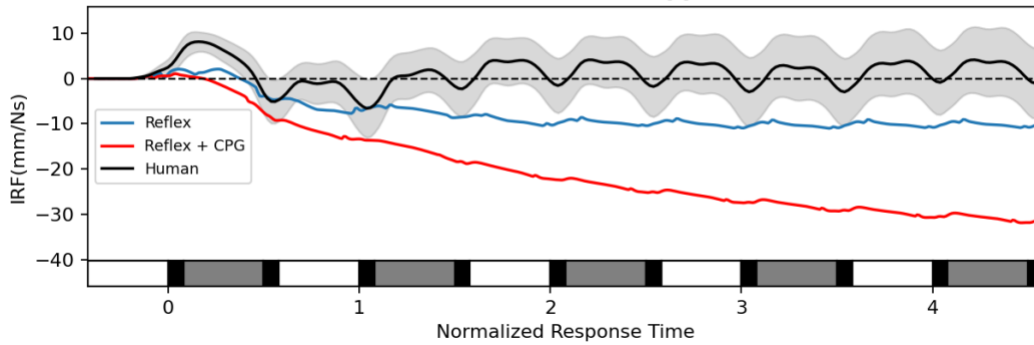


Figure 5-4) Comparing the Pelvis AP position response to the mechanical perturbations in the models and human. **A.** demonstrates the ϕ IRF responses in heat maps that have two independent variables: perturbation phase on the horizontal axis and normalized response time on the vertical axis. **B.** takes a vertical slice of the ankle AP response heat maps and depicts the ϕ IRF for the perturbations applied at mid swing (phase = -0.2). Black shaded areas depict experimental ϕ IRFs with 95% confidence interval, and solid blue and red lines show the Reflex model and the Reflex+CPG direct ϕ IRFs.

5.3.3 Muscular Responses:

The aim of this study was to examine whether adding a CPG to a counteractive model of human walking (Song and Geyer 2015) would help it produce phase specific responses. In chapter 4, we have observed that the older version of the studied model here (i.e., Geyer and Herr 2010) was not capable of producing (i) the early stance modulation of the anterior muscles and (ii) the late stance modulation of the GAS muscle. Therefore, in this study, we focused our analysis on these 2 groups of responses that we found the Geyer and Herr (2010) model failed to reproduce.

Early Stance Strategy: In the experimental data, in response to the perturbations during swing, the human participants showed positive responses at early stance for the anterior muscles including TA and VAS. We observed that neither model was able to reproduce the human TA response to the force perturbations (**Figure 5-5**). The average response for both models from late swing to early stance is close to zero. Thus, the models' responses are consistent with the effect produced by time shifts. On the other hand, for humans the average response is positive, which indicates an increase in the excitation of TA.

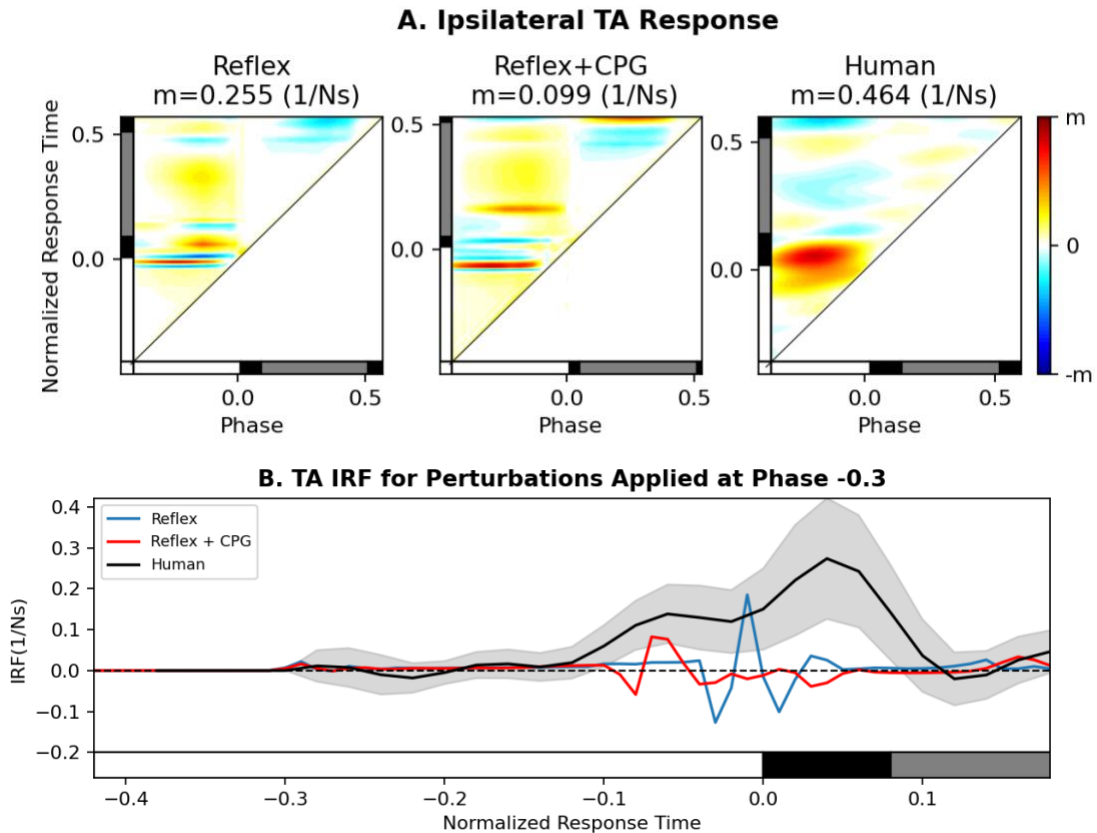


Figure 5-5) Comparing ipsilateral TA response to the mechanical perturbations in the models and human. **A.** demonstrates the ϕ IRF responses heat maps. **B.** takes a vertical slice of the ankle AP response heat maps and depicts the ϕ IRF for the perturbations applied at mid swing (phase = -0.3).

Unlike the TA responses, the average VAS responses from late swing to early stance seem to be substantially positive for both models and for humans (**Figure 5-6**) Comparing ipsilateral VAS response to the mechanical perturbations in the models and human. **A.** demonstrates the ϕ IRF responses heat maps. **B.** takes a vertical slice of the ankle AP response heat maps and depicts the ϕ IRF for the perturbations applied at mid swing (phase = -0.2)). In both models, the VAS muscle had force feedback mechanisms which were indirectly affected by the perturbation. The mechanical perturbations caused flexion of the hip joint (not shown) and shortened the VAS muscle length. Due to the muscle force-length relationship, the changes in the

muscle length increased its force, thus increasing the force-feedback induced excitations at its peak value. In addition to the force-feedback mechanism, the VAS muscle excitation has implemented in it a proportional-derivative reflex mechanisms that uses information about the knee joint angle to prevent hyperextension. The mechanical perturbation also caused extension of the knee joint (not shown). Due to the phase-specific nature of the knee hyperextension, this reflex mechanism caused an increase in VAS excitation right before heel strike in the Reflex+CPG model.

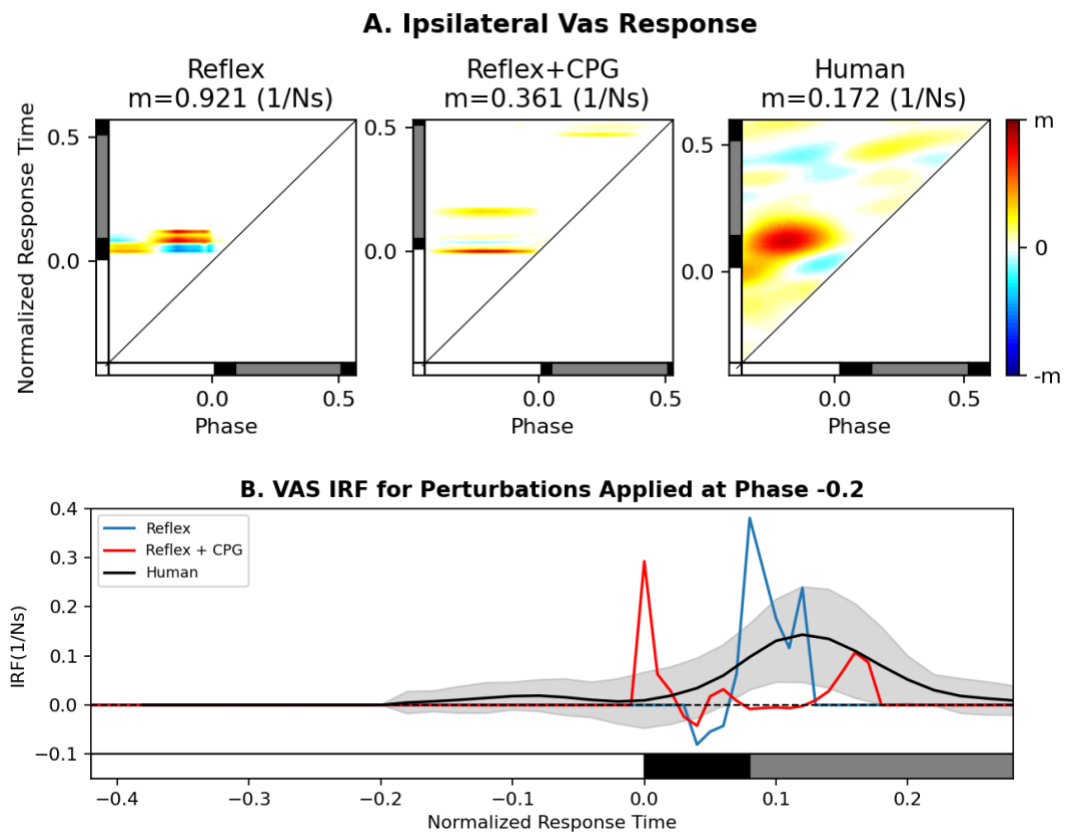


Figure 5-6) Comparing ipsilateral VAS response to the mechanical perturbations in the models and human. **A.** demonstrates the ϕ IRF responses heat maps. **B.** takes a vertical slice of the ankle AP response heat maps and depicts the ϕ IRF for the perturbations applied at mid swing (phase = -0.2)

Late stance strategy: The other strategy that we observed in human participants in response to the forward perturbation of the swing leg was a decrease in the excitation of the contralateral GAS muscle during late stance. In both models, the GAS muscle excitation was a product of a force feedback reflex mechanism. Therefore, like the VAS muscle, we expected the addition of the CPG to help improve the timing of the GAS response. However, in both models we observed a decrease in the excitation of the GAS muscle during late stance (**Figure 5-7**). The magnitude of the response was smaller in the reflex model, but the models did not show any other substantial differences.

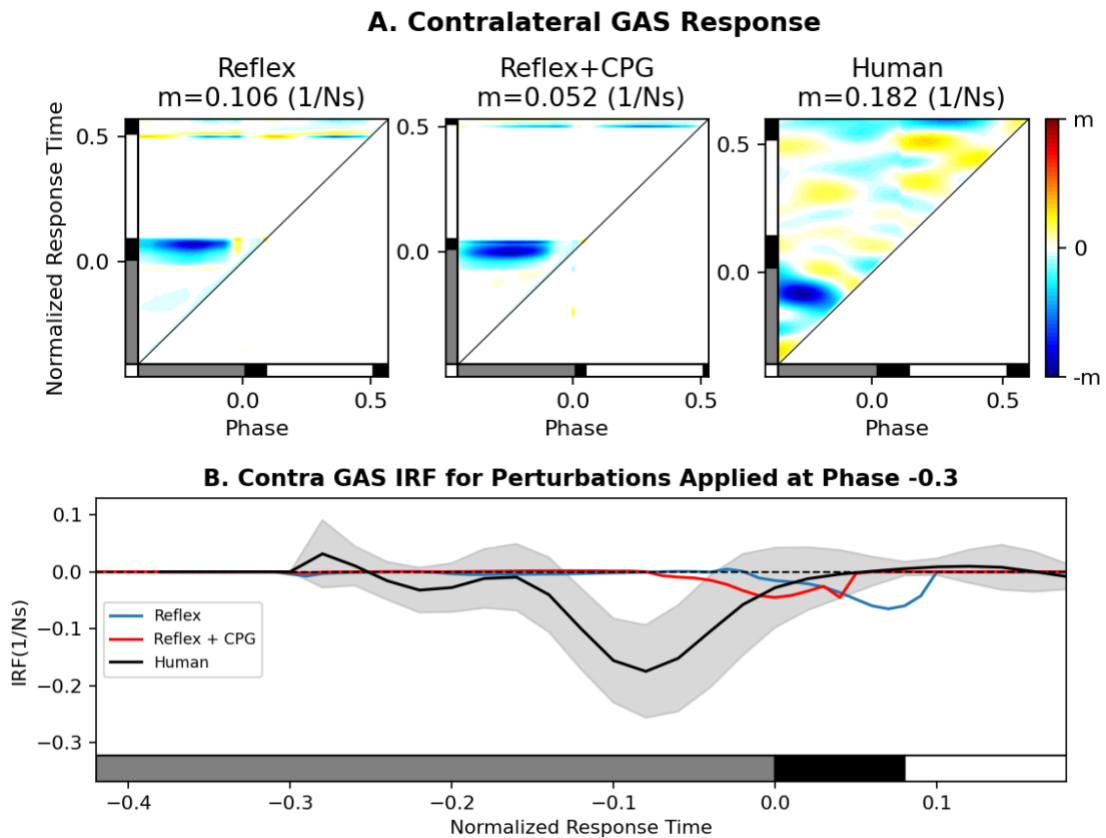


Figure 5-7) Comparing Contralateral GAS response to the mechanical perturbations in the models and human. **A.** demonstrates the ϕ IRF responses heat maps. **B.** takes a vertical slice of the ankle AP response heat maps and depicts the ϕ IRF for the perturbations applied at mid swing (phase = -0.3).

5.4 Discussion:

To further understand the neural mechanisms involved in control of human walking, in this study we compared the response of two neuromechanical models of human walking with previously collected experimental data (Rafiee and Kiemel 2020). We hypothesized that adding a CPG to a counteractive model of human walking (Song and Geyer, 2015) would improve the timing of at least subset of the muscular responses and would consequently positively affect the subsequent kinematic responses. However, our results did not show substantial differences between the responses of the two neuromechanical models. In this section, we first compare the models' responses with those of the humans and then attempt to understand why the addition of the CPG did not affect any of the muscular responses to a large extent.

5.4.1 Neuromechanical Models vs Human

In general, we observed that the initial kinematic responses were similar across the models and human (**Figure 5-3**) Comparing the Ankle AP position response to the mechanical perturbations in the models and human. **A.** demonstrates the ϕ IRF responses in heat maps that have two independent variables: perturbation phase on the horizontal axis and normalized response time on the vertical axis. The color coding of the heat maps from cold to hot indicates the value of the ϕ IRFs (white for 0, yellow and red for positive, and blue for negative). The value m , specified above each heatmap, is the maximum absolute response value which we used to define the color map (see color bar). The diagonal line in the heat map corresponds to a response measured at the same time the perturbation is applied. The ϕ IRF is 0 (white) below this line. **B.** takes

a vertical slice of the ankle AP response heat maps and depicts the ϕ IRF for the perturbations applied at mid swing (phase = -0.3). Black shaded areas depict experimental ϕ IRFs with 95% confidence interval, and solid blue and red lines show the Reflex model and the Reflex+CPG direct ϕ IRFs.), which indicates that the plant is represented well in the models. However, the muscular responses were found to be much more variable. We first address whether this difference in behavior could be attributed to the fact the human participants walked on a treadmill, whereas the neuromechanical models simulated overground walking. We know that the priorities of the neural controller in overground walking vs treadmill walking can be different in response to large perturbations. However, previous experimental studies using visual perturbations have shown that when walking on the treadmill, human participants did not correct a much larger forward displacement of the pelvis several cycles after the perturbation (Rafiee and Kiemel 2020). **Figure 5-8** compares the magnitude of the AP pelvis forward displacement in response to the visual perturbations with the mechanical perturbations used in this study. The data suggests that the perturbations in this study were small enough that the limited space of the treadmill did not introduce any restriction on foot-placement strategies.

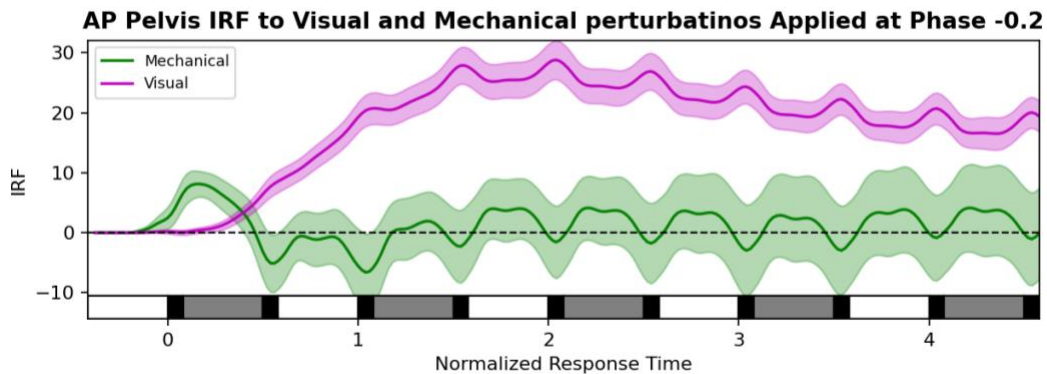


Figure 5-8) Comparing AP Pelvis response to the mechanical vs visual perturbations applied at mid swing (phase = -0.2) in human. The shaded areas depict experimental ϕ IRFs with 95% confidence interval.

5.4.2 Reflex Model vs Reflex+CPG Model

In the rest of this chapter, we compare the two neuromechanical models of human walking. In chapter 4 we found that a counteractive model of human walking (Geyer and Herr 2010) cannot produce most phase-specific muscular responses observed in human walking. Rather, most responses occurred with a fixed delay after the onset of perturbation. We argued that to implement phase-specific responses, the neural controller should have information about the phase of the system. To give the model phase information, we proposed using a CPG.

We compared the effect of the controllers on local stability of human walking by calculating the phase-dependent muscular responses of the models to perturbations. The observed phase-dependent responses can be attributed either to changes in the magnitude of average muscle waveform or the effect of time shifts on the average waveform. We expected that a Reflex+CPG model, in which the contribution of reflex to neural control is halved, to reduce the responses caused by change in the magnitude

of average waveform. Indeed, we observed smaller magnitude of responses in the Reflex+CPG model than the Reflex model. However, in most cases the ratio of the two models' responses were not 1 to 2. This observation indicates the important effect of time shifts in the responses.

We expected that a CPG, whose functional role is to set the timing of the muscle excitations, to help the model reproduce responses that are due to time shifts. However, we found the response of the Reflex model and the Reflex+CPG model to be very similar. Both models were able to reproduce the early stance VAS (**Figure 5-6**) Comparing ipsilateral VAS response to the mechanical perturbations in the models and human. **A.** demonstrates the ϕ IRF responses heat maps. **B.** takes a vertical slice of the ankle AP response heat maps and depicts the ϕ IRF for the perturbations applied at mid swing (phase = -0.2) and the late stance GAS responses (**Figure 5-7**) to mechanical perturbations, which the older version of the Reflex model (Geyer and Herr, 2010) failed to reproduce. This improvement can be attributed to the fact that the Song and Geyer (2015) model is dominantly controlled by sequential modules that gate the reflex mechanisms. In a way these sequential modules function as an implicit neural clock and produce similar phase-specific responses that we expected the combination of CPG and spinal reflexes to produce. Our general hypothesis was correct; incorporating mechanisms that account for the phase-dependency of non-counteractive responses helps a model to appropriately time the responses to perturbations. These two models used different mechanism to account for this phase-dependency. Given the important roles CPGs play in neural control of mammalian locomotion (Hultborn and Nielsen, 2007), their involvement in producing

these types of phase-specific responses in neural control of human walking is very plausible.

However, as discussed in the introduction, accounting for the phase-dependency of muscle modulations is not sufficient for producing all human muscular responses. In particular, we observed that neither model was able to reproduce the TA response to the mechanical perturbations. Previously, we have hypothesized that the early-stance increase in the excitation of TA compensates for the error in foot placement by propelling the pelvis forward relative to the stance foot (Rafiee and Kiemel 2020). Since the TA excitation in the model was controlled through a stretch reflex mechanism and did not depend on any mechanisms of compensating in errors of foot-placement, we did not expect that adding a CPG to the model would be sufficient for reproducing human responses. In the future, we plan to predict the neural feedback from the experimental data and then add those feedback components to the model. For example, the TA excitation will include some sort of “cutaneous” feedback. This cutaneous feedback would be a proportional controller that corrects for the errors in the relative position of the foot and pelvis from its desired value at heel strike.

Chapter 6 : Conclusions

This thesis aimed at expanding the current understanding of the neural control of human locomotion. In particular, it sought to examine the role of different muscle modulations in maintaining the local stability of human walking and the mechanisms that the nervous system uses to produce these muscle modulations.

In study one, we investigated the role of early stance modulation of the ankle dorsiflexor muscle, TA, in correcting for errors in foot placement. To investigate the role of TA in speed control during early stance, we imposed a restriction on ankle dorsiflexion using a taping method, which limited the ability of this muscle to accelerate the body forward during early stance. We characterized the kinematic and muscular responses of this “restricted” walking to mechanical perturbations and compared the results with those from “normal” human walking. We observed that as intended the dorsiflexion restriction compromised the TA’s ability to perform work. Even though strategies varied between subjects, several subjects showed indication of adaptation of the neural feedback so that it produced smaller TA responses at early stance. This change in the dorsiflexor muscle excitation also had the kinematic consequences of smaller dorsiflexion response at early stance. Our hypothesis was that if the early-stance modulation of TA indeed plays an important role in speed control, then in the absence of its contribution, the nervous system either would use alternative speed control strategies or would suffer consequences. We observed that with the diminished contribution of TA to speed control, the nervous system increased the

excitation of the other anterior muscle group, namely VAS modulation at early stance. This strategy helped accelerate the COM forward and compensated for the errors in foot placement, thus our hypothesis was supported.

In studies two and three, we used computer simulation of human walking to investigate the neural mechanisms responsible for producing the stabilizing responses observed in human locomotion. In a previous study (Rafiee and Kiemel 2020), we classified responses of human walking to small mechanical perturbations that resulted in forward displacement of the swing leg as counteractive and non-counteractive based on the latency of the responses and whether we could hypothesize a reflex mechanism to produce them or not. In study two we tested the previous counteractive / non-counteractive classification of the muscular responses. To this end, we examined the response of a counteractive model of human walking (Geyer and Herr, 2010) to external mechanical perturbations and compared its results to those from experimental studies (Rafiee and Kiemel, 2020). Our results supported the previous categorization. The model was able to reproduce the responses that we have categorized as counteractive but could not reproduce phase-specific muscle modulations that compensated for the errors in foot-placement. We concluded that implementing such strategies would require a more sophisticated control.

Finally, as a follow up to study two, in study three we compared different types of neural mechanisms that can stabilize human walking. Study two suggested that the implementation of the non-counteractive strategies requires a more sophisticated control involving mechanisms such as a clock or a state estimator. Therefore, in study

three, we developed a hybrid controller by adding a CPG to a newer version of the counteractive model of human walking in study two (Song and Geyer, 2015). To investigate whether the hybrid model reproduced human responses to external perturbations better than the purely counteractive model, we characterized and compared the responses of both models to the same external perturbations. We found that both models performed better than the model in study two (Geyer and Herr, 2010); however, no substantial differences were observed between the models. This finding suggests that the structure of the chosen counteractive model is such that it behaves as if it already has a CPG.

Completely understanding the role of the neural feedback in maintaining the local stability of human walking remains a challenge in the field of motor control. In this thesis, we provided additional evidence on the role of early stance TA modulation in foot-placement strategies and hypothesized neural mechanisms responsible for producing such non-counteractive strategies.

Appendices

Appendix I: Smoothing the Song & Geyer (2015) Model

The original Geyer model has 9 modules that are binary.

<i>st</i> :	leg in stance
<i>st_csw</i> :	leg in stance & contra-leg in swing
<i>st_sw0</i> :	leg in stance & initiate swing
<i>st_st</i> :	leg in stance & keep in stance
<i>sw</i> :	leg in swing
<i>sw_flex_k</i> :	leg in swing & flex knee
<i>sw_hold_k</i> :	leg in swing & hold knee
<i>sw_stop_l</i> :	leg in swing & stop leg
<i>sw_hold_l</i> :	leg in swing & hold leg

These modules depend on several parameters, some of which are binary:

<i>ci</i> :	ipsilateral leg contact at the current time point
<i>cip</i> :	ipsilateral leg contact at the previous time point
<i>cc</i> :	contralateral leg contact at the current time point
<i>bc_sw_init</i> :	brain command, initiate swing (which leg to transition into swing at double support)

and some are continuous:

φ :	knee angle
φ_{tgt} :	brain command, target knee angle
α :	foot-placement, hip angle - 0.5 knee angle
α_{tgt} :	brain command, desired foot-placement
α_{δ} :	brain command,
d_{α} :	brain command, hip velocity - 0.5 knee velocity
GRF_i :	ipsilateral leg ground reaction force

GRF_c : contralateral leg ground reaction force

The Geyer model uses ground reaction data, GRF_i , to determine if the leg is in swing

($ci = 0$) or stance ($ci = 1$):

if $GRF_i > 0.1$:

$ci = 1$ [0-G]

else ($GRF_i \leq 0.1$):

$ci = 0$

Based on current (ci) and previous (cip) ground contact information, the Geyer model divides gait cycle into 4 sequential parts, (the order of the commands is important since the early lines can be overwritten). Here, we summarize the original code:

if $cip == 0$ & $ci == 1$: **(When the foot touches the ground)**

$st = 1$ [1-G]

$sw = 0$ [2-G]

$sw_flex_k = 0$ [3-G]

$sw_hold_k = 0$ [4-G]

$sw_stop_l = 0$ [5-G]

$sw_hold_l = 0$ [6-G]

if $st == 1$: **(During stance control)**

$st_csw = 1 - cc$ [7-G]

$st_sw0 = bc_sw_init$ [8-G]

$st_st = 1 - st_sw0$ [9-G]

if $cip == 1$ & $ci == 0$: **(When the foot loses contact)**

```

st = 0 [10-G]
st_csw = 0 [11-G]
st_sw0 = 0 [12-G]
st_st = 0 [13-G]
sw = 1 [14-G]
sw_flex_k = 1 [15-G]

```

```

if sw == 1:          (During swing control)
    if sw_flex_k == 1:
        if  $\varphi < \varphi_{tgt}$ :
            sw_flex_k = 0 [16-G]
            sw_hold_k = 1 [17-G]
        else (sw_flex_k == 0):
            if sw_hold_k == 1:
                if  $\alpha < \alpha_{tgt}$ :
                    sw_hold_k = 0 [18-G]
                if  $\alpha < \alpha_{tgt} + \alpha_{\delta}$  :
                    sw_stop_l = 1 [19-G]
            if sw_stop_l == 1 & d_alpha > 0:
                sw_hold_l = 1 [20-G]

```

Here, we attempted to find smooth implementation of these lines of code:

The first step was to define the ground contact variable, ci , as a smooth function of the ground reaction force, GRF_i . To this end, we used the following equation:

$$ci = g(s_{p_c} * (GRF_i - 0.1) + 0.5) \quad [0-M]$$

, where s_{p_c} is the contact force smoothing factor and

$$g(x) = \frac{f(x)}{(f(x)+f(1-x))},$$

$$f(x) = \begin{cases} 0 & x \leq 0 \\ e^{-\frac{1}{x}} & x > 0 \end{cases}$$

Using [0-M] guarantees a smooth transition from 0 to 1 when GRF_i changes from 0 to 0.2. Note that in the limit of large s_{p_c} , [0-M] is mathematically equivalent to [0-G]. In addition, [0-M] allows for maintaining a fine resolution that can be achieved even with small s_{p_c} . In our implementation, we set $s_{p_c} = 5$.

(General stance and swing dynamics)

We used the ci as specified in [0-M] to determine the stance and swing dynamics. Consider [1-G] and [10-G] in the Geyer model. These conditions set the dynamics of the variable st . When the “first ground contact” condition is met, st is set to 1 [1-G]. st does not change until the “lose contact” condition is met, where st is set to 0 [10-G], and it remains 0 until the next ground contact. Conceptually, the ground contact information, ci , and the stance module, st , are the same; therefore, we used the following single line of code to define the st dynamics:

$$st = ci \quad [1-M]$$

Similarly, line [2-G] and [14-G] set the dynamics of the variable sw . When the “first ground contact” condition is met, sw is set to 0 [2-G] and remain 0 until the next “lose contact” condition is met, where sw is set to 1 [14-G]. Given the contrasting nature of st and sw , we defined sw as follows:

$$sw = 1 - st \quad [2-M]$$

(Stance modules dynamics)

The stance modules dynamics are all conditioned on st . When st is 0, these modules are set to 0 [11-13-G] and when st is 1, these values obey equations [7-9-G]. Therefore, we approximated the stance modules dynamics as follows:

$$st_csw = st * (1 - cc) \quad [3-M]$$

$$st_sw0 = st * bc_sw_init \quad [4-M]$$

$$st_st = st * (1 - st_sw0) \quad [5-M]$$

(Swing modules dynamics)

In the original Geyer model, the swing modules dynamics not only are conditioned on sw , but also on the flex-knee dynamics [16-20-G]. If the flex-knee dynamics are met, the rest of the swing modules are set to 0. Therefore, to calculate the swing modules, first the flex-knee condition had to be assessed. We defined the variable $flexk1$ that is 1, when the conditions for flexing the leg are met and is 0 otherwise (see [6-M]).

In the Geyer model, [16-G] sets the variable sw_flex_k to 0, if the conditions for flexing the leg are met (i.e., $flexk1 = 1$); otherwise, it does not change sw_flex_k . This condition checks for the leg to be already flexing and the knee angle, φ , to be smaller than a target knee angle, φ_tgt . In practice, [16-G] only acts on the model during early swing. Therefore, here, to define $flexk1$, we distinguished between the early and late swing, using the foot-placement variable, α . $flexk1$ is set to 1, when $\varphi > \varphi_tgt$ and $\alpha > 1.5$; otherwise $flexk1$ is set to 0. To ensure a smooth implementation of these conditions, we used tanh function [6-M]:

$$flexk1 = \left(0.5 + 0.5 * \tanh \left(s_{p_k1} * (\varphi - \varphi_tgt) \right) \right) * \left(0.5 + 0.5 * \tanh \left(s_{p_k2} * (\alpha - 1.5) \right) \right)$$

[6-M]

The dynamics of the rest of the modules during swing was approximated using $flexk1$.

(Flex knee dynamics)

In the Geyer code, lines [3-G], [15-G] and [16-G] set the dynamics of the sw_flex_k . When the “first ground contact” condition is met, sw_flex_k is set to 0 [3-G]. sw_flex_k does not change until the “lose contact” condition is met, where sw_flex_k is set to 1 [15-G]. During swing, [16-G] sets the dynamics of sw_flex_k . Therefore, the flex knee dynamics can be approximated as follows:

$$sw_flex_k = sw * flexk1$$

[7-M]

(Hold knee dynamics)

[17-G] & [18-G] set the dynamics of the sw_hold_k . When the leg is in swing (i.e., $sw = 1$), if the knee is flexing (i.e., $flexk1 = 1$), sw_hold_k is set to 0 [17-G]. If the knee is not flexing (i.e., $flexk1 = 0$), the relationship between the foot-placement variable α with its target value, α_tgt , sets the dynamics of the sw_hold_k [18-G]. [8-M] is our attempt at a smooth implementation of the hold knee dynamics:

$$sw_hold_k = sw * (1 - flexk1) * \left[0.5 + 0.5 * \tanh \left(s_{p_hk} * (\alpha - \alpha_tgt) \right) \right]$$

[8-M]

(Stop leg dynamics)

Similarly, dynamics of sw_stop_l depends on both the sw and $flexk1$. When the leg is in swing and the knee not flexing (i.e., $flexk1 = 0$), the sw_stop_l dynamics depends on the relationship between the foot-placement variable α and a threshold close to its target value, $\alpha_tgt + \alpha_delta$ [19-G]. Conceptually, if the leg is in swing and the knee is not flexing, the knee is in hold condition; therefore, we approximated the sw_stop_l as follows:

$$sw_stop_l = sw_hold_k * \left[0.5 + 0.5 * \tanh \left(s_{p_sl} * (\alpha - \alpha_tgt + \alpha_delta) \right) \right]$$

[9-M]

(Hold leg dynamics)

Lastly, sw_hold_l dynamics depends on sw_stop_l . When the leg is in swing, the knee is not flexing and the stop leg condition is satisfied, the sw_hold_l dynamics depend on the sagittal leg angular velocity d_α [20-G]. [10-M] is a smooth approximation of sw_hold_l :

$$sw_hold_l = sw_stop_l * [0.5 + 0.5 * \tanh(s_{p_hl} * d_\alpha)] \quad [10-M]$$

Bibliography

- Allen, N.E., Sherrington, C., Paul, S.S., Canning, C.G., 2011. Balance and falls in Parkinson's disease: a meta-analysis of the effect of exercise and motor training. *Mov. Disord.* 26, 1605–1615.
- Aoi, S., Ogihara, N., Funato, T., Sugimoto, Y., Tsuchiya, K., 2010. Evaluating functional roles of phase resetting in generation of adaptive human bipedal walking with a physiologically based model of the spinal pattern generator. *Biol. Cybern.* 102, 373–387.
- Bauby, C.E., Kuo, A.D., 2000. Active control of lateral balance in human walking. *J. Biomech.* 33, 1433–1440.
- Boakes, J.L., Rab, G.T., 2006. *Muscle activity during walking.* Hum. Walk. Lippincott Williams Wilkins Baltim.
- Brown, I.E., Loeb, G.E., 2000. A reductionist approach to creating and using neuromusculoskeletal models, in: *Biomechanics and Neural Control of Posture and Movement.* Springer, pp. 148–163.
- Cho, Y., Kim, S., Jeon, I., Ahn, S., Kwon, O., 2015. Effect of treadmill walking with ankle stretching orthosis on ankle flexibility and gait. *J. Phys. Ther. Sci.* 27, 1257–1260. <https://doi.org/10.1589/jpts.27.1257>
- Collins, S., Ruina, A., Tedrake, R., Wisse, M., 2005. Efficient Bipedal Robots Based on Passive-Dynamic Walkers. *Science* 307, 1082–1085. <https://doi.org/10.1126/science.1107799>
- Delafontaine, A., Gagey, O., Colnaghi, S., Do, M.-C., Honeine, J.-L., 2017. Rigid Ankle Foot Orthosis Deteriorates Mediolateral Balance Control and Vertical Braking during Gait Initiation. *Front. Hum. Neurosci.* 11. <https://doi.org/10.3389/fnhum.2017.00214>
- Den Otter, A.R., Geurts, A.C.H., Mulder, T., Duysens, J., 2004. Speed related changes in muscle activity from normal to very slow walking speeds. *Gait Posture* 19, 270–278.
- Dietz, V., Colombo, G., Müller, R., 2004. Single joint perturbation during gait: neuronal control of movement trajectory. *Exp. Brain Res.* 158, 308–316.
- Dietz, V., Quintern, J., Boos, G., Berger, W., 1986. Obstruction of the swing phase during gait: phase-dependent bilateral leg muscle coordination. *Brain Res.* 384, 166–169.
- Dingwell, J.B., Kang, H.G., 2007. Differences Between Local and Orbital Dynamic Stability During Human Walking. *J. Biomech. Eng.* 129, 586–593. <https://doi.org/10.1115/1.2746383>
- Dingwell, J.B., Marin, L.C., 2006. Kinematic variability and local dynamic stability of upper body motions when walking at different speeds. *J. Biomech.* 39, 444–452.
- Duysens, J., Forner-Cordero, A., 2018. Walking with perturbations: a guide for biped humans and robots. *Bioinspir. Biomim.* 13, 061001.

- Dzeladini, F., Van Den Kieboom, J., Ijspeert, A., 2014. The contribution of a central pattern generator in a reflex-based neuromuscular model. *Front. Hum. Neurosci.* 8, 371.
- Eng, J.J., Winter, D.A., Patla, A.E., 1994. Strategies for recovery from a trip in early and late swing during human walking. *Exp. Brain Res.* 102, 339–349.
- Faisal, A.A., Selen, L.P., Wolpert, D.M., 2008. Noise in the nervous system. *Nat. Rev. Neurosci.* 9, 292.
- Gad, A.F., 2021. PyGAD: An Intuitive Genetic Algorithm Python Library. ArXiv210606158 Cs Math.
- Geboers, J.F., Drost, M.R., Spaans, F., Kuipers, H., Seelen, H.A., 2002. Immediate and long-term effects of ankle-foot orthosis on muscle activity during walking: A randomized study of patients with unilateral foot drop. *Arch. Phys. Med. Rehabil.* 83, 240–245. <https://doi.org/10.1053/apmr.2002.27462>
- Gerritsen, K.G., van den Bogert, A.J., Hulliger, M., Zernicke, R.F., 1998. Intrinsic muscle properties facilitate locomotor control—a computer simulation study. *Motor Control* 2, 206–220.
- Geyer, H., Herr, H., 2010. A muscle-reflex model that encodes principles of legged mechanics produces human walking dynamics and muscle activities. *IEEE Trans. Neural Syst. Rehabil. Eng.* 18, 263–273.
- Grey, M.J., Mazzaro, N., Nielsen, J.B., Sinkjær, T., 2004. Ankle extensor proprioceptors contribute to the enhancement of the soleus EMG during the stance phase of human walking. *Can. J. Physiol. Pharmacol.* 82, 610–616.
- Grey, M.J., Nielsen, J.B., Mazzaro, N., Sinkjær, T., 2007. Positive force feedback in human walking. *J. Physiol.* 581, 99–105.
- Grillner, S., Wallen, P., 1985. Central pattern generators for locomotion, with special reference to vertebrates. *Annu. Rev. Neurosci.* 8, 233–261.
- Günther, M., Ruder, H., 2003. Synthesis of two-dimensional human walking: a test of the λ -model. *Biol. Cybern.* 89, 89–106.
- Hill, A.V., 1938. The heat of shortening and the dynamic constants of muscle. *Proc R Soc Lond B* 126, 136–195.
- Hof, A.L., 2008. The ‘extrapolated center of mass’ concept suggests a simple control of balance in walking. *Hum. Mov. Sci.* 27, 112–125. <https://doi.org/10.1016/j.humov.2007.08.003>
- Hof, A.L., Vermerris, S.M., Gjaltema, W.A., 2010. Balance responses to lateral perturbations in human treadmill walking. *J. Exp. Biol.* 213, 2655–2664. <https://doi.org/10.1242/jeb.042572>
- Holmes, P., Full, R.J., Koditschek, D., Guckenheimer, J., 2006. The dynamics of legged locomotion: Models, analyses, and challenges. *SIAM Rev.* 48, 207–304.
- Hultborn, H., Nielsen, J.B., 2007. Spinal control of locomotion—from cat to man. *Acta Physiol.* 189, 111–121.
- Jo, S., 2007. A neurobiological model of the recovery strategies from perturbed walking. *Biosystems* 90, 750–768. <https://doi.org/10.1016/j.biosystems.2007.03.003>

- Jo, S., Massaquoi, S.G., 2007. A model of cerebrocerebello-spinomuscular interaction in the sagittal control of human walking. *Biol. Cybern.* 96, 279–307. <https://doi.org/10.1007/s00422-006-0126-0>
- Joshi, V., Srinivasan, M., 2019. A controller for walking derived from how humans recover from perturbations. *J. R. Soc. Interface* 16, 20190027. <https://doi.org/10.1098/rsif.2019.0027>
- Karas, M.A., Hoy, D.J., 2002. Compensatory Midfoot Dorsiflexion in the Individual with Heelcord Tightness: Implications for Orthotic Device Designs. *JPO J. Prosthet. Orthot.* 14, 82–93.
- Kiemel, T., Logan, D., Jeka, J.J., 2016. Using perturbations to probe the neural control of rhythmic movements. *ArXiv Prepr. ArXiv160701746*.
- Kuo, A.D., 2002. The Relative Roles of Feedforward and Feedback in the Control of Rhythmic Movements. *Motor Control* 6, 129–145. <https://doi.org/10.1123/mcj.6.2.129>
- Lehmann, J.F., Condon, S.M., Price, R., 1987. Gait abnormalities in hemiplegia: their correction by ankle-foot orthoses. *Arch. Phys. Med. Rehabil.* 68, 763–771.
- Liu, M.Q., Anderson, F.C., Pandy, M.G., Delp, S.L., 2006. Muscles that support the body also modulate forward progression during walking. *J. Biomech.* 39, 2623–2630. <https://doi.org/10.1016/j.jbiomech.2005.08.017>
- Loeb, G.E., Brown, I.E., Cheng, E.J., 1999. A hierarchical foundation for models of sensorimotor control. *Exp. Brain Res.* 126, 1–18. <https://doi.org/10.1007/s002210050712>
- Logan, D., Kiemel, T., Jeka, J.J., 2017. Using a system identification approach to investigate subtask control during human locomotion. *Front. Comput. Neurosci.* 10, 146.
- Maki, B.E., McIlroy, W.E., 1997. The Role of Limb Movements in Maintaining Upright Stance: The “Change-in-Support” Strategy. *Phys. Ther.* 77, 488–507. <https://doi.org/10.1093/ptj/77.5.488>
- Martelli, D., Luo, L., Kang, J., Kang, U.J., Fahn, S., Agrawal, S.K., 2017. Adaptation of Stability during Perturbed Walking in Parkinson’s Disease. *Sci. Rep.* 7, 17875.
- Masud, T., Morris, R.O., 2001. Epidemiology of falls. *Age Ageing* 30, 3–7.
- Matthews, P.B., 1991. The human stretch reflex and the motor cortex. *Trends Neurosci.* 14, 87–91.
- Matthis, J.S., Fajen, B.R., 2014. Visual control of foot placement when walking over complex terrain. *J. Exp. Psychol. Hum. Percept. Perform.* 40, 106–115. <https://doi.org/10.1037/a0033101>
- Murai, A., Yamane, K., 2011. A neuromuscular locomotion controller that realizes human-like responses to unexpected disturbances, in: 2011 IEEE International Conference on Robotics and Automation. Presented at the 2011 IEEE International Conference on Robotics and Automation (ICRA), IEEE, Shanghai, China, pp. 1997–2002. <https://doi.org/10.1109/ICRA.2011.5979965>
- Nashner, L.M., 1980. Balance adjustments of humans perturbed while walking. *J. Neurophysiol.* 44, 650–664.

- Neptune, R.R., Kautz, S.A., Zajac, F.E., 2001. Contributions of the individual ankle plantar flexors to support, forward progression and swing initiation during walking. *J. Biomech.* 34, 1387–1398.
- Norlin, R., Odenrick, P., 1986. Development of Gait in Spastic Children with Cerebral Palsy: *J. Pediatr. Orthop.* 6, 674–680.
<https://doi.org/10.1097/01241398-198611000-00006>
- Ogihara, N., Yamazaki, N., 2001. Generation of human bipedal locomotion by a bio-mimetic neuro-musculo-skeletal model. *Biol. Cybern.* 84, 1–11.
- Olney, S.J., Richards, C., 1996. Hemiparetic gait following stroke. Part I: Characteristics. *Gait Posture* 4, 136–148. [https://doi.org/10.1016/0966-6362\(96\)01063-6](https://doi.org/10.1016/0966-6362(96)01063-6)
- Ota, S., Ueda, M., Aimoto, K., Suzuki, Y., Sigward, S.M., 2014. Acute influence of restricted ankle dorsiflexion angle on knee joint mechanics during gait. *The Knee* 21, 669–675. <https://doi.org/10.1016/j.knee.2014.01.006>
- Patla, A.E., 2003. Strategies for dynamic stability during adaptive human locomotion. *IEEE Eng. Med. Biol. Mag.* 22, 48–52.
- Patla, A.E., Prentice, S.D., Robinson, C., Neufeld, J., 1991. Visual control of locomotion: strategies for changing direction and for going over obstacles. *J. Exp. Psychol. Hum. Percept. Perform.* 17, 603.
- Pearson, K., Ekeberg, Ö., Büschges, A., 2006. Assessing sensory function in locomotor systems using neuro-mechanical simulations. *Trends Neurosci.* 29, 625–631.
- Perrin, D.H., McLeod, I., 2018. *Athletic Taping, Bracing, and Casting, 4E.* Human Kinetics.
- Perry, J., Davids, J.R., 1992. Gait analysis: normal and pathological function. *J. Pediatr. Orthop.* 12, 815.
- Prochazka, A., Ellaway, P., 2012. Sensory systems in the control of movement. *Compr Physiol* 2, 2615–27.
- Proctor, J., Holmes, P., 2010. Reflexes and preflexes: on the role of sensory feedback on rhythmic patterns in insect locomotion. *Biol. Cybern.* 102, 513–531.
<https://doi.org/10.1007/s00422-010-0383-9>
- Purves, D., Augustine, G.J., Fitzpatrick, D., Hall, W.C., LaMantia, A.S., McNamara, J.O., White, L., 2014. *Neuroscience, 2008.* Boeck Sinauer Sunderland Mass 15–16.
- Rafiee, S., 2017. *Lower-Body Mechanical Perturbation of Gait to Identify Neural Control (PhD Thesis).*
- Rafiee, S., Kiemel, T., 2020. Multiple strategies to correct errors in foot placement and control speed in human walking. *Exp. Brain Res.*
<https://doi.org/10.1007/s00221-020-05949-x>
- Rankin, B.L., Buffo, S.K., Dean, J.C., 2014. A neuromechanical strategy for mediolateral foot placement in walking humans. *J. Neurophysiol.* 112, 374–383.
- Romkes, J., Brunner, R., 2007. An electromyographic analysis of obligatory (hemiplegic cerebral palsy) and voluntary (normal) unilateral toe-walking. *Gait Posture* 26, 577–586.

- Romkes, J., Hell, A.K., Brunner, R., 2006. Changes in muscle activity in children with hemiplegic cerebral palsy while walking with and without ankle-foot orthoses. *Gait Posture* 24, 467–474.
<https://doi.org/10.1016/j.gaitpost.2005.12.001>
- Sinkjær, T., Andersen, J.B., Larsen, B., 1996. Soleus stretch reflex modulation during gait in humans. *J. Neurophysiol.* 76, 1112–1120.
- Song, S., Geyer, H., 2017. Evaluation of a neuromechanical walking control model using disturbance experiments. *Front. Comput. Neurosci.* 11, 15.
- Song, S., Geyer, H., 2015. A neural circuitry that emphasizes spinal feedback generates diverse behaviours of human locomotion. *J. Physiol.* 593, 3493–3511.
- Srinivasan, M., Ruina, A., 2006. Computer optimization of a minimal biped model discovers walking and running. *Nature* 439, 72.
- Taga, G., 1998. A model of the neuro-musculo-skeletal system for anticipatory adjustment of human locomotion during obstacle avoidance. *Biol. Cybern.* 78, 9–17. <https://doi.org/10.1007/s004220050408>
- Taga, G., 1995. A model of the neuro-musculo-skeletal system for human locomotion. *Biol. Cybern.* 73, 97–111.
- Tahir, U., Hessel, A.L., Lockwood, E.R., Tester, J.T., Han, Z., Rivera, D.J., Covey, K.L., Huck, T.G., Rice, N.A., Nishikawa, K.C., 2018. Case Study: A Bio-Inspired Control Algorithm for a Robotic Foot-Ankle Prosthesis Provides Adaptive Control of Level Walking and Stair Ascent. *Front. Robot. AI* 5. <https://doi.org/10.3389/frobt.2018.00036>
- Takakusaki, K., 2013. Neurophysiology of gait: from the spinal cord to the frontal lobe. *Mov. Disord.* 28, 1483–1491.
- Van de Crommert, H.W.A.A., Faist, M., Berger, W., Duysens, J., 1996. Biceps femoris tendon jerk reflexes are enhanced at the end of the swing phase in humans. *Brain Res.* 734, 341–344. [https://doi.org/10.1016/0006-8993\(96\)00885-2](https://doi.org/10.1016/0006-8993(96)00885-2)
- Vistamehr, A., Kautz, S.A., Neptune, R.R., 2014. The influence of solid ankle-foot-orthoses on forward propulsion and dynamic balance in healthy adults during walking. *Clin. Biomech.* 29, 583–589.
<https://doi.org/10.1016/j.clinbiomech.2014.02.007>
- Vlutters, M., Van Asseldonk, E.H.F., van der Kooij, H., 2018. Foot Placement Modulation Diminishes for Perturbations Near Foot Contact. *Front. Bioeng. Biotechnol.* 6. <https://doi.org/10.3389/fbioe.2018.00048>
- Wang, Y., Srinivasan, M., 2014. Stepping in the direction of the fall: the next foot placement can be predicted from current upper body state in steady-state walking. *Biol. Lett.* 10. <https://doi.org/10.1098/rsbl.2014.0405>
- Wereley, N.M., 1990. Analysis and control of linear periodically time varying systems (PhD Thesis). Massachusetts Institute of Technology.
- Wolpert, D.M., Ghahramani, Z., Jordan, M.I., 1995. An internal model for sensorimotor integration. *Sci. Wash.* 269, 1880.
- Wood, B.H., Bilclough, J.A., Bowron, A., Walker, R.W., 2002. Incidence and prediction of falls in Parkinson's disease: a prospective multidisciplinary study. *J. Neurol. Neurosurg. Psychiatry* 72, 721–725.

- Wu, A.R., Simpson, C.S., van Asseldonk, E.H.F., van der Kooij, H., Ijspeert, A.J., 2019. Mechanics of very slow human walking. *Sci. Rep.* 9, 1–10. <https://doi.org/10.1038/s41598-019-54271-2>
- Yang, J.F., Stein, R.B., James, K.B., 1991. Contribution of peripheral afferents to the activation of the soleus muscle during walking in humans. *Exp. Brain Res.* 87, 679–687.
- Zaytsev, P., Hasaneini, S.J., Ruina, A., 2015. Two steps is enough: No need to plan far ahead for walking balance, in: 2015 IEEE International Conference on Robotics and Automation (ICRA). Presented at the 2015 IEEE International Conference on Robotics and Automation (ICRA), pp. 6295–6300. <https://doi.org/10.1109/ICRA.2015.7140083>
- Zehr, E.P., Komiyama, T., Stein, R.B., 1997. Cutaneous Reflexes During Human Gait: Electromyographic and Kinematic Responses to Electrical Stimulation. *J. Neurophysiol.* 77, 3311–3325. <https://doi.org/10.1152/jn.1997.77.6.3311>